12-2015

Depositional Facies and Sequence Stratigraphy of Niagaran-Lower Salina Reef Complex Reservoirs of the Guelph Formation, Michigan Basin

Matthew J. Rine

DEPOSITIONAL FACIES AND SEQUENCE STRATIGRAPHY OF NIAGARAN-LOWER SALINA REEF COMPLEX RESERVOIRS OF THE GUELPH FORMATION, MICHIGAN BASIN

by

Matthew J. Rine

A thesis submitted to the Graduate College
in partial fulfillment of the requirements
for the degree of Master of Science
Geosciences
Western Michigan University
December 2015

Thesis Committee:

Dave Barnes, Ph.D.
William Harrison III, Ph.D.
Charlotte Sullivan, Ph.D.
Peter Voice, Ph.D.

DEPOSITIONAL FACIES AND SEQUENCE STRATIGRAPHY OF NIAGARAN-LOWER SALINA REEF COMPLEX RESERVOIRS OF THE GUELPH FORMATION, MICHIGAN BASIN

Matthew J. Rine, M.S.

Western Michigan University, 2015

Hydrocarbon reservoirs in the Niagara-Lower Salina Reef Complex in the Michigan Basin have been extensively studied since the early 1960's. These reservoirs host an immense hydrocarbon resource, existing as closely-spaced, highly-compartmentalized reservoirs that have produced >500 million barrels of oil and 2.9 trillion cubic feet of natural gas. Previous studies depict these "pinnacle reefs" as tall, symmetrical towers with a random distribution of facies. This study utilizes abundant core data (32 cores, 20-acre spacing), thin-section petrography, and petrophysical wire-line logs to reconstruct the geometry, facies distributions, depositional history, and sequence stratigraphy of the Columbus III Reef Complex within the Southern Niagaran-Lower Salina Reef Trend. This study indicates that there are three depositional sequences, which include a lower bioherm complex, the middle Niagaran reef complex, and the uppermost Lower Salina A-1 Carbonate. These sequences are highly influenced by relative sea level fluctuations within the Michigan Basin, and can be correlated to global sea level changes. This new stratigraphic model allows for better predictability within the Michigan Basin, particularly in reefs without abundant well control. The high-resolution model also permits more accurate correlations between the Lower Salina shallow-water carbonate factory and the surrounding inter-reef and basin center carbonates (A-1 Carbonate).

ACKNOWLEDGMENTS

I would like to thank my committee for their guidance throughout this project. Sincere thanks are extended to my advisor, Dave Barnes, who allowed me a great deal of independence and for providing professional criticism and worldly knowledge throughout the process. Dr. William Harrison III, for allowing me to tap into his never-ending knowledge and dedication for Michigan geology. Dr. Charlotte Sullivan, for her unparalleled enthusiasm for the fascinating realm of carbonates. Linda Harrison, Jennifer Trout, and the rest of the MGRRE staff for their help in navigating and utilizing the core repository. Dr. Peter Voice for his attention to detail, and Dr. Stephen Kaczmarek for his critical eye. Thank you to all of my mates for their camaraderie and competitive push through challenging times. I would like to thank Battelle, Bluewater Gas Storage, and the Michigan Basin Geological Society (MBGS) for their generous financial support. Special personal thanks to my mother, Victoria, who instilled in me a passion for discovery. And to my girlfriend, Nicole, who was incredibly supportive during my studies.

Matthew J. Rine

TABLE OF CONTENTS

Table of Contents—continued

Table of Contents—continued

Table of Contents—continued

LIST OF TABLES

LIST OF FIGURES

List of Figures—continued

LIST OF PLATES

List of Plates—continued

CHAPTER I

INTRODUCTION

Purpose of Investigation

Silurian Niagaran Pinnacle Reef oil fields comprise an immense hydrocarbon resource, existing as highly geologically compartmentalized, closely-spaced reservoirs within the Michigan Basin. These oil and gas fields have produced over 500 million barrels of oil and 2.9 trillion cubic feet of natural gas (State of Michigan production records, 2015). A number of important basic geological relationships in the Silurian reef succession, related to the origin and geological controls on hydrocarbon reservoir occurrence and quality, are not yet fully resolved. Of special interest and direct application to further exploitation of reef reservoirs are high resolution sequence stratigraphic relationships, interpretation of ancient carbonate and evaporite environments related to reef complexes, modes and timing of diagenesis, and application of these relationships to high-resolution static geological models.

The need for additional reservoir characterization data during the initial discovery period (1960's) of Niagaran pinnacle reef hydrocarbon reservoirs resulted in the recovery of hundreds of cores, which include both on reef sections as well as potential pay intervals within off-reef, flank localities. Due to the wealth of whole cores, petrophysical core analysis data, and geophysical log suites, high-resolution reservoir characterization in the context of enhanced oil recovery (EOR) operations is possible in many fields. Although many reef reservoirs have been produced in the Michigan Basin, only 5% of the discovered fields have undergone development beyond primary production. With an average primary recovery of 26% and an average secondary recovery around 12.5% (Harrison, 2015, personal communication), these reef reservoirs are currently being targeted for EOR projects with the potential of 180 to 200 million barrels of unrecovered reserves (Grammer et al., 2008).

Despite the economic importance of pinnacle reef hydrocarbon reservoirs, initial studies are in conflict regarding stratigraphic models for the reef complexes and related strata. Detailed stratigraphic and lithofacies studies in core and other subsurface data were conducted by Gill (1973), Huh (1973), and Budros (1974) and serve as fundamental references for this study. Since this early work was completed, sequence stratigraphic principles and depositional models for carbonate systems have evolved (Kerans and Tinker, 1997) and are especially useful in the understanding of these geologically complex reefs (Grammer et. al, 2010). The main stratigraphic and sedimentological controversies in the literature address the complex geometric juxtaposition of two incompatible sedimentary successions, the Lower Silurian organic reef complexes (Niagaran/Guelph Formation), and the Upper Silurian non-fossiliferous carbonate, and evaporite strata (lower Salina Group) that encase the reefs.

The current study represents a detailed stratigraphic and sedimentological investigation of a typical southern Niagaran pinnacle reef trend reservoir. The primary objective of this study is to create a more accurate and detailed depositional model for the Columbus III reef complex in St. Clair Co., Michigan. Additional objectives include (i) understanding the stratigraphic relationships between on and off-reef strata, (ii) establishing the precise geometry of the reef complex and the three-dimensional internal sediment distribution patterns, and (iii) accurately characterizing the internal facies stacking architecture in order to better understand the sequence stratigraphic evolution of the reef complex.

Fundamental Questions

- *Can sequence stratigraphic models more effectively constrain and predict the lateral and vertical facies distribution of the Niagara and Salina Groups in the Michigan Basin?*

- *What are the main geological controls on Niagaran pinnacle reef sediment distribution patterns?*
- *How did Niagara and Salina sedimentation record changes in both eustatic sea-level and Michigan Basin subsidence?*
- *What is the general geometry of the reef and how are sediments spatially distributed within the reef complex?*

Geologic Setting

The Early-Late Silurian Michigan Basin

The Michigan Basin is roughly circular in shape and covers an area of 122,000 square miles (316,000 square kilometers), encompassing large parts of the upper and lower peninsulas of Michigan and adjacent areas of eastern Wisconsin, northeastern Illinois, northern Indiana, northwestern Ohio, and western Ontario. It is an intracratonic depression bounded by persistent, structurally stable areas: the Canadian Shield in Ontario to the north and northeast; the Findlay Arch in Ohio to the southeast; the Kankakee Arch in Indiana and Illinois to the southwest; and the Wisconsin Arch in Wisconsin to the west (Catacosinos et al., 1991; Cohee and Landes, 1958, Fig. 1.1). Basin subsidence was initiated during the Precambrian and reached maximum rates during Late Silurian to Middle Devonian (Howell and van der Pluijm, 1999). Rocks of Silurian age occur throughout most of the basin and account for over 30 percent of the estimated 108,000 cubic miles of sediment in the basin (Cohee and Landes, 1958).

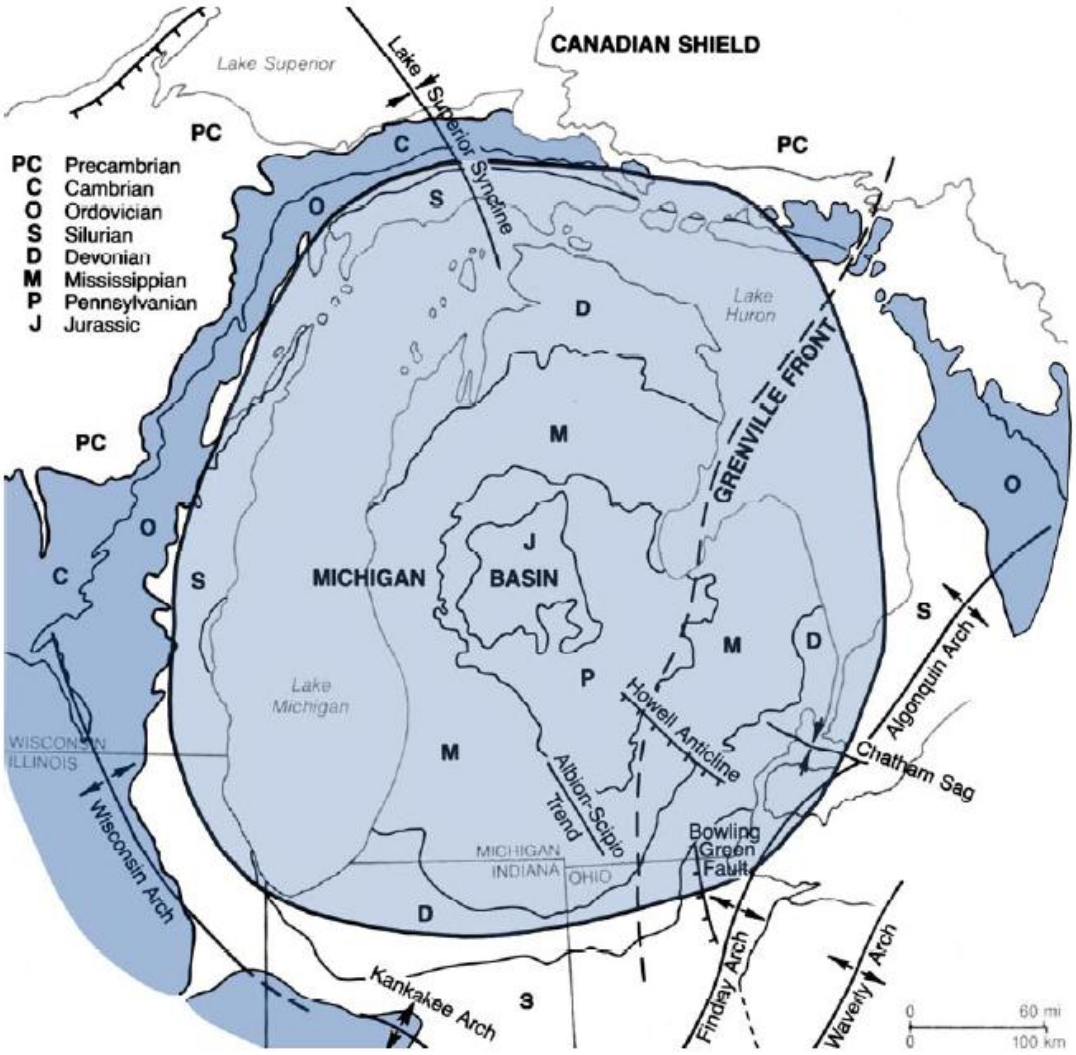

Figure 1.1. Detailed regional map of the Michigan Basin showing structural and basement elements (modified from Catacosinos et al., 1991).

Lithostratigraphic units in the Niagara and the lower Salina Groups (see Fig. 1.2) are the main focus of this study. The Manistique Group underlying the Niagara Group is also Niagaran in age (upper Llandoverian-lower Wenlockian). The Niagara Group is divided into the Gray Niagara (Lockport Dolomite), the Brown Niagara (Guelph Formation), the A-0 Carbonate (Cain Formation; Gill et. al, 1978), A-1 Evaporite, and the lower section of the A-1 Carbonate (Ruff Formation; Budros, 1974). The overlying Salina Group consists, from the base upwards, of the upper section of the A-1 Carbonate

(Ruff Formation), A-2 Evaporite, A-2 Carbonate, B Evaporite, B Unit, C Unit, D Evaporite, E Unit, F Evaporite, and G Unit. The upper Salina section is overlain by the Bass Islands Group, which is lithologically uniform and areally persistent. Disagreement regarding intra-reef and off-reef stratigraphy and sedimentology has dominated studies of Silurian pinnacle reef complexes since the onset of reef exploration. The age of the lower and upper parts of the reef buildups and opposing reef growth models will be thoroughly assessed and evaluated in this study.

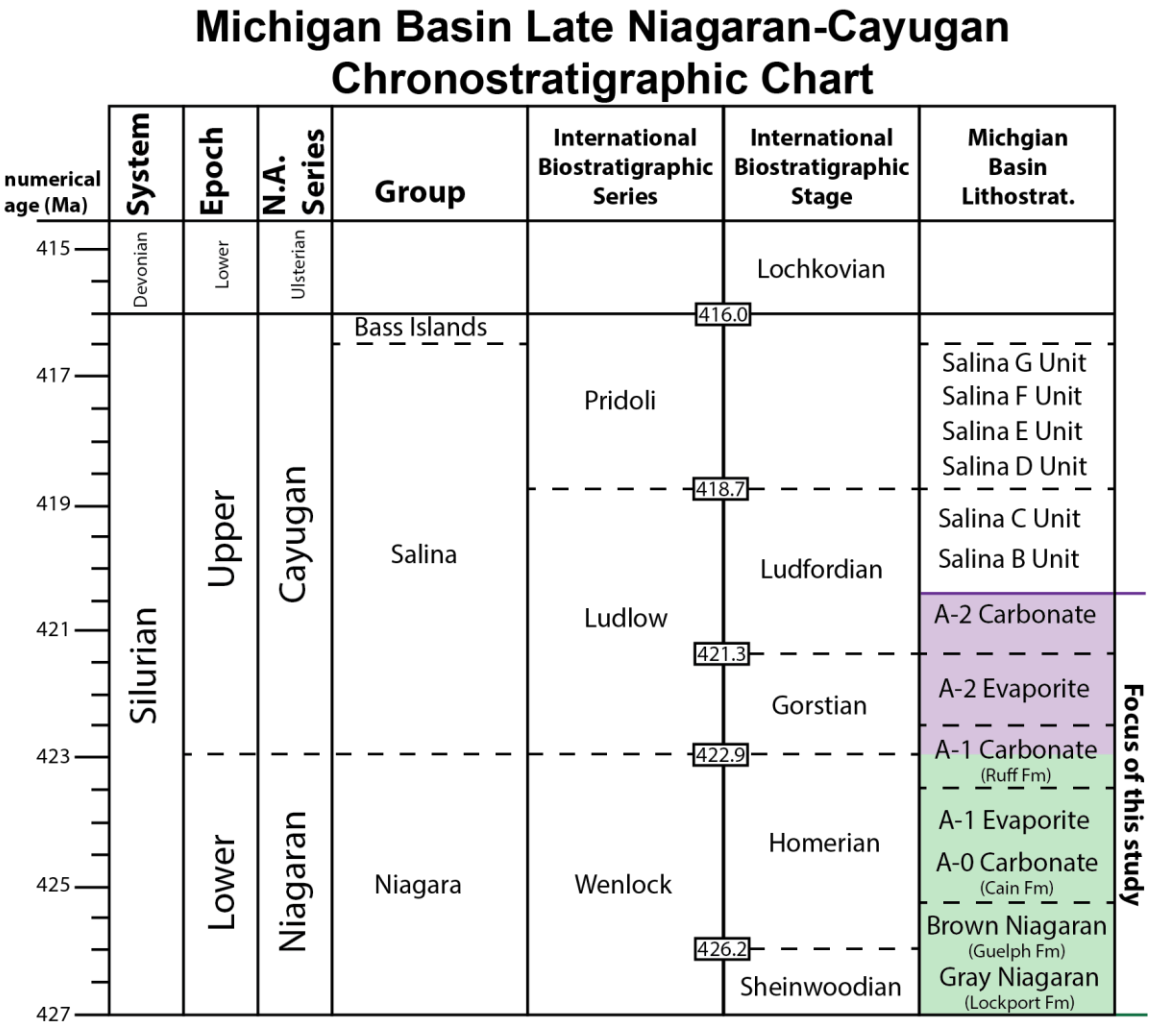

Figure 1.2. Chronostratigraphy of the Niagaran reefs and their encasing strata, Niagara and Salina Groups, in the Michigan Basin subsurface as determined in this study. Numerical ages for Silurian Stages are from Cramer et al. (2011).

The beginning of Lower Silurian carbonate deposition in the Michigan Basin coincided with the initiation of a major transgression of the North American continental interior platform (Briggs, 1978). This transgression was most likely synchronous with the rapid growth of the mid-ocean ridge, which reached a maximum during the Wenlockian deposition of the Lockport-Guelph carbonates (Briggs, 1978). In Michigan, the Niagaran (Lower Silurian) is represented by the isolation of the central Michigan Basin from the global ocean by the construction of a continuous belt of organic carbonate banks around the basin margin (Mesolella, 1974). At this time the basin was located between 20-25° South latitude (Fig. 1.3). This low-latitude location of the basin provided favorable environmental conditions for carbonate reef growth until the late Niagaran and the Cayugan (Mesolella, 1974). At this time reef growth halted and the basin was dominated by arid conditions (Briggs, 1978). Restriction of the basin resulted in a highly evaporitic regime and deposition of primarily evaporitic strata of the Salina Group, as well as restricted carbonate successions (Briggs, 1978). In contrast, during Niagaran deposition, the Michigan basin was characterized by normal marine salinity and open marine circulation (Mesolella, 1974).

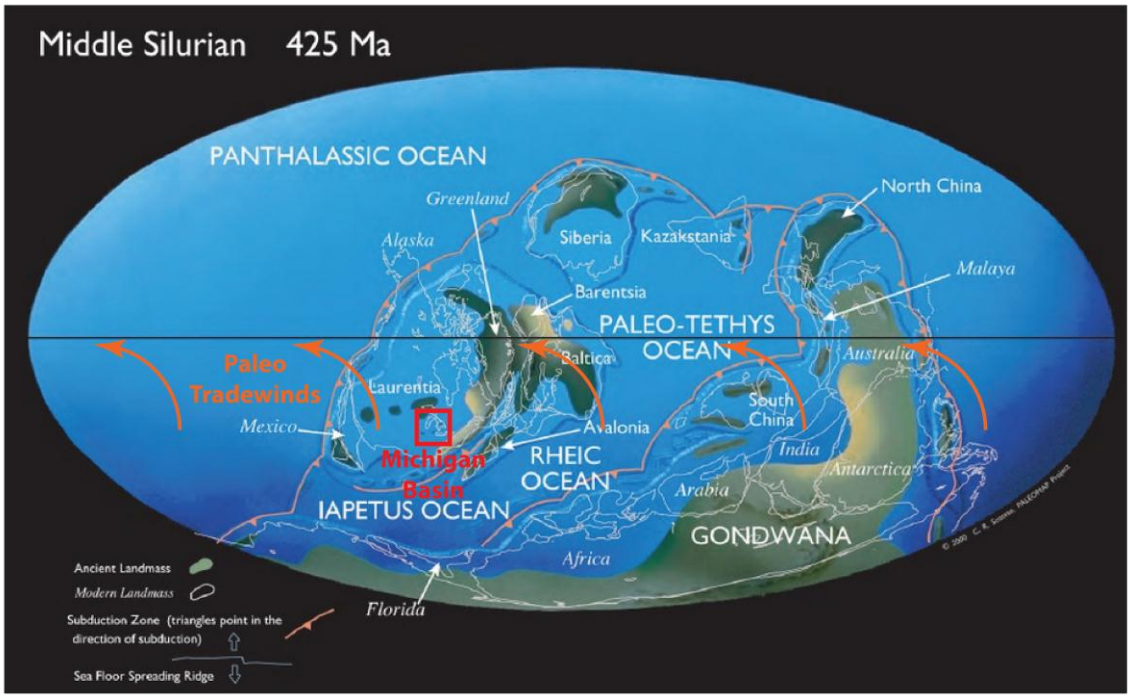

Figure 1.3. Silurian global reconstruction from the Scotese PALEOMAP Project (http://www.scotese.com). Michigan Basin is located between 20-25° south of the equator in a tropical to sub-tropical environment. General paleo-wind direction consists of southeasterly trade winds across the Michigan Basin.

At the beginning of the Upper Silurian (Cayugan) conditions in the Michigan Basin were transitional to intensively evaporative, associated with the gradual withdrawal of the sea to the central part of the basin. The location of the Michigan Basin had also shifted north a few degrees, resulting in the transition from humid tropics into the arid tropical belt. The regression of sea water from the Michigan Basin may have been triggered by the cessation of active spreading at an ocean ridge system, resulting in emergence of the North American cratonic interior platforms as sea water slowly returned to the ocean basins (Briggs, 1978). This relative sea-level fall resulted in the progressive exposure and demise of the Guelph Formation carbonate banks and pinnacle reefs as well as the subsequent deposition of gypsum, halite, and potash salts in the basin center due to almost complete desiccation of the basin (Gill, 1977). Potassium-rich sylvite deposits are easily identified in wire-line logs by a prominent gamma ray increase due to the natural

radiation of potassium present in the potash. As documented by Leibold (1992), these potash salts are underlain by a regressive package of halite and overlain by a transgressive package of halite, totaling as much as 400 feet (122 m) of evaporites in the basin center (see Fig. 1.4).

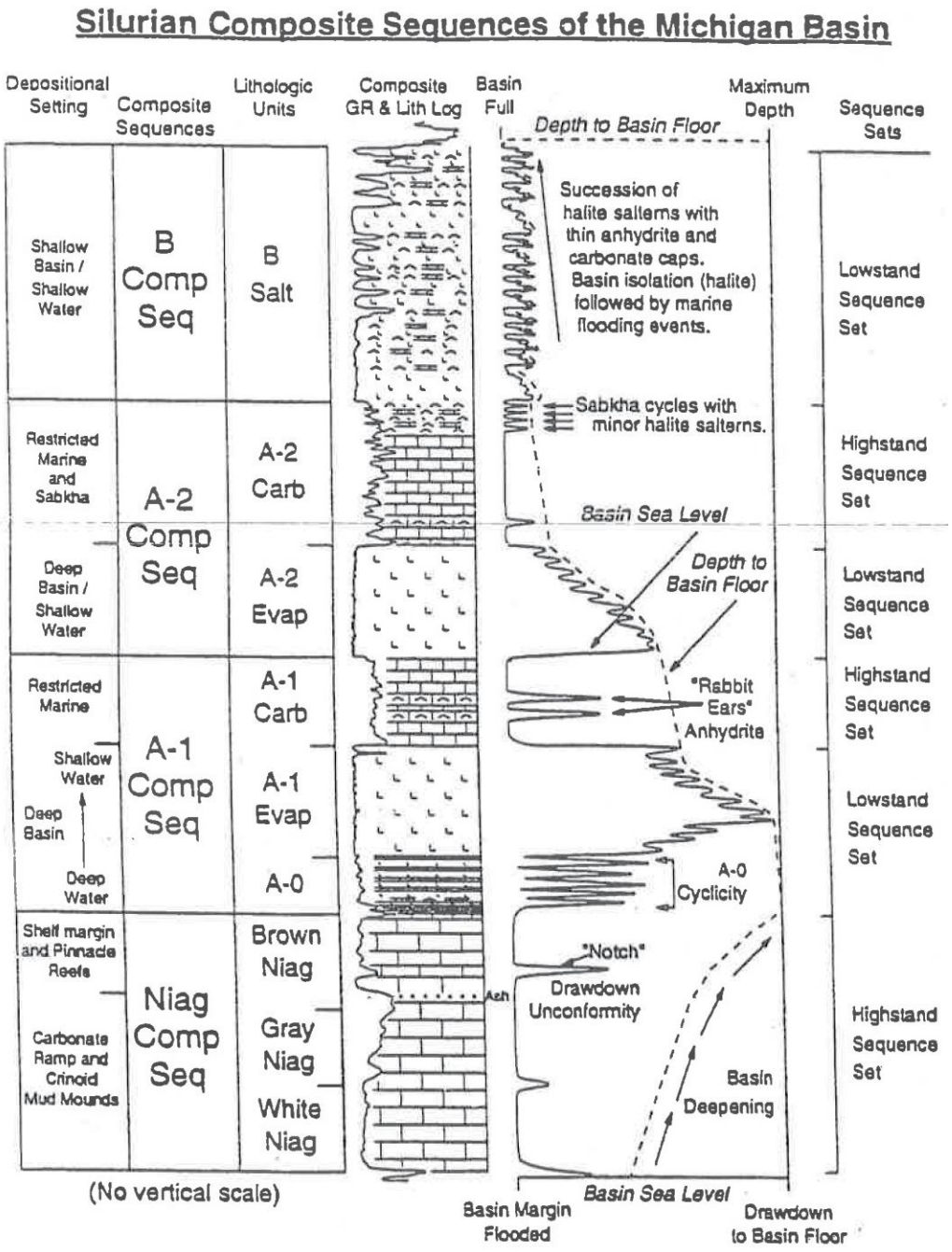

Figure 1.4. Summary of the composite sequences of the Niagara and lower Salina Groups in the Michigan Basin from Leibold (1992). The solid lined curve represents the approximate sea level within the basin, while the dashed line represents the depth to the basin floor.

The subsequent transgressive deposits (A-1 Carbonate) filled the middle part of the basin as relative sea-level began to rise and continued to onlap the basin margins. The first Salina Group Unit to onlap the southern margin of the basin was the A-2 Carbonate (Gill, 1977). The restricted nature of the A-1 Carbonate biota (largely cyanobacterial with a complete absence of hard parts of any macrofossils) also suggests that the Salina marine conditions never returned to normal open-marine conditions prevalent during Niagaran time in the Michigan Basin. The A-2 Carbonate unit is overlain by the Salina B, D, and F Salts (and several heterolithic units; C Shale, E Unit, and G Shale), which mark the end of Salina deposition.

Previous studies suggest that subsidence rates differed at the northern and southern margins of the basin (Budros, 1974; Briggs and Briggs, 1974). Subsidence in the north was greater as inferred by taller, narrower reef geometry compared to shorter, more laterally extensive geometry along the southern margin (Ells, 1967). Reef geometry and carbonate-evaporite unit thicknesses will be discussed later because they are important for discerning tectonic history as well as diagenetic and reef growth models.

Silurian Pinnacle Reefs

Silurian pinnacle reef complexes are isolated, topographically-high carbonate buildups and exist in two well-defined belts in the subsurface of the Michigan Basin. Both reef trends are completely encased by younger salt, anhydrite, and fine-grained carbonate strata (Fig. 1.5). As defined by Lowenstam (1950), a reef is "the product of the actively building and sediment-binding biotic constituents, which, because of their potential wave resistance, have the ability to erect rigid, wave resistant topographic

structures." The reefs were deposited on a ramp-like slope that deepened toward the basin center. They vary in size depending on their location in the basin. The average reef is about 300 feet (107 m) in height and the tallest reefs exceed 700 feet (210 m). The northern trend reefs are typically smaller in diameter, but are taller than the broad, shorter southern trend reefs. In general, the height of reefs increases basinward on both the northern and southern slopes (Fig. 1.6). To date, over 1,100 reefs have been identified in the northern and southern trends at depths ranging from 2,200 to 7,000 feet (733 to 2,135 m) in the subsurface (State of Michigan history of Niagaran reef fields).

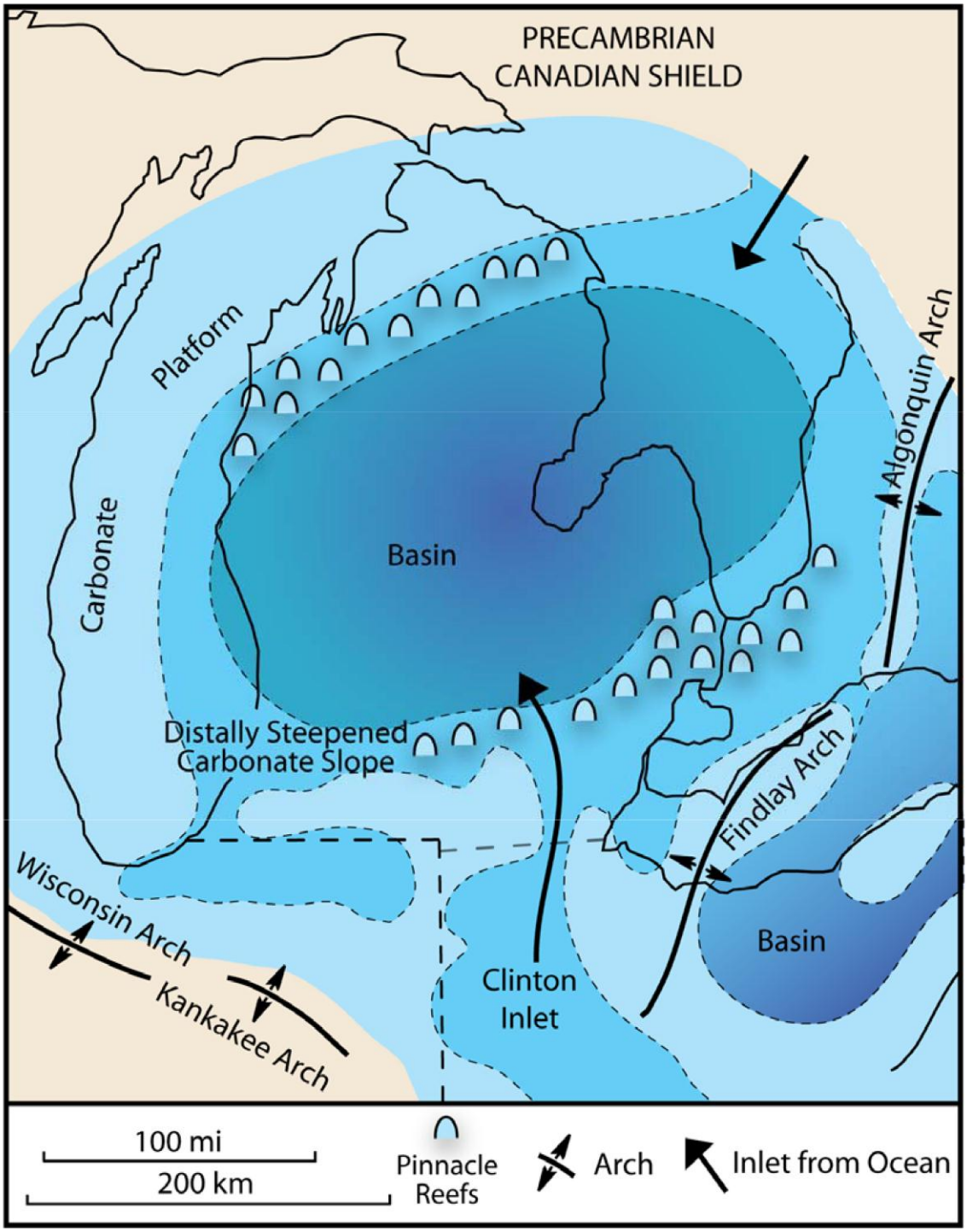

Figure 1.5. The generalized depositional environments of the Michigan Basin in the Silurian during Niagaran deposition, composed of a carbonate platform with reef bank, carbonate ramp with pinnacle reefs, and a deep basin center. Modified from Burgess and Benson (1969).

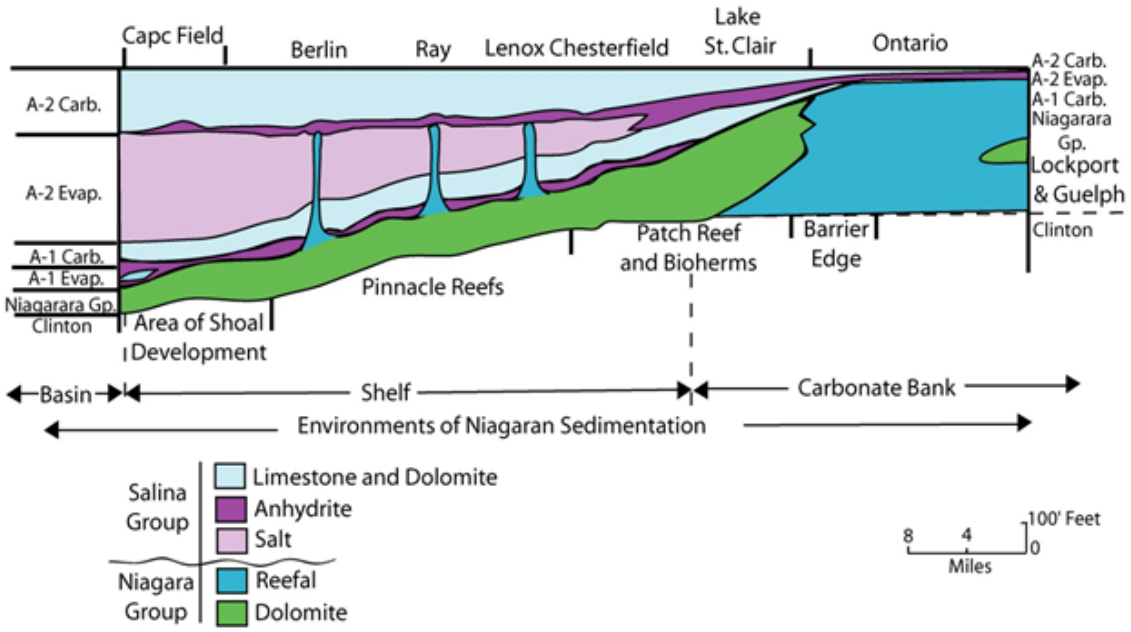

Figure 1.6. Schematic cross section extending from the shelf edge into the center of the Michigan Basin during Silurian time. Modified from Burgess and Benson (1969).

Previous studies (Ells, 1967; Mesolella, 1974) concluded that deposition of Niagaran rocks occurred in three major depositional environments. The first depositional environment is a shallow, laterally extensive carbonate bank which extends as a circular belt around the outermost edge of the Michigan Basin (see Fig. 1.5). These strata occur in a belt 15 to 20 miles (24-32 km) wide in the north and 50 miles (80 km) wide in the south. This carbonate bank or barrier reef environment was composed of a variety of shallow-water carbonate facies including patch reefs, back-reef lagoonal deposits, and fore-reef mudstone and grainstone deposits (Mesolella, 1974). The second depositional environment is the gently sloping ramp where the Silurian pinnacle reef complexes developed. These are commonly referred to as "pinnacle reefs" because their reef flanks have been observed to slope from 30 to 45 degrees, and therefore have been depicted as tall, narrow structures. Previous studies have generally depicted Michigan pinnacle reefs as having symmetrical and random facies distributions. However, I contend here that

previous characterizations are based on poor well control in an individual field, and that facies distributions are asymmetrical and predictable. The third depositional setting is the deep basin center where little to no carbonate sediment accumulated during Niagaran time. Ells (1967) attributed the various reef geometries observed on the carbonate bank and pinnacle reef ramp to varying rates of tectonic subsidence, with the greatest rates of subsidence towards the basin center and slower rates at the basin edges. Subsidence-controlled reef geometry agrees with basin-centered subsidence model for the Silurian by Howell and van der Pluijm (1999).

The Silurian pinnacle reef models of Gill (1973) and Huh (1973) were developed using core materials and petrographic thin sections. These authors, and others (Balogh, 1981; Charbonneau, 1990; Briggs, 1974; Mesollela, 1974), subdivided each reef complex into three and occasionally four distinct growth stages; the Biohermal Stage, Organic Reef Stage, Supratidal Island Stage, and Tidal Flat Stage (see Fig. 1.7). The present study builds on this genetic model using a much higher density of cores and wire-line logs.

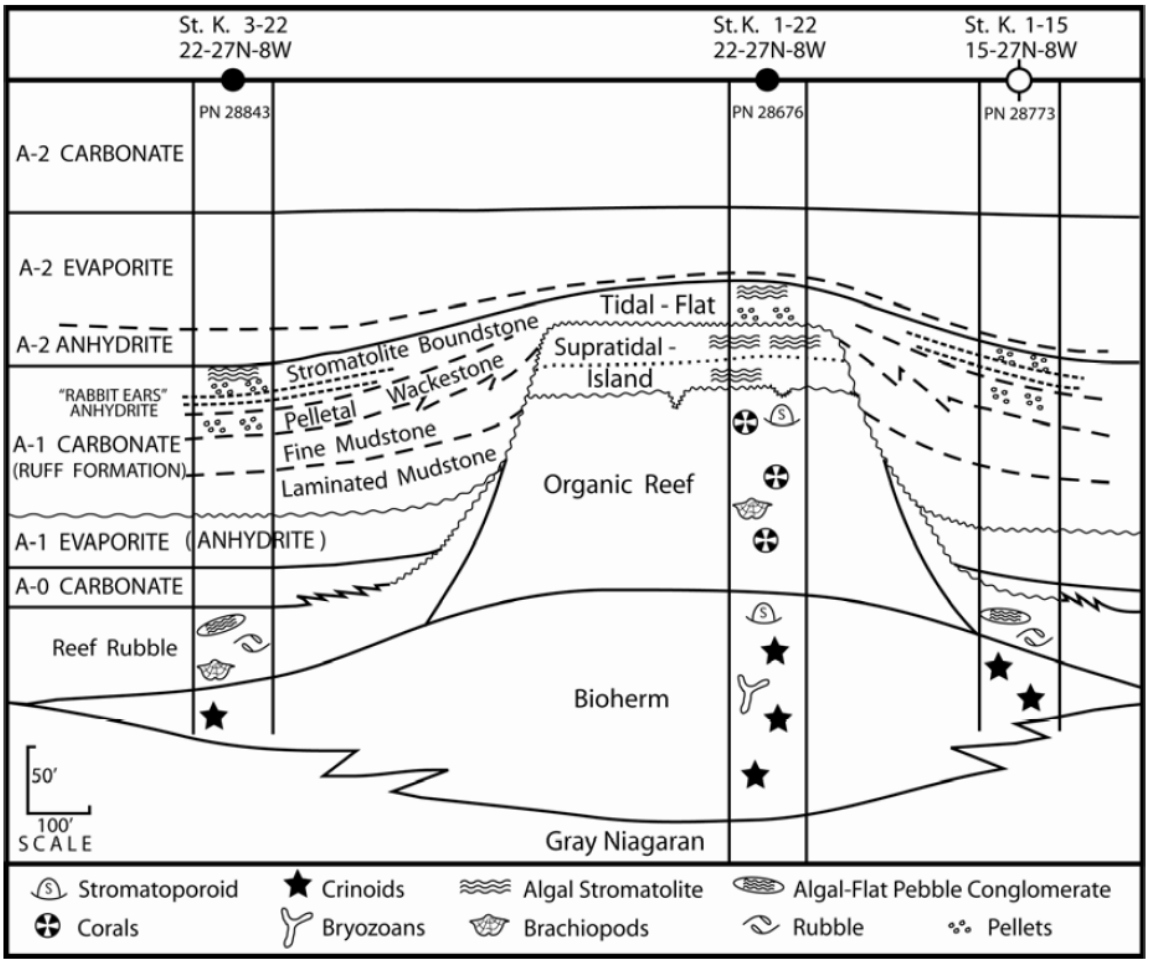

Figure 1.7. Vertically exaggerated model of the Kalkaska 21 reef complex in the Northern Pinnacle Reef Trend from Ritter (2008) as modified from Huh (1973).

The depositional model by Huh (1973) suggests that the portion of the reef complex that belongs to the Guelph Formation evolved in two stages: 1) the initial biohermal stage, and 2) a subsequent organic reef stage. The organic reef stage was followed by a period of subaerial exposure and later capped by the algal stromatolite stage (Salina Group) atop the reef crest (Huh, 1973). The timing and duration of this unconformity is a major source of controversy amongst published depositional models and will be discussed later.

The carbonate mud-rich biohermal strata are inferred to have been deposited

below storm wave-base in a low energy environment and represent the beginning of the stabilization period preceding reef growth (Gill, 1973; Huh, 1973). Gill (1973) subdivided the bioherm into three principle depositional facies: skeletal wackestone, biohermal core, and skeletal-lithoclastic packstone. These facies are differentiated based on relative abundance and size of fossil biota in relation to carbonate mud (Dunham, 1962), and the proportions of intraclasts. These biohermal facies always lie stratigraphically below the organic reef but a gradational transition between the two units typically occurs (Gill, 1973; Huh, 1973). This transition to organic reef growth is marked by changes in faunal assemblage, more grain-rich lithofacies and occasional hardgrounds. The bioherm biota existed in low energy conditions and were transitional to a new community of organisms adaptable to the high energy and turbulent, wave-influenced conditions necessary for organic reef growth (Gill, 1973; Huh, 1973).

The organic reef stage described by Gill (1973) and Huh (1973) consists of four main depositional facies consisting of carbonate sediment components dominated by: (i) in-place skeletons of reef-builders/framework organisms, (ii) grainy reef detritus, (iii) skeletal reef dwellers, and (iv) pelletal mudstone. Typically, the contribution of reef dwellers and reef builders is expressed by the relative amounts of skeletal materials by the different faunal groups inhabiting the reef environment. The primary framework building organisms (reef builders) that inhabited the reef core are stomatoporoids, tabulate corals, bryozoans, and algae. While the organic reef core and bioherm facies can constitute hundreds of feet of any vertical section in core, it is important to note that on average less than 30 percent of the reef core is represented by frame-builders in growth position (Gill, 1973; Huh, 1973). The majority of the growth stage is interstratified with deposits of coarse-grained skeletal wackestone (reef dwellers), which consist of fragments of organisms comprising principally crinoids, bryozoans, rugose corals, small colonial tabulate corals, and brachiopods (Gill, 1973). Shaver (1974) attributed increasing species diversity, increased organic productivity, and a higher abundance of

skeletal material near the margin of the Silurian reef outcrops in Northern Indiana (Wabash Platform) to increased environmental complexity as the reef crest approached sea level.

Organic reef deposits are capped by caliche, vadose, and shallow peritidal deposits providing strong evidence of subaerial exposure. These caliche and vadose deposits exist mostly in the upper 20 to 30 feet (6 to 9 m) of reef core/bioherm successions. Reef rubble conglomerate is present in successions adjacent to reef core areas at the base of the reef slope. Huh (1973) identified a distinct internal stratification of this reef rubble conglomerate in the Kalkaska 21 Reef Complex. He noted that the lower part of the reef rubble conglomerate is represented by intraclastic rubble shed from the active reef core during the organic reef growth stage due to turbulent water conditions and down-slope movement of sediment. In contrast, the upper part of reef rubble-dominated successions comprises distinct lithoclastic material composed of laminated caliche crusts eroded from caliche deposits that capped the reef during subaerial exposure of the reef core (Huh, 1973).

Cyanobacterial stromatolites, lithoclastic breccias, and burrowed, pelletal mudstones, which formed under peritidal conditions, overlie the exposure surface on the reef crest and represent the stromatolitic cap stage of the Salina Group (Gill, 1973). The cyanobacterial stromatolites are indicative of an intertidal to supratidal environment whereas the burrowed mudstone represents short phases of submergence to shallow subtidal conditions (Gill, 1973). The flat-pebble lithoclastic breccias are interpreted as gently reworked, partially lithified cyanobacterial stromatolite mats that were eroded during exposure. The absence of normal marine organisms and the abundance of cyanobacterial laminations and fecal pellets are further evidence that marine waters during Salina deposition were restricted and hypersaline. Evidence for normal marine conditions during Salina deposition is not observed within the Michigan Basin.

The reef complex growth stages are well documented and are for the most part in

agreement. One point of contention is the placement and nature of unconformities between stages. Huh (1973) worked on Northern trend reefs and recognized two unconformities bounding the supratidal stage with a possible third unconformity in the middle. This is contradicted by Gill (1973) and others who have developed their reef growth models based on different reefs located around the basin.

Models for Pinnacle Reef Growth

Three contrasting depositional models for pinnacle reef development are presented in Mesolella et al. (1975), entitled "reef-evaporite controversy" of the Michigan Basin. The main point of disagreement is whether the upper parts of pinnacle reef complexes are Niagaran or Cayugan (Salina) in age. The first model (see Fig. 1.8), supported by Gill (1975), Briggs (1978), and Balogh (1981), suggests that the entire pinnacle reef sequence (from the crinoidal bioherm at the base, to the top of the stromatolitic cap at the crest in the reef crest sections) is of Niagaran age and was completely deposited prior to the A-1 Evaporite of the Salina Group and the A-1 Carbonate. This model also places the Niagara-Salina contact on the reef complex crest at the base of the A-2 Evaporite, which directly overlies the stromatolitic cap. Proponents of this model contend that the observed shallowing-upward faunal succession in the reef section (crinoidal to coral to cyanobacterial) reflects normal marine salinities. Normal marine conditions, it is argued, are followed by increasing salinity during late Niagaran time, which culminated in deposition of the A-1 Evaporite in the center of the basin and around the reef margins.

The second reef model suggests that there was contemporaneous deposition of thick anhydrite and halite deposits occurring in deeper interreef areas during pinnacle reef growth (see Fig. 1.9). The strongest proponent of this model was Jodry (1969) who suggested that "the reefs never stood more than a few feet or tens of feet above the

surrounding sediments." Felber (1964) argued that deposition of the A-1 Anhydrite was contemporaneous with growth of the upper algal biostrome in the reef (thus implying that the A-1 unit was deposited in deep water). Biostratigraphic data show that the A-1 Carbonate of the Salina Group is latest Ludlow and Pridoli in age, whereas the coral-bearing zones of the reefs date as Wenlock or older (Berry and Boucot, 1970). These data disqualify the second depositional model, but, do not disprove the first or third models.

The third model is supported by the work of Huh (1973), Sharma (1966), Mesolella (1975), Sears and Lucia (1979), and Shaver (1974). This model suggests that there were two or three distinct stratigraphic discontinuity-bounded episodes of carbonate deposition on the crest of the pinnacle reef complexes (see Fig. 1.10). This model proposes that during Wenlockian time, a massive stromatoporoid barrier-reef complex existed along the margins of the basin while stromatoporoid/coral-built, pinnacle reefs were growing basinward along the shelf. Deposition of the A-1 Evaporite occurred following a sea level drawdown and the development of exposure surfaces on the reef core prior to sea-level rise during early Cayugan. Once sea level over-topped the crest of the exposed Wenlock pinnacle reefs, sedimentation was re-initiated on the reef tops with restricted marine, evaporite-prone, predominantly algal stromatolite accumulations. Rejuvenation of reef complex growth is represented by a "tidal flat stage" marking the end of reef complex growth prior to A-2 Evaporite deposition (Huh, 1973). This model suggests that the restricted tidal flat carbonate strata in the upper parts of pinnacle reef complexes are stratigraphically equivalent to the A-1 Carbonate. The major difference between these models is that the third one accounts for at least one significant phase of subaerial exposure during the evolution of the entire Niagara- lower Salina reef complex. This model is also unique in that it describes *quasi-contemporaneous deposition* in which two distinct depositional settings; one carbonate-dominated and the other evaporite-dominated, were nearly contemporaneous but not strictly synchronous (Mesolella, 1974).

This model allows for the upper parts of the pinnacle reef complexes (including the stromatolitic cap) to be Cayugan in age, but not necessarily age-equivalent to the Cayugan evaporites.

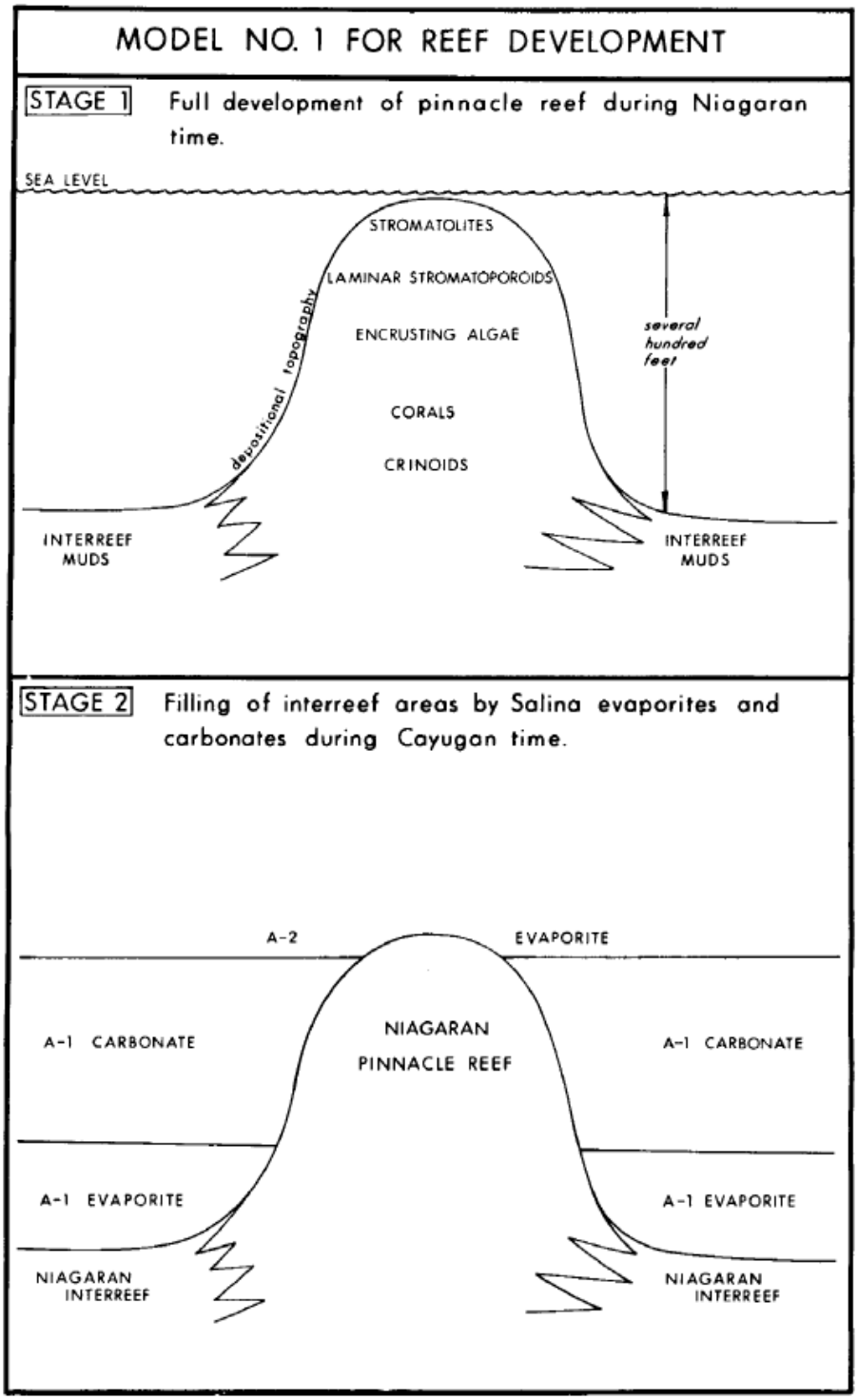

Figure 1.8. Depositional model 1 for pinnacle reef development (Mesolella, 1974).

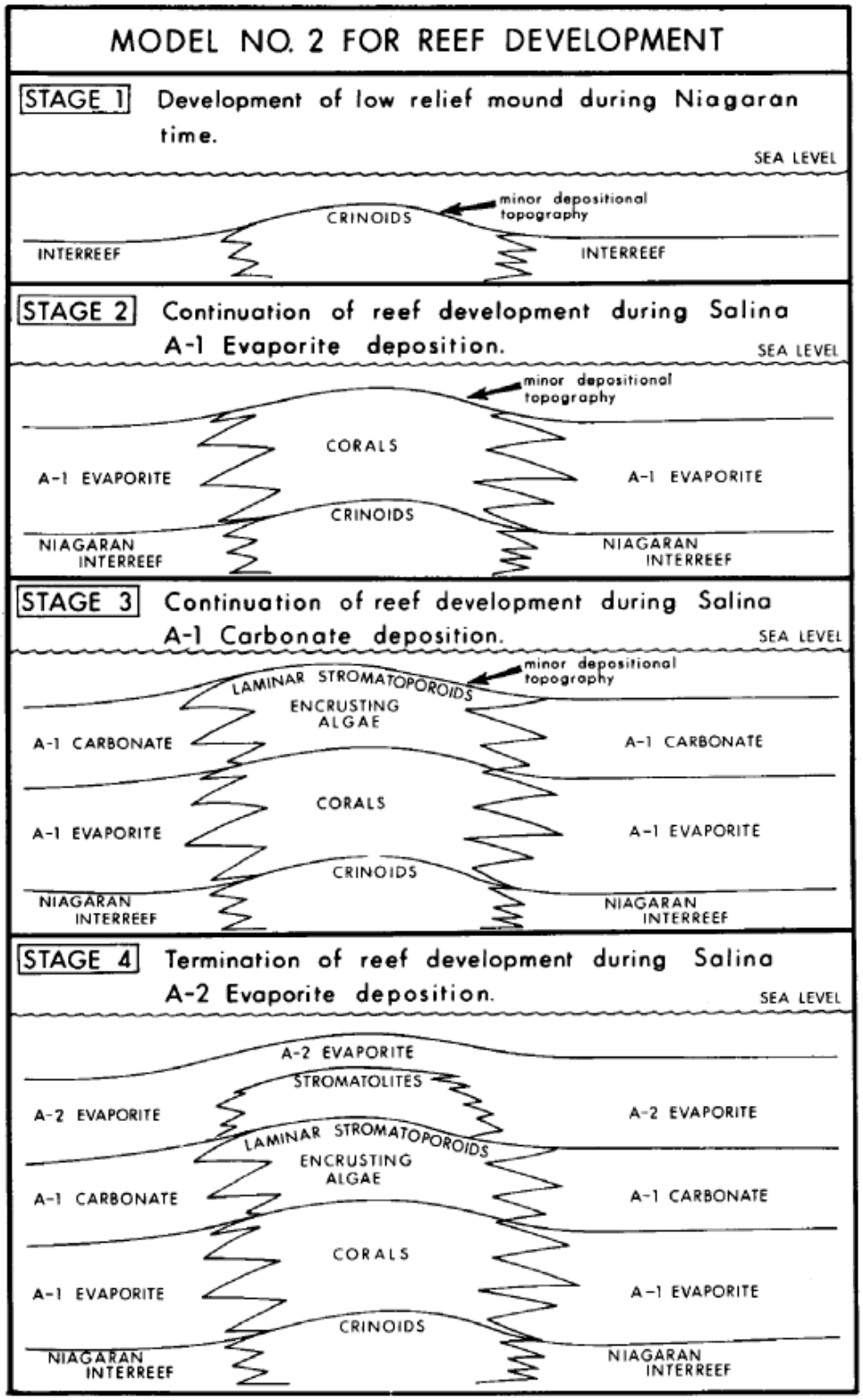

Figure 1.9. Depositional model 2 for pinnacle reef development (Mesolella, 1974).

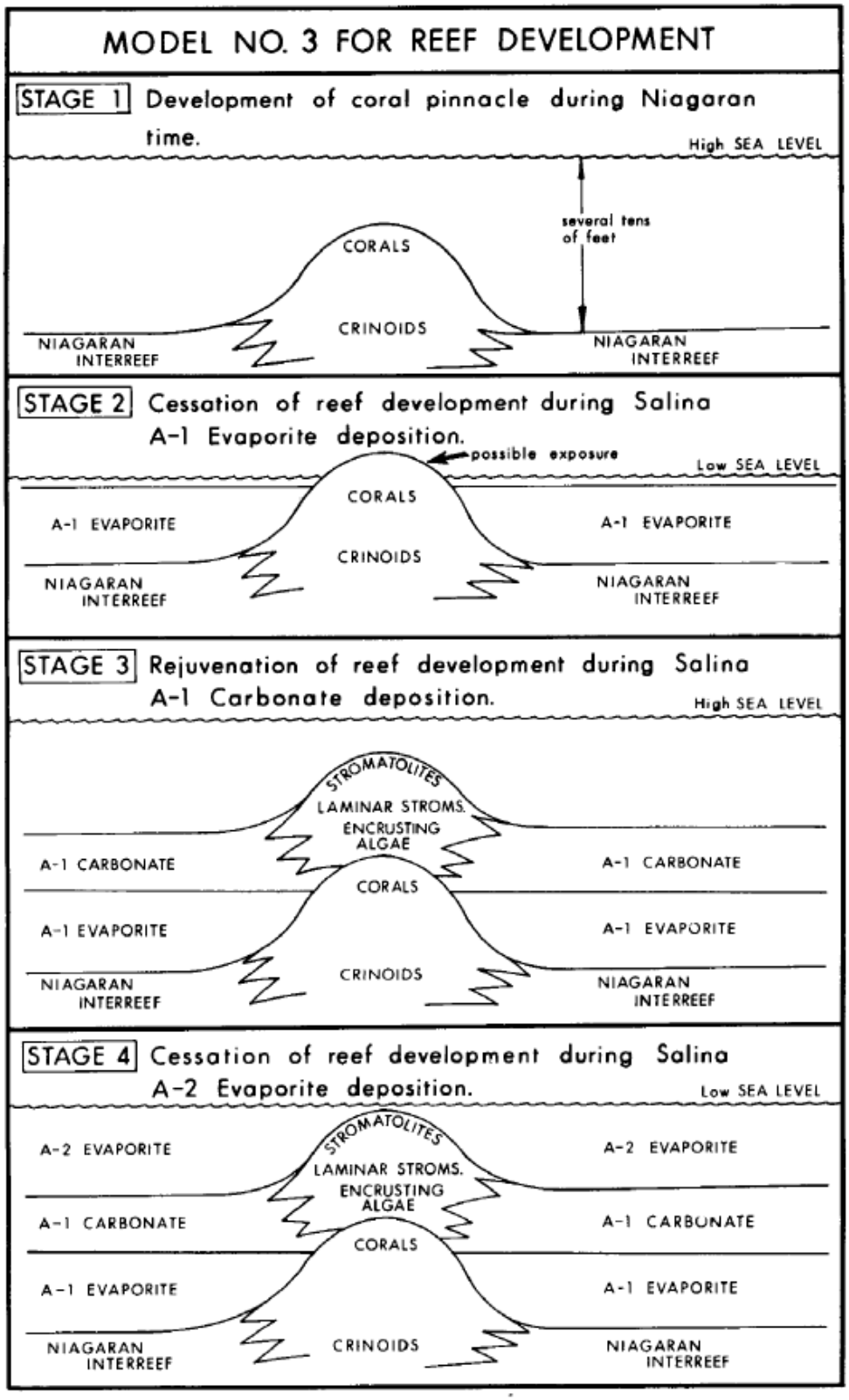

Figure 1.10. Depositional model 3 for pinnacle reef development (Mesolella, 1974).

Recent studies (Noack, 2008; Ritter, 2008; Wold, 2008; and Qualman, 2009) have investigated the magnitude and positions of these major unconformities, but no single model is yet unequivocally confirmed. The current study will attempt to clarify some of the conflicts between these models using stratigraphic relationships observed in the Columbus III Field in southeastern Michigan.

Silurian Sea Level

The Silurian is marked by seven 30+ meter, third order eustatic sea-level fluctuations each occurring over 1-3 million years (Ross and Ross, 1996, see Fig. 1.11). These third-order scale sea level fluctuations are thought to be superimposed on a large second-order rise and fall that covered the entire Silurian Period (Ross and Ross, 1996). The sea level curves created by Ross and Ross (1996) were the result of a combination of biostratigraphic and lithostratigraphic studies from the Illinois, Appalachian, and Estonian Basins. Contradicting Silurian sea level curves have been compared to the Ross and Ross (1996) curve to identify major discrepancies (see Fig. 1.12). The curve produced by Haq and Shutter (2008) was determined using sequence stratigraphy and includes 15 eustatic sea level high stands with fluctuations up to 140 meters. Disagreement with Haq and Shutter's (2008) methodology of using current offlap break points to reconstruct relative sea level resulted in the use of Ross and Ross' (1996) eustatic curve for comparison in this study.

Although the curve of Ross and Ross (1996) has minor disagreements with the Haq and Shutter (2008) curve, it is very similar to that of Johnson's (2010) curve, whose research strategy placed a premium on biological fabric from carbonate deposits rich in brachiopods, corals, stromatoporoids, bryozoans, trilobites, and others. The agreement between the Ross and Ross (1996) curve and the Johnson (2010) curve was justification

for using these curves for later comparison of Silurian sea level fluctuations interpreted in this study for the Michigan Basin.

The other two Silurian sea level curves used for comparison were that of Shaver (1996) and Spengler and Read (2010; see Fig. 1.12). Shaver (1996), who studied the Silurian reef-outcrops in northern Indiana and western Ohio, also attempted to re-create relative sea level curves for the Great Lakes Region. Spengler and Read (2010) used a combination of biostratigraphy and lithostratigraphy to perform a high-resolution sequence stratigraphic study of the Silurian Wabash Platform, directly southwest of the Michigan Basin. The Spengler and Read (2010) curve is also in very close agreement to that of Ross and Ross (1996) and Johnson (2010).

The majority of vertical growth in Michigan Basin pinnacle reefs occurred during Wenlockian time, a geological time period during which there appears to be one or two, third order-scale-eustatic sea level changes based on the Ross and Ross (1996) curve (see Fig. 1.11). The major controversy of the previously described reef growth models is where these third order sequence boundaries are observed in the reefs and surrounding strata. This study uses evidence presented in previous studies to resolve the locations and magnitudes of these boundaries to better identify genetically related packages.

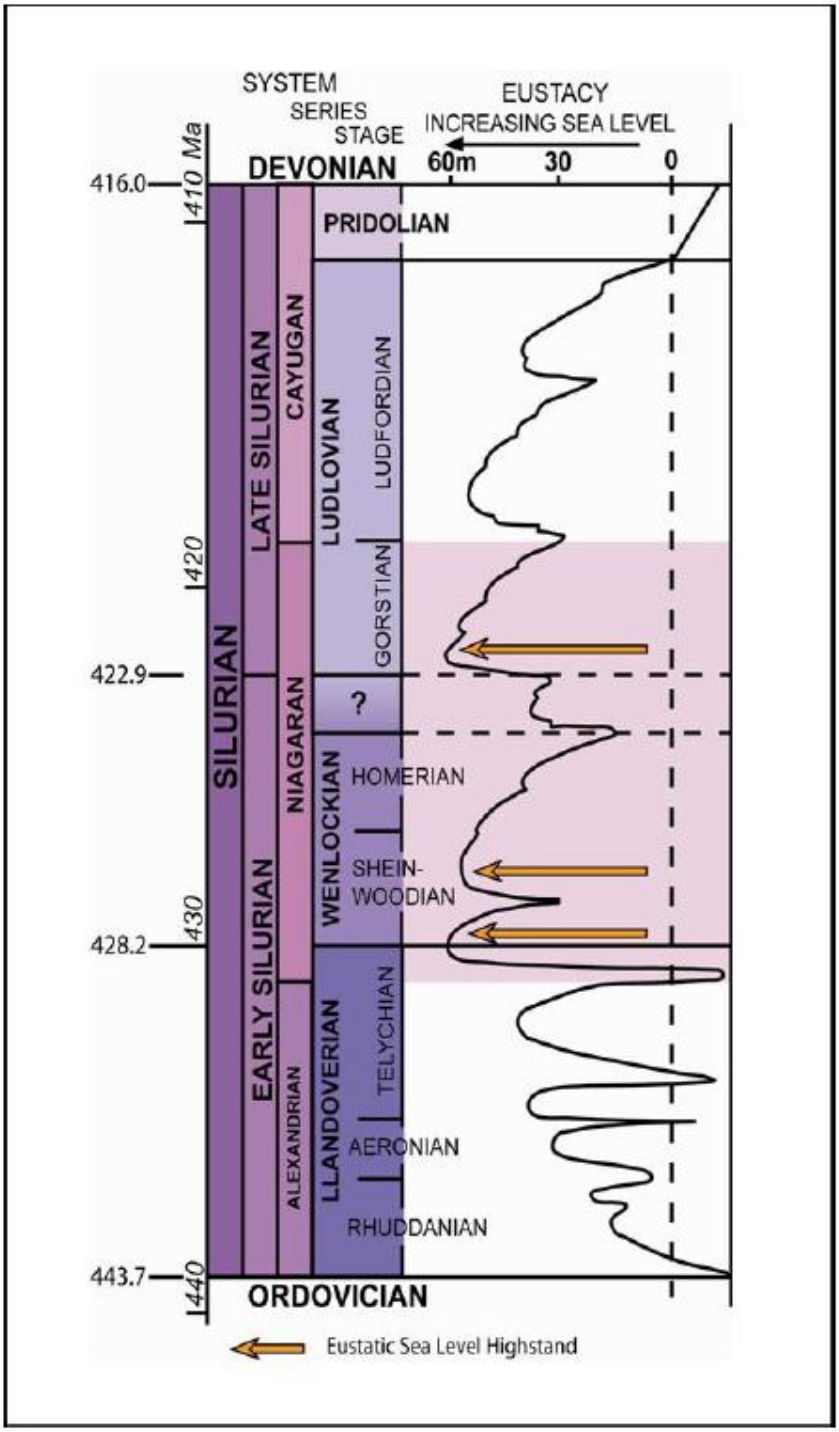

Figure 1.11. Seven 3rd order eustatic sea level fluctuations interpreted for the Silurian. Sea level high stands from the Sheinwoodian to Gorstian are identified with arrows. Figure from Ritter (2008) as modified from Ross and Ross (1996).

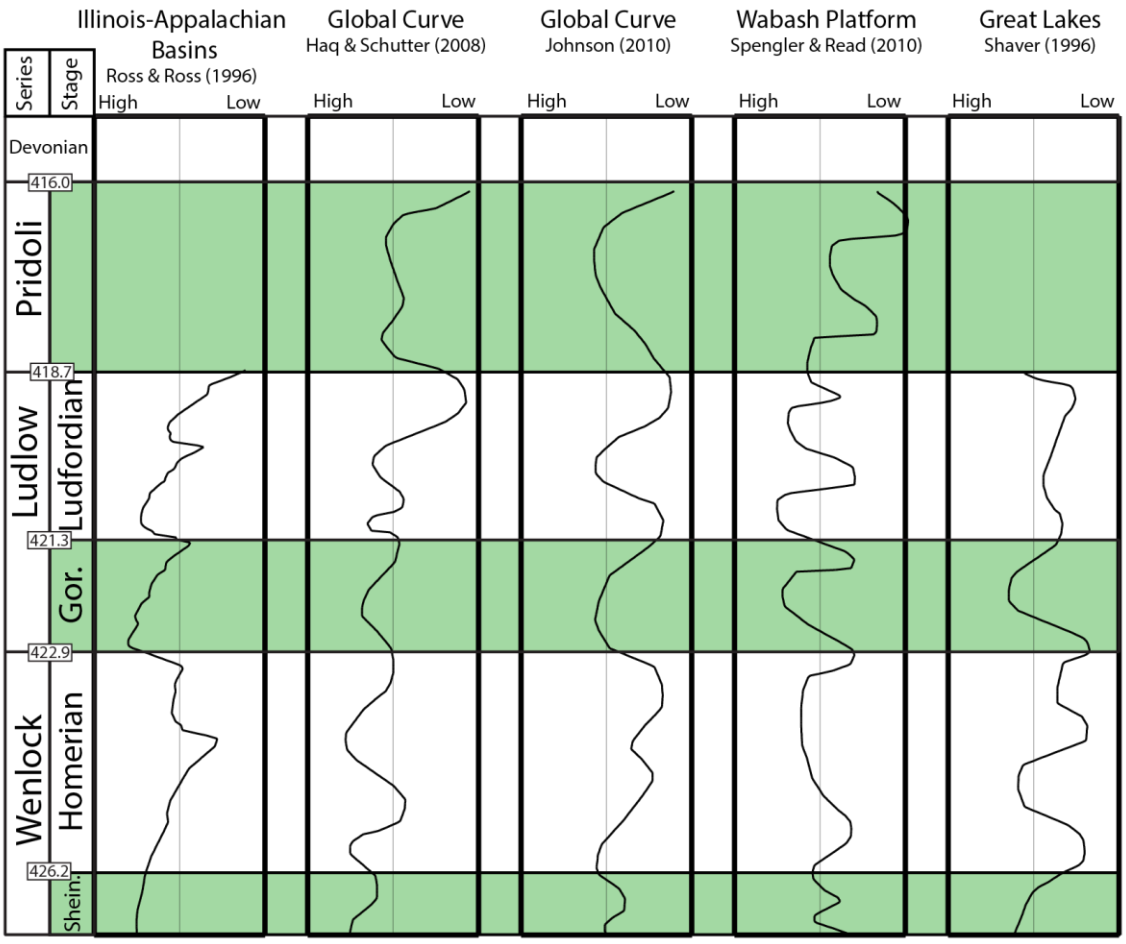

Figure 1.12. Compilation of global and regional sea level reconstructions for the middle to upper Silurian. Data from Ross and Ross (1996), Haq and Schutter (2008), Johnson (2010), Spengler and Read (2010), and Shaver (1996).

Oil and Gas Significance

Study of the Michigan Basin Silurian reefs and evaporites was launched in the early 1950's as hydrocarbon exploration accelerated in southeast Michigan. Initial exploration led to the discovery of hundreds of reefs in the southern trend by the 1960's. In 1961, two of the largest reef discoveries in southeast Michigan (Belle River Mills Field and Ray Field) were found using gravity techniques which relied on the density

contrast between the carbonate reefs and their encasing evaporites. Gravity studies were successful in the southern trend because pinnacle reefs occur at shallow depths (less than 3,500 feet [1,067 m], compared to reefs in the northern trend, all currently at depths greater than 3,500 feet [1,067 m] below the surface). The evolution of seismic reflection technology as well as a better understanding of the Michigan Basin further resulted in oil and gas exploration success in the northern Niagaran Pinnacle Reef trend.

An extensive program of hydrocarbon exploration began in 1967 along the northern trend of the Michigan Basin and it was a successful petroleum producing area by 1969. Prior to 1969, commercial production of hydrocarbons was limited to one producing well (the Hamlin pool) in Mason County (Mesolella, 1974). This changed in 1969, with the effective use of seismic reflection techniques, which led to the drilling of three test wells, all of which produced commercial quantities of petroleum. To date, the combined northern and southern reefs have produced over 500 million barrels of oil and 2.9 trillion cubic feet of natural gas (State of Michigan production records, 2015).

One major conundrum pertaining to pinnacle reef production is the distribution of dolomite versus limestone within the reservoirs. Although thorough observations have been made of reefs composed entirely of dolomite, some entirely of limestone, and others of inter-bedded dolomite and limestone, the controls on dolomitization are still poorly understood. Reef reservoirs composed mostly of dolomite have been far more productive than those composed solely of limestone, and reefs that are inter-bedded limestone and dolomite produce the majority of hydrocarbons from dolomitic intervals. This is an important observation when evaluating the distribution and quality of reservoirs in individual reef complex fields.

Although the majority of the pinnacle reef fields in the Michigan Basin are thought to be discovered, there is still great potential for secondary/enhanced oil recovery. The average primary recovery of reef reservoirs is 26% and the average secondary recovery is about 12.5% with only about 5% of the fields in basin having undergone anything past primary recovery (State of Michigan production records, 2015). It is estimated that as much as 180 to 200 million additional barrels of incremental oil may be economically recoverable using enhanced oil recovery techniques (State of Michigan production records, 2015). Due to the compartmentalized nature of these reefs, they are also currently used for both cyclic gas injection-withdrawal and carbon dioxide enhanced oil recovery programs. The Columbus III reef field in southeast Michigan is an example of a gas storage field used in this study. The majority of gas storage fields currently exist in southeastern Michigan while the CO_2 EOR programs exist along the northern trend in Otsego County.

Columbus III Field

The Columbus III Field is located in St. Clair County, Michigan, along the southern pinnacle reef trend in the Michigan Basin (Fig. 1.13). The field was first discovered in December, 1968, by Sun Oil Corporation with the completion of the Harold Winn #1 well (permit #27465). Extensive development drilling followed and the field has had a total of 114 boreholes (89 vertical and 25 horizontal) completed to date. Initial estimates of stock tank oil-initially-in-place (STOIIP) for the field ranged from 11,000,000 to 15,000,000 barrels of oil (bbls), but recent volume calculations performed for the purpose of this study estimate somewhere between 22,000,000 to 27,000,000 bbls.

To date, the field has produced about 8,500,000 bbls of oil, which is about 31-39% of the original oil in place estimated in this study.

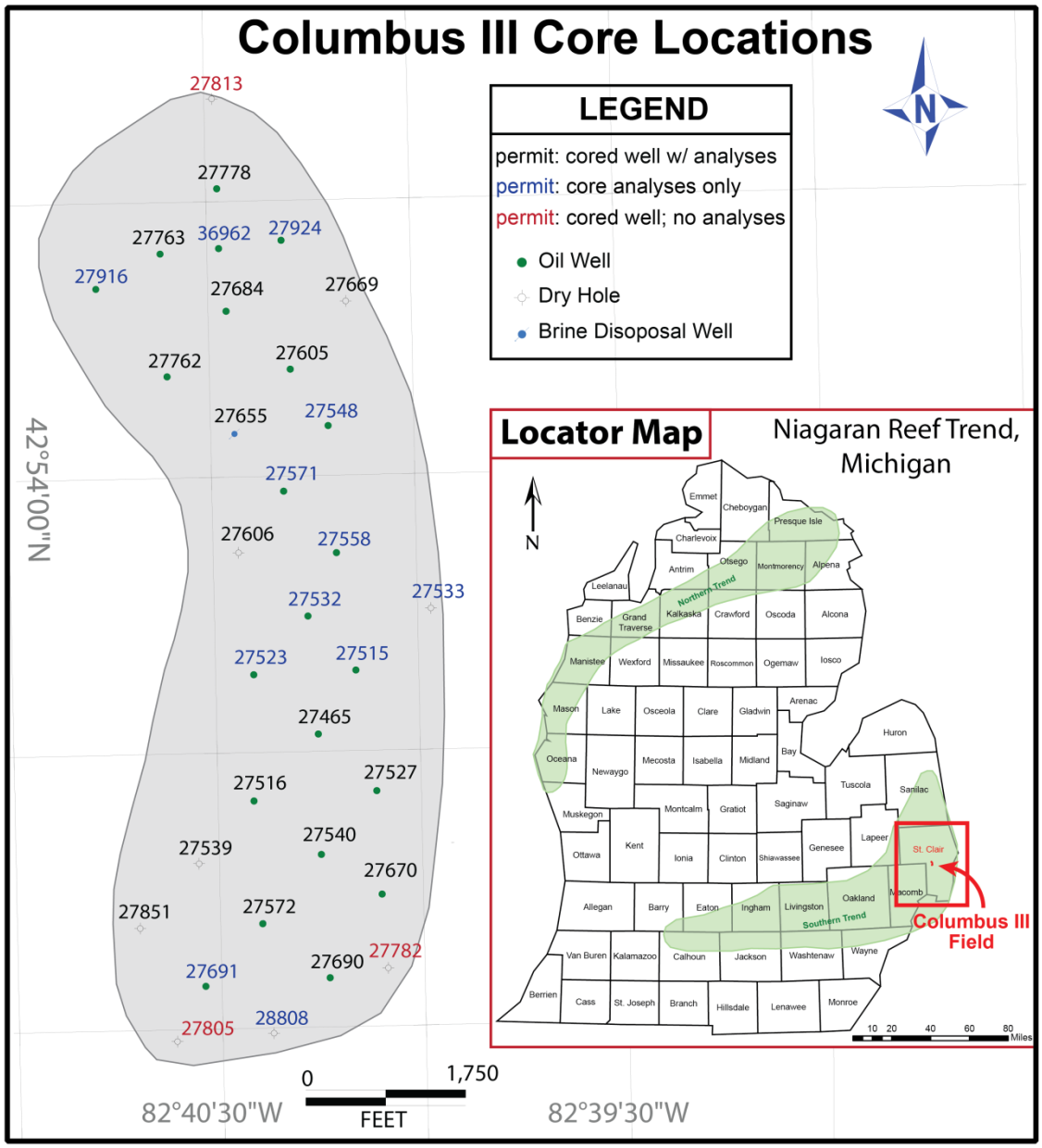

Figure 1.13. Map of Columbus III Field showing the location of cored wells and core analyses wells in proximity to the reef. The gray outline marks the transition from reef flank to regional inter-reef deposits. The Columbus III Field is located in St. Clair County, Michigan, within the Southern Niagaran Reef Trend belt.

After primary production began in 1969, secondary recovery efforts followed in September, 1974, with the re-injection of gas and water. These enhanced oil recovery techniques continued until 2004 when the field was converted to gas storage. Prior to this conversion, the field had only one gas injection well which was injecting relatively small amounts of gas each year (16,500 cubic feet of gas in 2004). By 2006, the field had 14 gas injections wells and was injecting and withdrawing upwards of 30,000,000 cubic feet of natural gas per year. Management of a complicated reservoir system such as this has a strong need for a static earth model, which in-turn can be used for dynamic fluid-flow modeling.

One of the main reasons that the Columbus III field was an excellent candidate for geological modeling was the abundance of whole core and geophysical log data. Of the 89 vertical wells drilled (114 total; 25 horizontal), a total of 32 wells recovered whole core, with conventional, whole core analyses conducted on 29 of those cores. Twenty of the 32 cores were available for observation at the Michigan Geological Repository for Research and Education (MGRRE) at Western Michigan University, with all 29 of the core analyses reports available for use. In terms of cored well position within the reef complex, 11 wells represent reef crest to reef apron and 9 are located on reef flank positions. Additionally, 72 of the 114 wells have geophysical logs that were used in the analysis. Permit files, deviation surveys, and production history data were also used as ancillary data in this study.

CHAPTER II

DATA AND METHODS

Core Description and Interpretation

Core material was analyzed and described using a hand-lens and 10X magnification binocular microscope. Attributes that were recorded include lithology, dolomite crystal size, pore types and distribution (rock fabric), fossil content, sedimentary structures, and stratigraphic surfaces. Diagenetic features that were noted include fracturing, dissolution, oil staining, and salt plugging. Some of this information, such as dolomite crystal size, was primarily obtained using thin sections. Dilute (5%) hydrochloric acid (HCl) was used in combination with geophysical log signatures (discussed later) to discriminate limestone ($CaCO_3$), which reacts more vigorously with HCl, than dolomite ($MgCa(CO_3)_2$).

The Dunham (1962) limestone classification scheme was used to classify depositional textures described in this study. This carbonate classification emphasizes texture, mud-content, and grain packing, which is typically related to degree of hydrodynamic activity and the environment of deposition. Depositional facies are obscured by intense dolomitization in all of the study cores, which resulted in at least partial destruction of original depositional fabrics and pore types. Where original depositional textures could not be identified in both hand sample and thin section due to intense dolomitization, rock types were identified as crystalline dolomites. Depositional facies descriptions were aided by previous studies of Niagaran reefs in both the northern and southern trends by Huh (1973), Gill (1973), and Budros (1974).

Conventional Whole Core Analysis

Conventional whole core analysis data was available for the 20 cores examined

for this study, as well as 9 additional cores that do not reside at MGRRE (see Fig. 2.1). The full diameter conventional whole core analysis data used for this study are limited to porosity and horizontal permeability. Data in the report included depth of sample, total core thickness analyzed, horizontal and vertical permeability, porosity, fluid saturations (oil and water), bulk density, and grain density. Air permeability was measured in the laboratory using the Hasseler Sleeve method[1]. Two horizontal measurements are taken at 90 degrees from each other and are represented as maximum permeability and permeability 90 degrees from maximum. Porosity was measured in the laboratory using the helium expansion method[2]. The whole core porosity and permeability data were converted into digital log format, with depth as the y-axis and porosity and permeability as the x-axis. These log curves were then imported into IHS Petra and Schlumberger Petrel workstations and used in combination with the other geophysical logs for the construction of cross-sections.

Geophysical Logs

Wire-line log interpretations were used in combination with core material to better identify depositional facies within the reef complex where core data were not available. Depositional facies and diagenetic overprinting (such as salt plugging or dolomitization) were correlated to wire-line log responses using a 3-D sequence stratigraphic framework interpreted from the core. Gamma ray (GR) and neutron

[1] A sample of known length and diameter is encased in an air-tight sleeve in a horizontal position and is injected with a fluid of known viscosity. The pressure drop across the sample and the flow rate are measured and permeability is calculated using the Darcy equation (Lucia, 2007; see Eq. 1).

$$Q = A\left(\frac{k}{\mu}\right)\left(\frac{\Delta P}{L}\right)$$

where Q is rate of flow, k is permeability, μ is fluid viscosity, $(\Delta P)/L$ is the potential drop across a horizontal sample, and A is the cross-sectional area of the sample.

[2] A dried sample is placed in a chamber of known volume and the pressure is measured with and without the sample, keeping the volume of gas constant (Lucia, 2007). The pressure difference then indicates the pore volume.

porosity (SNP) logs were used for the core-to-log correlations. Wire-line logs were also used for structural and stratigraphic cross-sections.

The gamma ray log was essential for identifying depositional facies and sequence stratigraphic boundaries in the non-cored wells in this study. The gamma ray log measures the total combined natural gamma ray radiation of uranium, potassium, and thorium, which differs from that of the spectral gamma ray measurement. Potassium and thorium are concentrated in the minerals that constitute insoluble residue in carbonate rocks, such as windblown silt, silicate rock fragments, and clays. This means that many carbonate facies can be correlated with current energy because the amount of insoluble residue is thought to be inversely proportional to current energy, rate of carbonate production, and siliciclastic input (e.g., carbonate grainstones deposited in high energy environments typically have low gamma ray signatures).

Because of the relatively low concentrations of radioactive material in most carbonates and evaporites (with the exception of Sylvite, KCl), the gamma ray log was displayed on an amplified scale of 0 to 50 API units (conventional display is 0 to 150). This allows for easier identification of smaller amplitude gamma ray log spikes that could be correlated from well to well in many cases. For example, a high gamma ray signature can be observed above the reef crest, which separates two distinct stratigraphic sequences (see Fig. 2.1). Also, a gradual increase in the gamma ray response can be indicative of a shallowing upward carbonate succession (see Fig. 2.1). These gamma ray features cannot be used without reference to core material, but can be very powerful once these log pattern relationships are integrated with core observations.

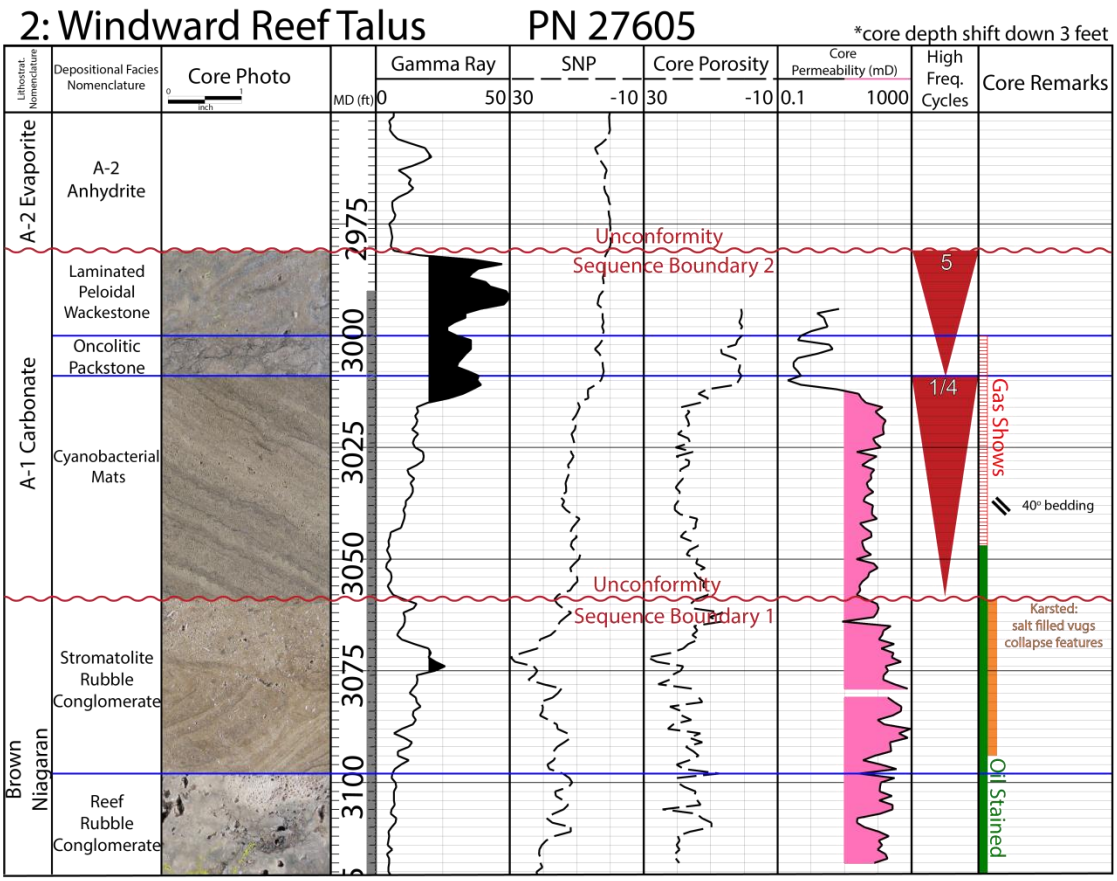

Figure 2.1. Single well cross section template used for well log analysis in this study with representative core photos. Well logs displayed are gamma ray, sidewall neutron porosity, core porosity, and core permeability. Perforated, cored, and salt plugged intervals are labeled. Depositional facies and lithostratigraphic nomenclature are labeled on the left hand tract. High frequency shallowing upward cycles are noted with upside-down red triangles.

The neutron log was available as either neutron count or sidewall neutron porosity. The neutron log measures the hydrogen ion concentration of the formation by measuring the capture of neutrons emitted by a neutron source. The hydrogen index of oil and water is usually assumed to be 1, but, because of its much lower density, gas has a significantly lower concentration of hydrogen and results in a lower neutron reading than expected from water or oil for the same porosity (known as the *gas effect*).

Sequence Stratigraphy and Stratigraphic Hierarchy

Sequence stratigraphy is a method used to determine chronostratigraphic relationships in stratigraphic successions by correlating genetically related units based on interpretations of depositional environments and the location of bounding discontinuities (Embry, 2009). A sequence stratigraphic model developed using available core provides a robust architectural framework for reducing uncertainty in the assignment of depositional facies during the creation of reef growth models of Silurian Michigan reefs. A robust sequence stratigraphic framework also provides an excellent foundation for and cross check of facies analysis and the interpretations of depositional history. Correlation of third and fourth order sequences from the reef crest to their inter-reef strata are facilitated by the sequence stratigraphic model. A sequence stratigraphic analysis consists of: 1) the spatial distribution of vertical sedimentary facies stacking patterns, 2) the recognition and correlation of stratigraphic surfaces that represent changes in depositional trends in the rock record and 3) the description and interpretation of resulting, genetic stratigraphic units bounded by those surfaces (Embry, 2009).

The fundamental components of sequence stratigraphy analysis are the identification of various identifiable surfaces that are bounding units of genetically related strata (Embry, 2009). These surfaces can exist as either material-based, as defined on the basis of observable physical characteristics, or time-based surfaces, as defined by the interpreted change in the direction of shoreline movement from the spatial distribution of vertical successions of sedimentary facies (e.g., landward or seaward movement). The material-based surfaces, as defined by Embry (1995, 2001), that are used for correlation are: 1) subaerial unconformity, 2) regressive surface of marine erosion, 3) shoreline ravinement, 4) maximum regressive surface, 5) maximum flooding surface, and 6) slope onlap surface. Each of these surfaces is characterized by a combination of observable attributes and can be identified in core and correlated to wire-

line logs in this study. The time-based surfaces (or chronostratigraphic surfaces) are defined on the basis of a specified event at an exact location, identifying time synchronous surfaces that punctuate rock successions.

Data Limitations

While core material was abundant in the Columbus III field, there were very few wells with wire-line logs or cores that were drilled in off-reef positions. This made it difficult to determine the lateral limits of certain flank depositional facies. The lack of biostratigraphic age constraints throughout the Niagara and Salina units also made it difficult to determine sequence magnitude in the basin and correlations outside of the basin.

A common problem faced when performing core-log correlations is shifting the core depth to match log depth. Typically the depths scribed on the core boxes are poorly labeled or there is a problem with depths scribed on the core slabs being different from those of the original depth markings. Gamma ray log signatures and core analyses depths (core analysis sample numbers) were the best methods for accurately matching core and log depths.

CHAPTER III

FACIES ANALYSIS

Reef Complex Type Sections

Due to the complex nature of carbonate deposition, depositional facies reflect a combination of biological factors, hydraulic regime, sea-water chemistry, and authigenic processes. Both the spatial and temporal distribution of facies that exist within a Silurian Pinnacle Reef Complex are affected by these major controls. Furthermore, autogenic controls on sediment production and accumulation in the carbonate factory are determined by the rates of subsidence, position of sea level, and depth of the euphotic zone (James et al., 2010). These autogenic controls are recorded in the sediments and help in better understanding the history of both Silurian Pinnacle Reef growth and the Michigan Basin as a whole. Creating a facies model for these ancient, biologically constructed structures is a challenge because reef growth was governed as much by interactions within the evolving biosphere as by universal physical and chemical laws (James and Wood, 2010).

This study aims to establish the importance of the prevailing wind direction and its major influence on the depositional profile and reef complex morphology. As noted earlier, the general paleo-wind direction during the Silurian consisted of southeasterly trade winds across the Michigan Basin, as the Basin was rotated roughly 45 degrees clockwise and located between 20-25° south of the Equator. These prevailing winds resulted in asymmetrical facies deposition on the reef complex (see Fig. 3.2), an observation that has not been accurately portrayed by previous depositional studies due to a lack of core coverage.

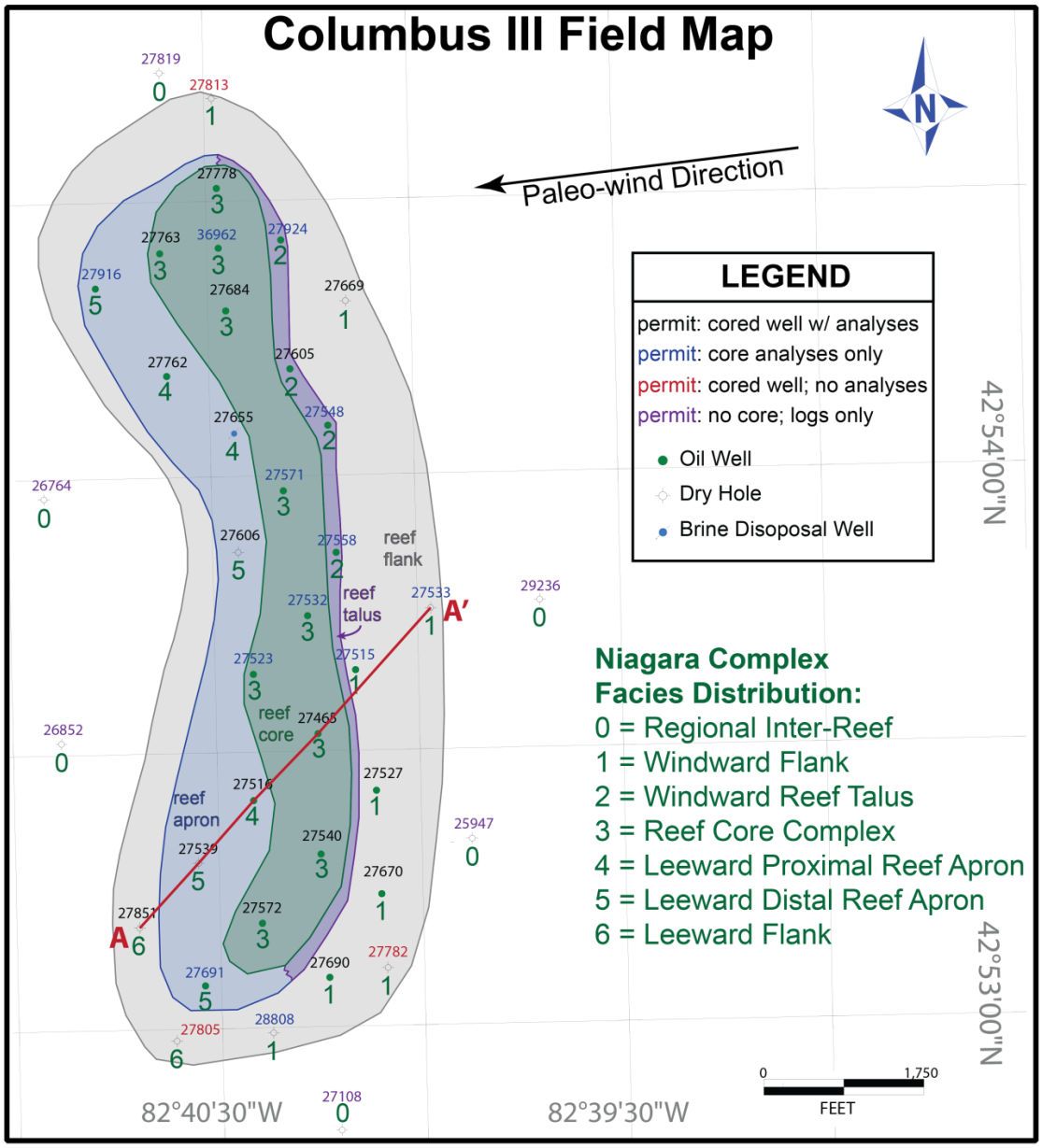

Figure 3.1. A map of the Columbus III field with numbers corresponding to Niagara Complex facies locations. This map is a synoptic time slice of the depositional facies distribution during reef complex growth in the Niagaran, prior to Salina deposition. The green polygon outlines the horizontal extent of reef complex core facies, the blue polygon the extent of the reef apron, the purple polygon the extent of the windward reef talus, and the gray polygon the extent of reef flank facies. The A to A' cross section line represents the cross section in Figure 3.2.

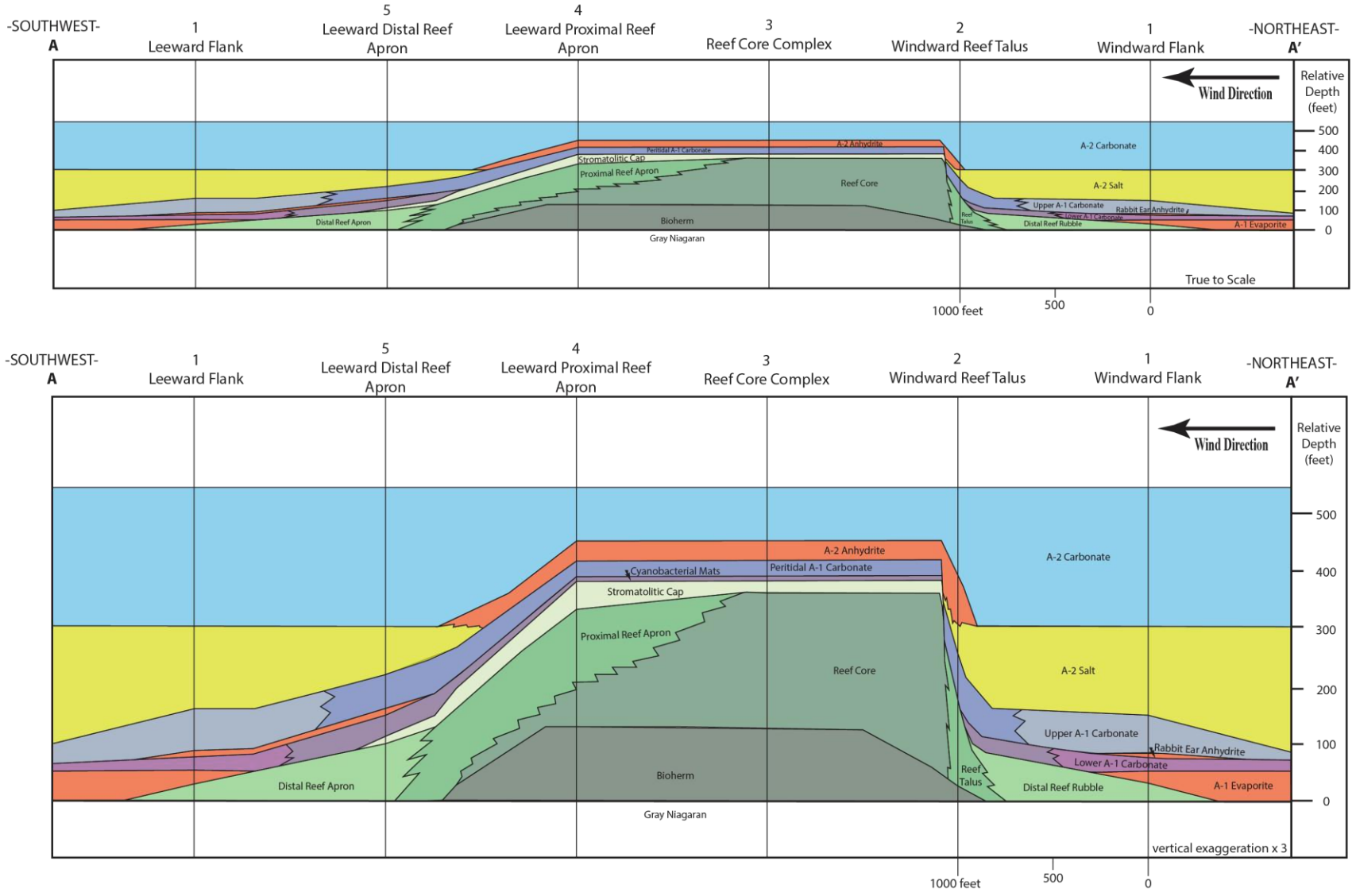
-SOUTHWEST-
A
1
Leeward Flank
5
Leeward Distal Reef Apron
4
Leeward Proximal Reef Apron
3
Reef Core Complex
2
Windward Reef Talus
1
Windward Flank
-NORTHEAST-
A'
Wind Direction
Relative Depth (feet)
500
400
300
200
100
0
A-2 Anhydrite
Peritidal A-1 Carbonate
Stromatolitic Cap
Proximal Reef Apron
Reef Core
A-2 Carbonate
A-2 Salt
Upper A-1 Carbonate
Rabbit Ear Anhydrite
Lower A-1 Carbonate
A-1 Evaporite
Distal Reef Apron
Bioherm
Reef Talus
Distal Reef Rubble
Gray Niagaran
True to Scale
1000 feet
500
0
-SOUTHWEST-
A
1
Leeward Flank
5
Leeward Distal Reef Apron
4
Leeward Proximal Reef Apron
3
Reef Core Complex
2
Windward Reef Talus
1
Windward Flank
-NORTHEAST-
A'
Wind Direction
Relative Depth (feet)
500
400
300
200
100
0
A-2 Anhydrite
Cyanobacterial Mats
Peritidal A-1 Carbonate
Stromatolitic Cap
Proximal Reef Apron
Reef Core
A-2 Carbonate
A-2 Salt
Upper A-1 Carbonate
Rabbit Ear Anhydrite
Lower A-1 Carbonate
A-1 Evaporite
Distal Reef Apron
Bioherm
Reef Talus
Distal Reef Rubble
Gray Niagaran
vertical exaggeration x 3
1000 feet
500
0

Figure 3.2. A true to scale (upper) and 3 to 1 vertically exaggerated (lower) stratigraphic cross-section of the Columbus III reef complex. The cross section is hung on the Gray Niagaran surface, which best represents the paleo-sea-floor during Niagaran time. Facies thicknesses were used from six wells, one at each type section location (1: 27533, 2: 27558, 3: 27465, 4: 27516, 5: 27539, 6: 27851; refer to Figure 3.1 field map for locations).

The main focus of this chapter is the identification of different depositional facies, their stacking patterns, and spatial distributions. In this study, the reef complex was described in 7 distinct major facies types (or type sections), representing sediment accumulation in different positions of the reef complex during Niagaran reef complex growth as a result of the paleo-wind direction and depositional environment (see Fig. 3.1). These facies types will be discussed in general in the paragraph below and then in detail in the following sections. It is important to recognize that the topographic structure, which formed during the Niagara reef complex growth, also controlled subsequent depositional patterns of the overlying Salina units. Therefore, distinct lateral distributions of Salina facies are also observed based on the paleo-topographic structure of the underlying Niagara complex. Aside from the three-dimensional sediment distribution patterns, these type section locations also exhibit distinctly different internal facies stacking architecture.

The reef core itself, consisting of wave-resistant binding reef constituents, exists in a narrow corridor (less than 1,500 feet or 460 m thick), which strikes roughly north to south (see Fig. 3.1, highlighted by green). The reef apron, which consists of carbonate mud and detrital carbonate scree shed mostly on the leeward side of the carbonate reef factory, has a greater areal extent than the reef itself. In the immediate windward direction of the reef core complex exists a very thin (less than 200 feet or 61 m thick) unit referred to as the windward reef talus. Laterally encompassing the reef complex in all directions are windward and leeward flank deposits, which thin in the inter-reef direction. A systematic approach was used by analyzing cores at each type section locality to

further examine the depositional facies, stacking patterns, and their spatial distributions. Depositional facies were determined based on similar depositional environments as well as contemporaneous deposition. Within each depositional facies (e.g. Reef Core), lithofacies were determined based on the Dunham (1962) classification scheme which emphasizes texture, mud-content, and grain packing (e.g. *skeletal wackestone* or *coral/stromatoporoid boundstone*).

Type Section 3: Reef Core Complex

The reef core complex represents the thickest accumulations of carbonate within the basin. The average thickness of the reef complex within the Columbus III field is 400 feet (122 m) from the top of the Gray Niagaran to the base of the A-2 Anhydrite (see Fig. 3.3). The reef complexes are composed of a variety of bounding and baffling fauna, including crinoids, bryozoans, brachiopods, tabulate corals, rugose corals, and stromatoporoids.

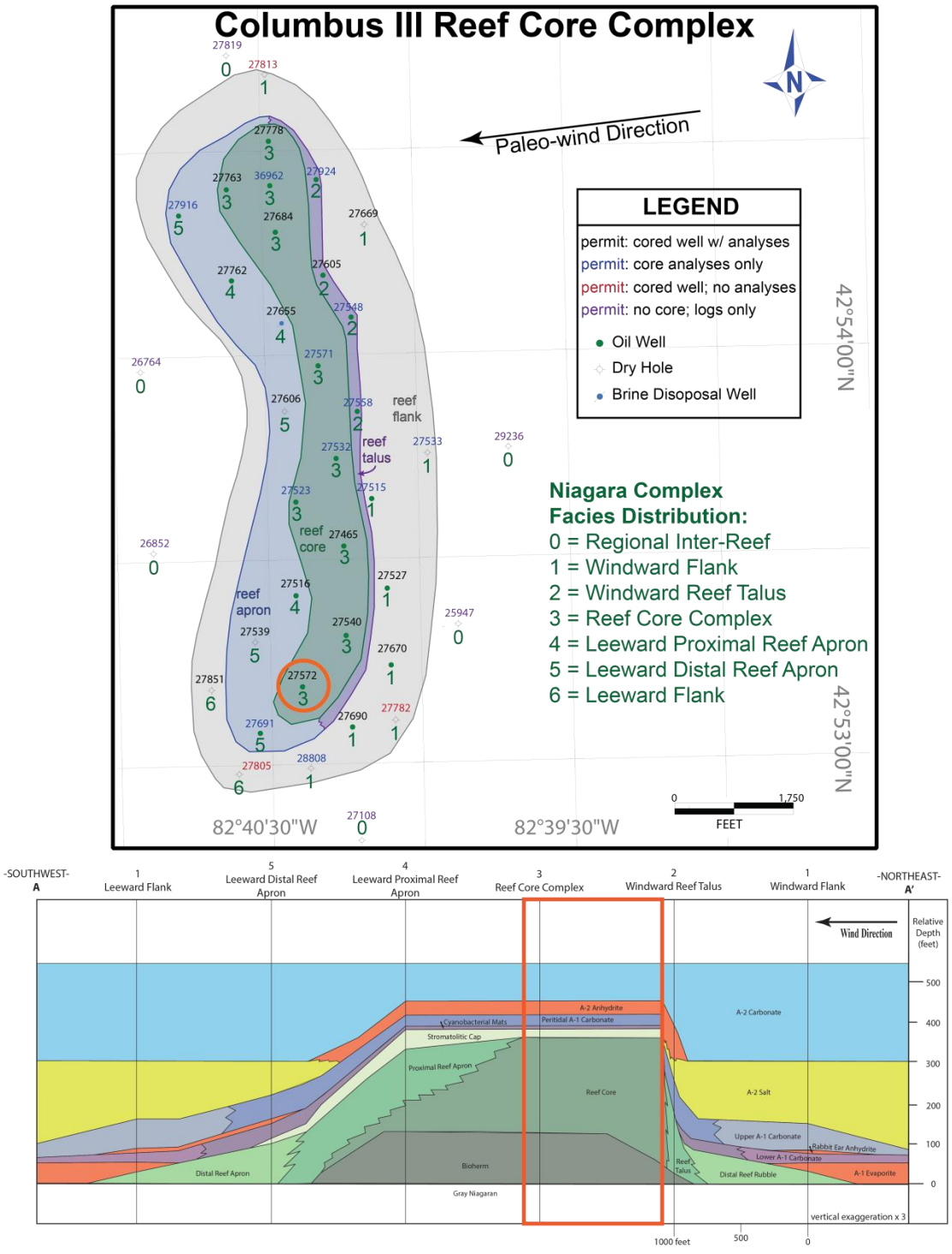

Figure 3.3. The Reef Core Complex type section location highlighted on the Columbus III Field map (upper) and reef complex cross-section (lower).

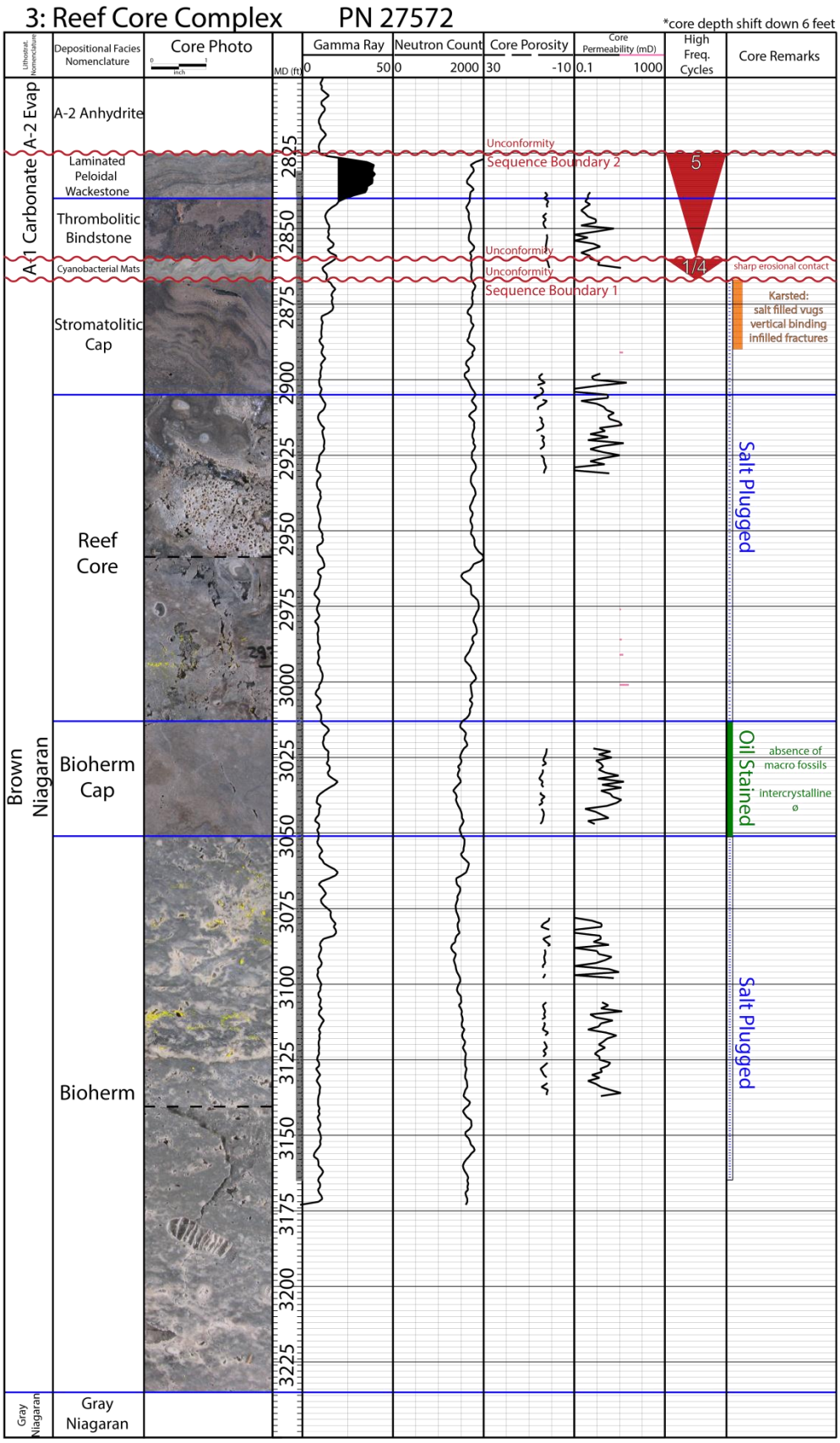
3: Reef Core Complex
PN 27572
*core depth shift down 6 feet
Lithostrat. Nomenclature
Depositional Facies Nomenclature
Core Photo
MD (ft)
Gamma Ray
0
50
Neutron Count
0
2000
Core Porosity
30
-10
Core Permeability (mD)
0.1
1000
High Freq. Cycles
Core Remarks
A-2 Evap
A-2 Anhydrite
A-1 Carbonate
Laminated Peloidal Wackestone
Thrombolitic Bindstone
Cyanobacterial Mats
Stromatolitic Cap
Reef Core
Bioherm Cap
Bioherm
Brown Niagaran
Gray Niagaran
Gray Niagaran
2825
2850
2875
2900
2925
2950
2975
3000
3025
3050
3075
3100
3125
3150
3175
3200
3225
Unconformity
Sequence Boundary 2
Unconformity
Unconformity
Sequence Boundary 1
5
1/4
sharp erosional contact
Karsted:
salt filled vugs
vertical binding
infilled fractures
Salt Plugged
Oil Stained
absence of macro fossils
intercrystalline ø
Salt Plugged

Figure 3.4. A single well cross-section of the 27572 well which illustrates the stack of facies for a reef core complex location within the Niagara-lower Salina reef complex. Displayed on the cross-section is lithostratigraphic nomenclature, depositional facies, core photos, wire-line logs (gamma ray, neutron count), core porosity and permeability data, and oil stained (green), salt plugged (blue), and cored (gray) intervals. Also noted are interpreted 3rd order sequence boundaries, smaller-scale unconformities, and shallowing upward cycles. Core depths were shifted down 6 feet (2 meters) to match wire-line log depths.

The base of the Reef Core Complex type section begins with the Gray Niagaran depositional facies (see Fig. 3.4). The Gray Niagaran is laterally extensive throughout the Michigan Basin and underlies all 7 reef complex type sections. The 27572 core did not penetrate the Gray Niagaran, and therefore was identified in logs from nearby wells due to its distinctive higher gamma ray signature compared to that of the overlying bioherm. Directly overlying the bioherm is the bioherm cap, followed by the reef core. The last depositional facies that belongs to the lithostratigraphic unit of the Brown Niagaran is the stromatolitic cap. A third-order sequence boundary separates the Brown Niagaran sediments from the overlying A-1 Carbonate sediments at this locality and will be further discussed in the reef growth model in the next chapter. The main focus of this chapter is the identification of different depositional facies, their stacking patterns, and spatial distributions.

Overlying the stromatolitic cap is the cyanobacterial mat facies of the A-1 Carbonate, which are separated by an unconformity, interpreted to be a third-order sequence boundary. These cyanobacterial mats are overlain by the thrombolitic bindstone facies, which are also separated by an unconformity, but of unknown magnitude. The thrombolitic bindstone gradationally transitions into the overlying laminated peloidal wackestone. The cored interval (as marked gray on the depth track, Fig. 3.4) ends in the laminated peloidal wackestone, but using the wire-line log data it is observed that it is overlain by the A-2 Anhydrite. Characteristics and initial interpretations of each depositional facies are as follows.

Bioherm

General Description: The bioherm is defined by two main lithofacies, a *crinoidal mudstone* and a *skeletal wackestone*. The two lithofacies interfinger throughout the vertical section with an increasing amount of *skeletal wackestone* towards the upper half of the bioherm. The contact between the underlying Gray Niagaran and the bioherm is observable by the transition from a light gray color to dark gray to brown. This contact also marks a gradual change in the faunal assemblage. The contact between the bioherm and the overlying bioherm cap is sharp, and marked by the absence of fossils, as well as the presence of a purely crystalline dolomite. The bioherm ranges from 83 to 175 feet (25 to 53 m) in thickness where it directly underlies the reef core complex throughout the Columbus III field.

The *crinoidal mudstone* consists predominately of a microcrystalline dolomite matrix which has a mottled gray and white appearance with crinoid ossicles scattered throughout. Stromatactis textures are abundant and this facies is predominately composed of dolomite. The crinoid fragments range from 0.2 to 10 mm in diameter and are present in varying abundances throughout this facies. Crinoid fragments do not show any preferred orientation.

The *skeletal wackestone* is mostly composed of crinoids and bryozoans with rare occurrences of tabulate corals (Favosites sp. and Halysites sp.), rugose corals, and tabular stromatoporoids at the top. The matrix is composed of brown to gray dolomicrite with stromatactis textures throughout. Branching bryozoa are generally found in colonies, or thickets, and are typically found alongside crinoids and pentamerid brachiopods. The presence of tabular stomatoporoids and tabulate corals is sporadic and restricted to the upper half of the bioherm. They may be in growth position but do not interlock to form a rigid framework. Colonial rugose corals have also been identified but are sparse (see Plate 1, Fig.1).

Preliminary Interpretation: The main characteristics of the bioherm are its mottled appearance and abundance of a microcrystalline dolomite matrix. The abundance of stromatactis textures is evidence for synsedimentary lithification, which is a common attribute for reefs of all ages. Even in biohermal mounds that are mostly mud, a surprising amount of void space produces internal cavity systems (James and Wood, 2010). The inner surfaces of these cavities are preferentially coated with automicrite (microcrystalline carbonate that is produced *in situ*), which can be an important cementing agent, ultimately resulting in the stromatactis texture. The cavities can also be filled with fine-grained sediment composed of bioclastic silt and mud that trickles into holes from above or skeletons that fall from the walls and ceilings after death (James and Wood, 2010). Overall, the entire bioherm package is interpreted as a deep water mud mound, originally composed of lime-mud, synsedimentary cements, automicrite, and internal cavities (stromatactis). Although the *skeletal wackestone* lithofacies consists of sparse tabulate corals and stomatoporoids, compared to the overlying reef core it is not as wave-resistant. The abundance of crinoids is further evidence for a deeper water environment, as crinoids clustered around the lower parts and peripheries of reefs (Wood, 1999). The biohermal mound is interpreted to have initiated below storm-weather wave-base (SWB; 60 feet or 18 m below sea-level) and grew above SWB but below fair-weather wave-base (FWB, 30 feet or 9 m below sea-level). The gradual increase in frame-building organisms towards the upper half of the bioherm is evidence for gradual growth into higher-energy (i.e. shallower water) conditions.

Bioherm Cap

General Description: The bioherm cap facies is described as a *crystalline dolomite*, and ranges from 3 to 10 feet (1 to 3 m) in thickness. This facies is composed

entirely of brown dolomite rhombs (as identified in thin section), with the main pore type being intercrystalline. This depositional facies is easily differentiated from the bioherm by the absence of fossils, stromatactis, and cements. The contact between the bioherm cap and the overlying reef core is sharp, and is marked by the abundance of wave-resistant fauna, such as stromatoporoids and tabulate corals.

Preliminary Interpretation: Because this facies only consists of dolomite rhombs with very few depositional textures preserved, interpretations of depositional environments are difficult to make on lithology alone. Therefore, it is important to use the stratigraphic position of this facies, between a deeper water biohermal mound and a shallower water reef boundstone, to produce the interpretation. In order for a reef to initiate, it needs a firm substrate on which to encrust (James and Wood, 2010). This means that in order to transition from the muddy substrate of the bioherm mound, there either had to be a rise in sea-level and creation of a hardground, or fall in sea-level and exposure of the bioherm crest. This exposure would likely have resulted in erosion, possible karsitification, and deposition of eroded carbonate debris in topographic lows within the bioherm mound and around the peripheries. Either a small unconformity, or drowning and creation of a hardground, would result in the sharp transition that is observed between the underlying bioherm to the overlying bioherm cap. No unequivocal evidence supports either model of sea level rise or fall, therefore this needs further investigation. This problem could potentially be resolved by looking at a reef complex that has not undergone intense dolomitization, where the depositional fabric of the bioherm cap was preserved.

Reef Core

General Description: The reef core is composed of two main lithofacies, the *coral/stromatoporoid boundstone* and *skeletal wackestone*. Similar to the underlying

bioherm, these two lithofacies interfinger throughout the vertical section and occur in varying thicknesses. Although organic reefs are thought to be mainly composed of frame-building organisms, the *coral/stromatoporoid boundstone* facies comprises less than 30% of the entire reef core, while the reef core itself comprises less than 50% of the entire Niagara Reef Complex. The *skeletal wackestone* facies is prevalent throughout the reef core and therefore the reef core is identified by its faunal assemblage rather than texture alone. The contact between the reef core and the overlying stromatolitic cap is gradational and marked by the appearance of stromatolitic cyanobacterial mats directly overlying spherical stromatoporoids of the reef boundstone. The reef core ranges from 151 to 264 feet (46 to 80 m) in thickness where it is not overlain by the proximal reef apron facies.

The *coral/stromatoporoid boundstone* lithofacies consists of the major frame-building organisms such as tabulate corals and stomatoporoids. The two main types of tabulate corals are Favosites sp. and Halysites sp., which exist as both well preserved complete fossils or as coral fragments. The stomatoporoids range in morphologies from massive (spherical or hemispherical) to encrusting. Due to the intense dolomitization of all reef core facies, the internal structures of the encrusting stromatoporoids are very difficult to identify. They are most commonly observed as homogenous masses with only faint traces of internal laminations (see Plate 2, Fig. 1). However, the massive (spherical) stromatoporoid morphologies are well-preserved and occur at the top of the reef core section (see Plate 2, Fig. 2). These are characterized by their relatively smooth and peripheral outline with spherical internal laminations. The structures of tabulate corals are more easily identified and more commonly used for determining the *coral/stromatoporoid boundstone* lithofacies. Salt plugging is prevalent throughout this facies and commonly occurs in the intraskeletal pore space of the tabulate corals. Synsedimentary cements are also abundant throughout the reef boundstone lithofacies and range from dark brown to light tan in color. Cements are difficult to differentiate

from encrusting stromatoporoids due to the obliteration of their internal structure by diagenesis.

The *skeletal wackestone* lithofacies comprises the majority of the reef core and is mostly composed of a lower energy, intra-reef faunal assemblage, including bryozoans, brachiopods, crinoids, and rugose corals, which are mostly observed as skeletal fragments but occasionally as whole fossils. The skeletal lithoclast abundance varies from 25-50%, characterizing these as *skeletal wackestone* to *packstone*. The remaining 50-75% is composed of a microcrystalline dolomite matrix. While very similar to the *skeletal wackestone* lithofacies described within the bioherm, the main difference is how it interfingers with the *coral/stromatoporoid boundstone* lithofacies. It also lacks the stromatactis texture which is prevalent throughout the bioherm. Rarely, lithoclasts occur in conglomerate intervals within the reef core as sub-rounded to angular clasts, ranging from 0.5 to 2 cm in diameter (see Plate 1, Fig. 3).

Preliminary Interpretation: The reef core facies is characterized by a mixed assemblage of organisms with numerous lithologic transitions between the *coral/stromatoporoid boundstone* and *skeletal wackestone*. Moore and Wade (2013) separate framework reefs into four elements: 1) the framework organism, including encrusting, attached, massive, and branching metazoans; 2) internal sediment, filling primary growth voids and bioeroded cavities; 3) the bioeroders, which break down reef elements by boring, rasping, or grazing; and 4) abiotic or microbial induced cement, which results in early lithification of reef sediments. These four elements combine to produce the different rock fabrics observed from different microenvironments at any given time in the formation of the reef. While reef-building organisms were growing upward into the wave-agitated zone, slightly deeper-water organisms were thriving between the ridges of dense coral and stromatoporoid growth. These intra-reef ridges or pockets accumulated skeletal sands and lithoclasts of reef material (see Plate 1, Fig. 3).

Also, cavities formed beneath laminar and convex massive stromatoporoids, from which cryptic crinoid, bryozoan, and brachiopod biotas are observed. Although slight variations in water-depth had a major impact on the different sub-facies within the reef core, these reef complexes are undoubtedly "organic reefs" as defined by Lowenstam (1950), as they had the ability to erect rigid, wave-resistant, topographic structures by a combination of frame-building, sediment retention, and binding processes. It is important to note that frame-building organisms do not comprise the bulk of the reef core, they are simply the frame that holds the reef complex together that traps detrital and chemically precipitated sediments. This is also seen in other reefs in the rock record (Wood, 1999).

Evidence for the reef core facies to be deposited in a shallow water environment is reflected by the abundance of wave-resistant organisms such as stromatoporoids throughout the section. Because the combined height of the reef core and the underlying bioherm reaches thicknesses of 400 feet (122 m), it was necessary to have a relative sea-level rise during the construction of these reef cores. The effects of eustatic sea-level and basin-centered subsidence will be later discussed.

Plate 1

core depth: 3086′ log depth: 3092′
Bioherm

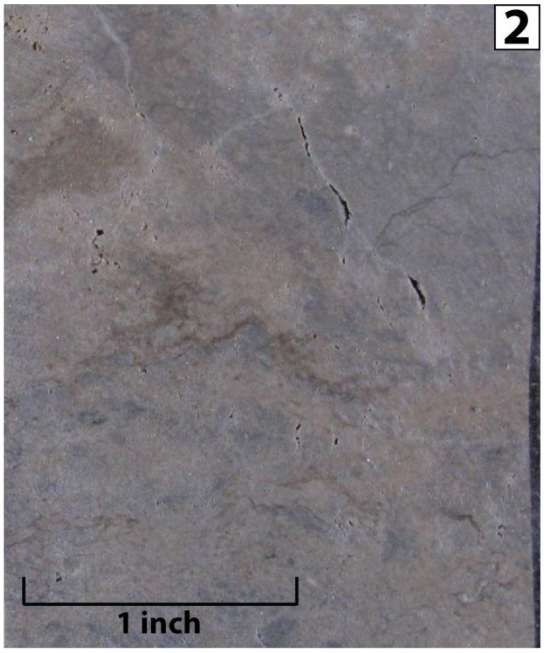

core depth: 3015′ log depth: 3021′
Bioherm Cap

core depth: 3001′ log depth: 3007′
Reef Core

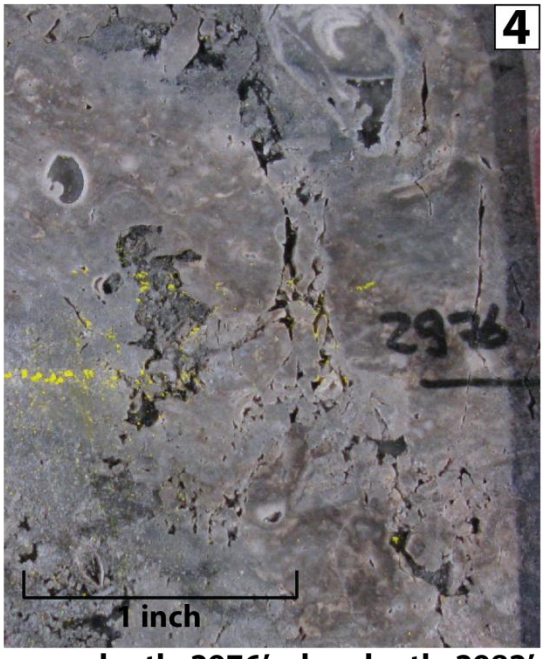

core depth: 2976′ log depth: 2982′
Reef Core

Plate 1. PN 27572 - Reef Core Complex Rock Types:

Fig. 1. Bioherm – *skeletal wackestone***.** Gray and white mottled appearance. Stromatactis textures towards the top with salt plugged rugose corals near the base. Crinoid ossicles throughout within a microcrystalline dolomite matrix.

Fig. 2. Bioherm cap – *crystalline dolomite***.** Composed entirely of dolomite rhombs with intercrystalline porosity. Brown coloring due to oil staining.

Fig. 3. Reef core – *skeletal wackestone***.** Intraclastic conglomerate with sub-rounded to angular clasts up to 2 cm in size.

Fig. 4. Reef core – *skeletal wackestone***.** Skeletal wackestone with crinoid ossicles, salt plugged pentamerid brachiopods, and synsedimentary cements within a microcrystalline dolomite matrix.

Stromatolitic Cap

General Description: The Stromatolitic cap, which directly overlies the reef core in this type location, is mostly composed of a *hemispheroid stromatolitic bindstone* and a *skeletal wackestone* lithofacies. Stromatolites can make up between 40-80% of this depositional facies, with the remaining rock being composed of *skeletal wackestone*. The amount of stromatolites per volume of rock increases upward towards the unconformable contact with the cyanobacterial mats of the A-1 Carbonate. This facies also represents the last appearance of reef core organisms in the vertical section. The contact between the stromatolitic cap and overlying laminar cyanobacterial mats is sharp and is associated with extensive karsting. These karsted surfaces were places where white, crinkly-laminated stromatolites belonging to the cyanobacterial mat facies encrusted along

fractures in various non-planar orientations (see Plate 2. Fig. 4). The underlying stromatolites belonging to the stromatolitic cap are also ripped up directly below the contact. The stromatolitic cap ranges from 28 to 37 feet (9 to 11 m) in thickness where it directly overlies the reef core.

The *hemispheroid stromatolitic bindstone* consists of dark brown, laterally-linked hemispheroid stromatolites (see Plate 2. Fig.3). It is easily distinguished from the overlying cyanobacterial mat facies (white in color) by its dark brown color. It also has fewer clasts of broken algal fragments. These laterally-linked hemispheroid stromatolites have domes ranging from 2 cm in diameter to 1 cm in height. The hemispheroids are often separated by flat lying laminations of up to 5 cm in length.

The *skeletal wackestone* consists of bioclastic fragments mostly composed of organisms found in the underlying reef core such as tabulate corals, stromatoporoids, and brachiopods. This lithofacies is very similar to that of the *skeletal wackestone* belonging to the reef core depositional facies. The amount of skeletal fragments ranges from 20-40%, with brachiopods the most commonly identified fossil. Synsedimentary cements are common and are similar in appearance, and therefore difficult to differentiate from flat-lying stromatolites.

Preliminary Interpretation: The stromatolitic cap marks a transition to shallower water depths from the underlying reef core. This appears to be a gradational transition because organisms that were prevalent in the underlying reef core are still found scattered throughout this facies. The increasing amount of laterally-linked hemispheroid stromatolites towards the top of this facies is interpreted as a shallowing upward sequence and an overall shift from early to late highstand. During deposition of this stromatolitic facies, which in some places is over 30 feet (9 m) thick, relative sea level continued to rise, however at a slower rate, in order to account for 30 feet (9 m) of intertidal deposition. Stromatolitic cap deposition is ultimately ceased by subaerial exposure and a third-order sea-level fall, which is recorded by vugs and fractures,

interpreted as karst features, spans tens of feet down from the exposure contact.

Cyanobacterial Mats

General Description: The cyanobacterial mats consists of two lithofacies, the *crinkly stromatolitic bindstone* and the *stromatolitic conglomerate*. Although both units are composed of stromatolites, very distinct differences are evident and important. The first main difference is the white to gray color of the cyanobacterial mats versus the dark brown of the underlying stromatolitic cap. A second major difference is the lack of a micritic matrix in the cyanobacterial mats. The final, and most important difference is the morphology of the stromatolites. The stromatolitic cap microbial structures are laterally-linked hemispheroids, while the cyanobacterial mats are thin and crinkly laminated. The contact between the cyanobacterial mats and the overlying thrombolitic bindstone is sharp (see Plate 3, Fig. 2) and a distinct change in textures as well as color from white to brown is observed. The cyanobacterial mats range from 6 to 10 feet (2 to 3 m) in thickness.

The *crinkly stromatolitic bindstone* lithofacies is almost completely composed of thin, crinkly laminated cyanobacterial stromatolites and associated fragments. The stromatolites have a distinct white to gray color and are almost completely devoid of a micritic matrix. The laminae that make up this lithofacies are very thin (mm- to sub-mm-scale) and appear to be in growth position.

The *stromatolitic conglomerate* consists entirely of broken fragments of the crinkly stromatolitic bindstone. The cyanobacterial mat fragments are elongated pebbles that range from silt size to small cobbles and exhibit no apparent sorting. The pebbles are often loosely packed within a darker gray micritic matrix.

Preliminary Interpretation: The cyanobacterial mats are interpreted to belong to a slightly shallower, more restricted depositional environment to that of the underlying

stromatolitic cap. While they both are composed of cyanobacterial mats, the cyanobacterial mats appear to belong to a higher-energy, storm-influenced environment due to the abundance of the stromatolitic conglomerate lithofacies composed of cyanobacterial mat pebbles, and therefore ranges from intertidal to supratidal. The whiter color of this facies is most likely the result of prolonged subaerial oxidation. The absence of any organisms that belong to the underlying reef core is evidence for more restricted marine waters compared to the more normal marine waters of the underlying Niagara units. This could be a result in a shift in the climatic regime, or simply an increased restriction of the Michigan Basin from the normal marine ocean waters. Huh (1973) argued that the crinkly laminations observed here were the result of the cyanobacterial mats which trapped sediment. More specifically, laminae were formed during cyclic growth of cyanobacterial mats and sediment influx. The complete disappearance of any reef core fauna in this facies is also evidence for a larger (3^{rd} order) sequence stratigraphic boundary between the cyanobacterial mats the underlying stromatolitic cap.

Plate 2

core depth: 2905′ log depth: 2911′
Reef Core

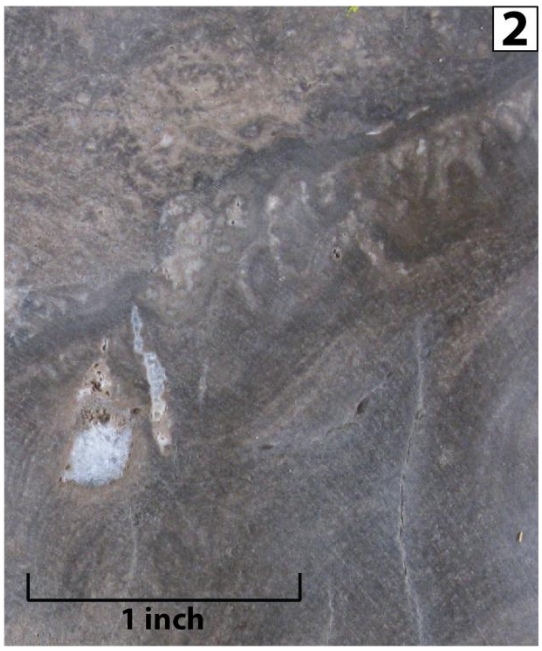

core depth: 2899′ log depth: 2905′
Stromatolitic Cap - Reef Core Contact

core depth: 2877′ log depth: 2883′
Stromatolitic Cap

core depth: 2861′ log depth: 2867′
Cyanobacterial Mats -
Stromatolitic Cap Contact
Sequence Boundary 1

Plate 2. PN 27572 - Reef Core Complex Rock Types:

Fig. 1. Reef core – *coral/stromatoporoid boundstone***.** Favosites sp. coral with overlying synsedimentary cements and potential encrusting stromatoporoids. Salt plugging occurs in vugs and fractures throughout the reef core facies.

Fig. 2. Stromatolitic cap - Reef core contact. Contact at the top of the reef core facies with spherical stromatoporoids (*coral/stromatoporoid boundstone*) at the bottom, directly overlain by the *skeletal wackestone* of the stromatolitic cap.

Fig. 3. Stromatolitic cap – *hemispheroid stromatolitic bindstone***.** Laterally-linked hemispheroid stromatolites.

Fig. 4. Cyanobacterial mats – Stromatolitic cap contact (sequence boundary 1). Contact between underlying brown, laterally-linked hemispheroid stromatolites (*hemispheroid stromatolitic bindstone*) and overlying white to gray, thin, crinkly laminated cyanobacterial stromatolites of the A-1 Carbonate (*crinkly stromatolitic bindstone*). The overlying white stromatolites are growing vertically along fractures between the underlying brown stromatolites.

Thrombolitic Bindstone

General Description: The *thrombolitic bindstone* facies exhibits different thrombolitic textures that vary from ribbon-like mesoclots (see Plate 3, Fig. 4) to irregular patchy mesoclots (see Plate 3, Fig. 3). The thrombolites have a mottled appearance with darker brown micrite and lighter tan sparry cement. The *thrombolitic bindstone* ranges from 20 to 34 feet (6 to 10 m) in thickness. This facies is easily differentiated from stromatolites of previously described facies, which have stratified internal fabrics, because of the thrombolites clotted internal fabric. It is also easily

differentiated from the underlying cyanobacterial mat facies by a distinct color contrast (white to brown), and is separated by a sharp, unconformable contact (see Plate 3, Fig. 2).

Preliminary Interpretation: The *thrombolitic bindstone* facies is interpreted to be deposited in a subtidal setting. Thrombolites are thought to be biogenic, with mesoclots derived from the calcification of microbial colonies in sediments (Kennard and James, 1986). Similar to that of stromatolites, thrombolites are also believed to exist in areas of environmental stress such as active tidal currents, low nutrients, or high salinities (James and Wood, 2010). This interpretation supports the hypothesis that marine waters were more restricted at the beginning of the underlying cyanobacterial mats deposition and during thrombolitic bindstone deposition. The internal fabrics of thrombolites are controlled by environmental changes, and therefore can aid interpretations. A facies distribution model of various types of thrombolites by Tang et al. (2013) places all thrombolitic types in the upper to lower subtidal zone, with stromatolites formed in the intertidal zone. The types of thrombolites observed here, with patchy and ribbon-like mesoclots, likely grew in the upper subtidal zone.

Plate 3

core depth: 2858′ log depth: 2864′
Cyanobacterial Mats

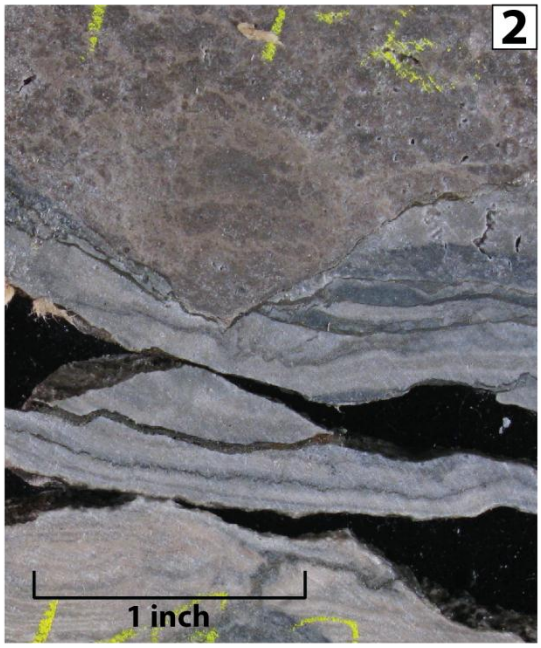

core depth: 2854′ log depth: 2860′
Thrombolitic Bindstone - Cyanobacterial Mats Contact Unconformity

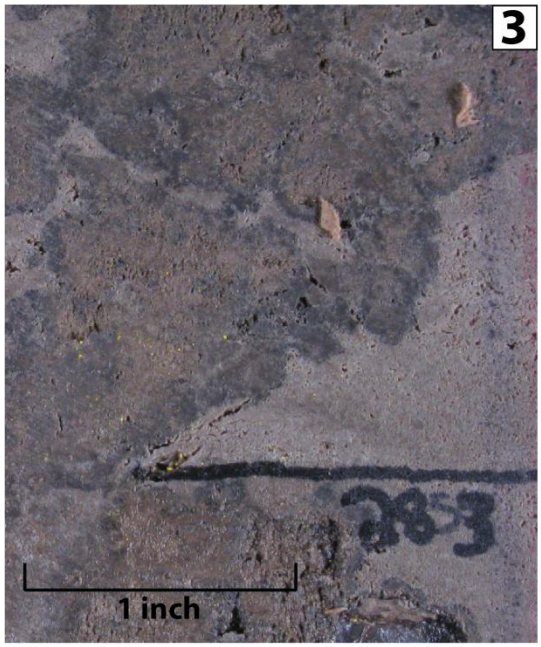

core depth: 2853′ log depth: 2859′
Thrombolitic Bindstone

core depth: 2844′ log depth: 2850′
Thrombolitic Bindstone

Plate 3. PN 27572 - Reef Core Complex Rock Types:

Fig. 1. Cyanobacterial mats – *crinkly stromatolitic bindstone* (bottom) and *stromatolitic conglomerate* (top)**.** White to gray, thin, crinkly-laminated cyanobacterial stromatolites. Conglomerate of elongated pebbles composed exclusively of stromatolite fragments.

Fig. 2. Thrombolitic bindstone – Cyanobacterial mats contact (unconformity). Sharp contact between underlying white cyanobacterial mats (*crinkly stromatolitic bindstone*) and overlying brown thrombolitic texture (*thrombolitic bindstone*).

Fig. 3. Thrombolitic bindstone – *thrombolitic bindstone***.** Mottled mudstone interpreted as a cyanobacterial boundstone (thrombolite). Irregular patchy mesoclots of darker brown micrite with a lighter tan sparry matrix.

Fig. 4. Thrombolitic bindstone – *thrombolitic bindstone***.** Thrombolitic texture with darker micritic ribbon-like mesoclots and less light tan matrix.

Laminated Peloidal Wackestone

General Description: The *laminated peloidal wackestone* facies exhibits well-developed laminations of peloids and pellets, which comprise up to 40% of the wackestone. Peloids are spherical or elliptical in shape and are encased in a brown, microcrystalline dolomite matrix. Thin laminations are wavy and parallel, and range from 1 to 3 mm in thickness and are most likely cyanobacterial mats. Randomly scattered anhydrite laths occur, cross-cutting horizontal laminations. This unit ranges from 8 to 15 feet (2 to 5 m) in thickness where it directly overlies the reef core complex and is composed almost entirely of dolomite.

Preliminary Interpretation: The grains that comprise up to 40% of the *laminated peloidal wackestone* are interpreted as fecal pellets and are evidence for an intertidal environment (Huh, 1973). The abundance of peloid grains indicates organisms living in

this subtidal environment, but marks the last evidence for significant biogenic carbonate deposition before the deposition of the overlying A-2 Evaporite unit.

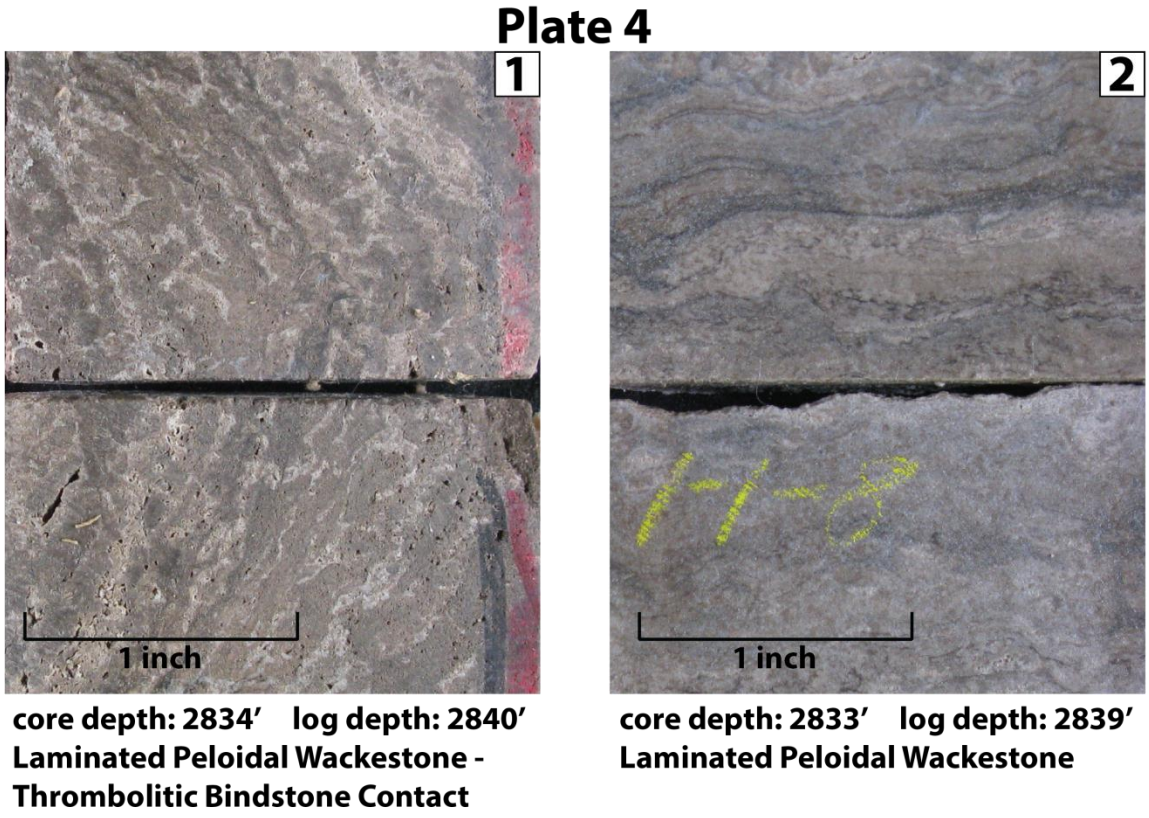

Plate 4. PN 27572 - Reef Core Complex Rock Types:

Fig. 1. Laminated peloidal wackestone – Thrombolitic bindstone contact. Mottled thrombolitic mosaic texture with vertically arranged mesoclots growing along a vertical fracture at the contact between the *laminated peloidal wackestone* and *thrombolitic bindstone* facies. The fracture is larger than the core photograph which does not capture the entire contact.

Fig. 2. Laminated peloidal wackestone. Well-developed laminations of peloidal grains which comprise up to 40% of the wackestone. Peloids are spherical or elliptical in shape and exist within a brown, microcrystalline dolomite matrix. Randomly scattered anhydrite laths occur, cross-cutting horizontal laminations.

Reef Core Complex Wire-Line Log Signatures

Although wire-line log data are sparse for the 27572 well, as well as the majority of the cored wells, distinct log signatures can be observed in the gamma ray log alone. The bases of the wire-line logs are in the bioherm, and therefore the gamma ray spike that is used to identify the top of the Gray Niagaran is not observed (see Fig. 3.4). The gamma ray intensities in the bioherm are intermediate and slightly higher than in the overlying clay-free organic reef rocks, but lower than the underlying argillaceous substrate of the Gray Niagaran. Within the bioherm, the neutron count log gradually decreases (porosity increases) upward and plateaus in the overlying bioherm cap. This high porosity interval in the bioherm cap also corresponds to the highest core permeability values, with some values greater than 10 mD (shaded in pink; see Fig. 3.4). This interval is also marked by oil staining, with the top of the oil staining capped by the base of salt plugging, which occurs at the base of the reef core and continues up through the top of the stromatolitic cap. It is observed that salt plugging plays a major role in reservoir quality throughout this field and almost always transitions into oil staining below. The reef core facies has very low gamma ray intensities with little variation from bottom to top. A slight gamma ray increase occurs near the top of the reef core as it transitions into the more clay-rich stromatolitic cap facies. The high gamma ray signature of the laminated peloidal wackestone at the top of the core is observed in all reef core complex locations and most likely represents a shift in climatic regime (discussed later).

Type Section 4: Leeward Proximal Reef Apron

Type section 4 is represented by a similar stack of facies as the Reef Core Complex, with the addition of the proximal reef apron facies. This type section location lies directly leeward from the previously described Reef Core Complex type section (see Fig. 3.5), and therefore has a very similar internal facies architecture. The main

difference is that in the Reef Core Complex location, the reef core and bioherm facies are a combined 330 feet (101 m) thick. In this type section, the reef core and bioherm facies are only 197 feet (60 m) thick and the overlying proximal reef apron is 128 feet (39 m) thick (refer to Fig. 3.6). Thus, both type sections are almost identical thicknesses, but are composed of a different stack of depositional facies. The leeward proximal reef apron contains a debris slope (scree) composed of broken and rolled fragments of lithified reef material, intermixed with detrital carbonate shed from the active carbonate factory in the reef core. This reef apron material was transported via waves and currents and re-deposited in the leeward direction.

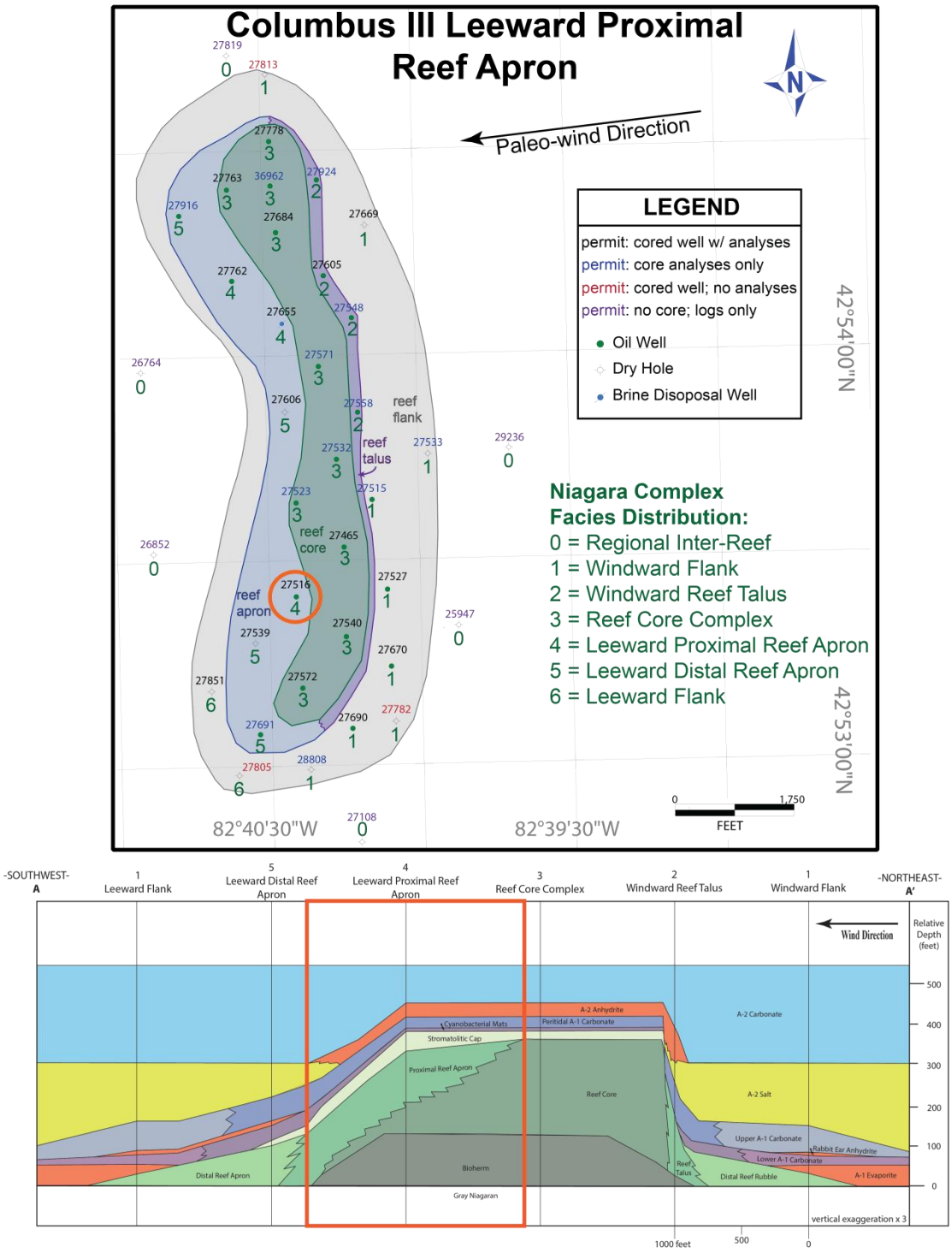

Figure 3.5. The Leeward Proximal Reef Apron type section location highlighted on the Columbus III Field map (upper) and reef complex cross-section (lower).

4: Leeward Proximal Reef Apron PN 27516

*core depth shift down 6 feet

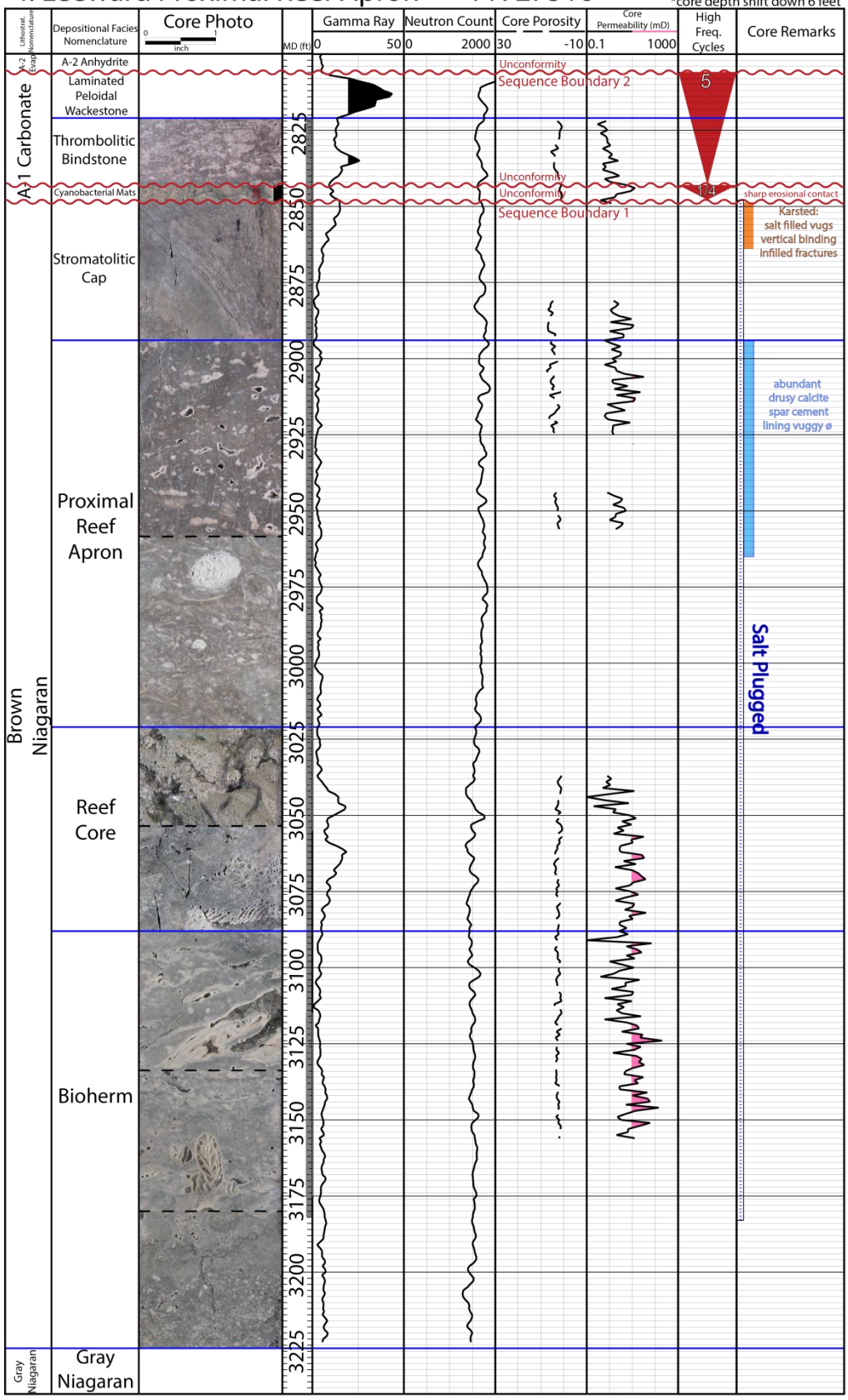

Figure 3.6. A single well cross-section of the 27516 well which illustrates the stack of facies for a leeward proximal reef apron location within the Niagara-lower Salina reef complex. Core depths were shifted down 6 feet to match wire-line log depths.

The base of the Leeward Proximal Reef Apron type section begins with the Gray Niagaran, which is directly overlain by the bioherm (see Fig. 3.6). The bioherm and overlying reef core consist of the same lithofacies described in the Reef Core Complex type section. However, the reef core facies is less than 60 feet (18 m) thick in this location and the overlying proximal reef apron is 128 feet (39 m) thick. The proximal reef apron is then overlain by the same facies succession as observed at the top of the Reef Core Complex type section: stromatolitic cap, cyanobacterial mats, and thrombolitic bindstone. Although the cored interval ends at the top of the thrombolitic bindstone facies, it is observed in wire-line logs that it is directly overlain by the laminated peloidal wackestone facies (high gamma ray signature), which is capped by the A-2 Anhydrite. Therefore, the only depositional facies that differs from the Reef Core Complex in this locality is that of the proximal reef apron, which is characterized by the following observations.

Proximal Reef Apron

General Description: The proximal reef apron is composed of two main lithofacies: *skeletal mudstone* and *skeletal wackestone*. The only difference between these lithofacies is the relative proportions of skeletal grains to mud. The *skeletal mudstone* has minor skeletal fragments, and is most identifiable by its abundance of drusy calcite spar cement lining vuggy porosity. The *skeletal wackestone* fauna consists of tabulate corals, brachiopods, bryozoans, and crinoids. Most fossils are not intact and appear to have been transported. The proximal reef apron is differentiated from the underlying reef core facies by the decrease in abundance of both reef bounding and reef dwelling organisms. The proximal reef apron is completely devoid of stromatoporoids.

It also is distinguishable by characteristic calcite cements which are prominent in the *skeletal mudstone* lithofacies. The proximal reef apron transitions into the overlying stromatolitic cap by the first occurrence of hemispheroidal stromatolites at a similar stratigraphic position as was observed for the stromatolitic cap atop the Reef Core Complex type section locality. The proximal reef apron ranges from 94 to 127 feet (29 to 39 m) in thickness in the leeward proximal reef apron location.

Preliminary Interpretation: The proximal reef apron facies is interpreted to be a product of the upwind, carbonate factory in the reef core. While reef communities are demonstrably wave-resistant, boreholes in modern reef complexes have shown that original framework can be almost completely obliterated, with between 40-90% of the entire volume consisting of rubble, sediment, and voids (Hubbard et al., 1990). The absence of stromatoporoids in the reef apron, which are the major frame-building organisms of the reef core, indicates that few if any wave-resistant structures existed in the proximal reef apron location. However, the presence of other reef core debris, such as tabulate corals and brachiopods, are evidence that the reef core was nearby. The vertical transition from reef core to proximal reef apron is interpreted to have resulted from progradation of the apron over the reef core.

Due to the lack of binding, wave-resistant organisms in growth position throughout the proximal reef apron facies, the interpreted water depth for this facies ranges from 30 feet (9 m), where it lies directly next to the Reef Core Complex crest, to 150 feet (46 m), where grains and skeletal clasts tens of meters from the reef core crest were deposited in calmer, deeper water environments. This range of water depths is interpreted from the present day thickness observed in core of the proximal reef apron facies at various locations throughout the Columbus III complex. This lateral transition away from the Reef Core Complex in the leeward direction marks the gradational facies transition from proximal to distal reef apron facies.

Plate 5

core depth: 2956′ log depth: 2962′
Proximal Reef Apron

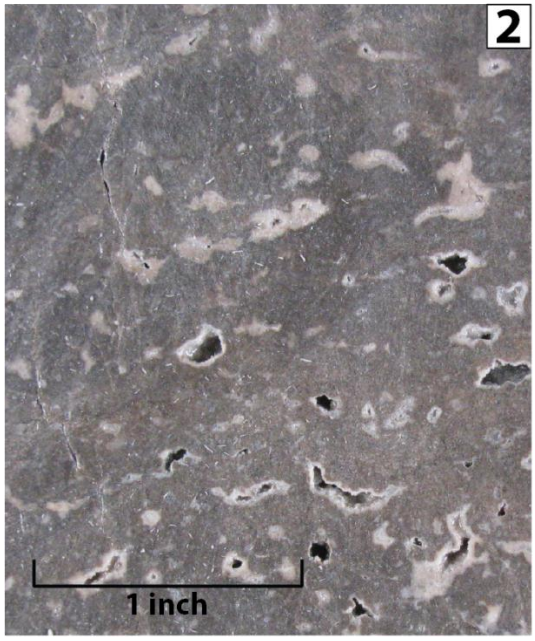

core depth: 2890′ log depth: 2896′
Proximal Reef Apron

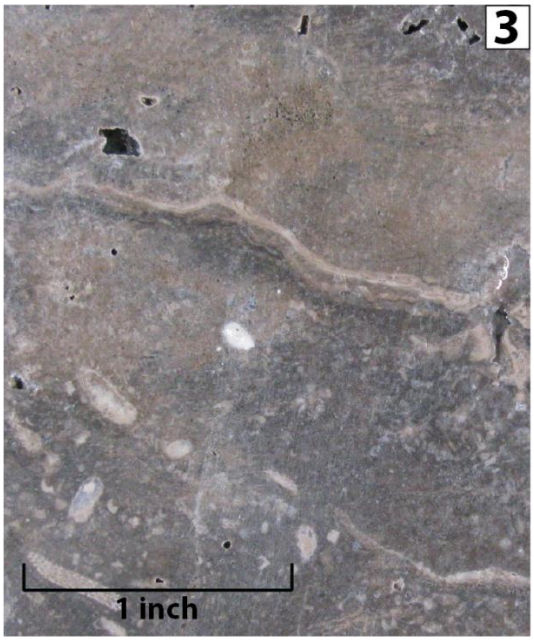

core depth: 2880′ log depth: 2886′
Stromatolitic Cap

core depth: 2854′ log depth: 2860′
Stromatolitic Cap

Plate 5. PN 27516 – Leeward Proximal Reef Apron Rock Types:

Fig. 1. Proximal reef apron – *skeletal wackestone***.** A skeletal wackestone with fragments of disarticulated brachiopods, bryozoans, and Halysites sp. corals.

Fig. 2. Proximal reef apron – *skeletal mudstone***.** Microcrystalline dolomite with vugs lined with drusy calcite spar cements.

Fig. 3. Stromatolitic cap – *skeletal wackestone***.** Skeletal fragments within a microcrystalline dolomite matrix with cements. Vuggy porosity composed of moldic pores is present.

Fig. 4. Stromatolitic cap – *hemispheroid stromatolitic bindstone***.** Steeply inclined hemispheroid stromatolite much larger than the core piece itself. Internal laminations are less than 1 mm thick.

Leeward Proximal Reef Apron Wire-Line Log Signatures

The wire-line logs for this type section began near the base of the bioherm (see Fig. 19). The gamma ray log response is relatively low throughout the bioherm and into the overlying reef core, where it gradually increases to about 20 API units in the middle of the reef core. There are horizontal stringers of permeability that range from 10 to 50 mD throughout the top of the bioherm and into the reef core, but salt plugging is pervasive from the top of the stromatolitic cap to the base of the cored interval in the bioherm. This core was completely devoid of oil staining throughout. The proximal reef apron has a very low gamma ray log signature through the entire section, identical to that of the nearby reef core, but increases from 0 to 20 API units within the stromatolitic cap. The gamma ray decreases slightly at the transition to the overlying cyanobacterial mats, increases slightly throughout the thrombolitic bindstone, and reaches its maximum of 45 API units within the laminated peloidal wackestone facies. The neutron count log shows

highest porosities to exist in the bioherm and reef core facies, and lower porosities in the proximal reef apron and overlying facies.

Type Section 5: Leeward Distal Reef Apron

Type section 5 is represented by a similar stack of facies observed in the Leeward Proximal Reef Apron, with the omission of the reef core facies. There also exists a slightly different stack of facies atop the cyanobacterial mat facies in the A-1 Carbonate, which is more representative of A-1 Carbonate facies observed in the flank locations of the reef complex. Because this type section is located further in the leeward direction of the Reef Core Complex than type section 4 (see Fig. 3.7), the distal reef apron facies is interpreted to be deposited contemporaneous with the growth of the reef core complex and proximal reef apron, but the reef building organisms never existed in this location. The distal reef apron facies in this type section are very similar to proximal reef apron facies of type section 4, with evidence for deeper water and further transport of material from the Reef Core Complex. The distal reef apron directly overlies the bioherm toe and is 87 feet (27 m) thick.

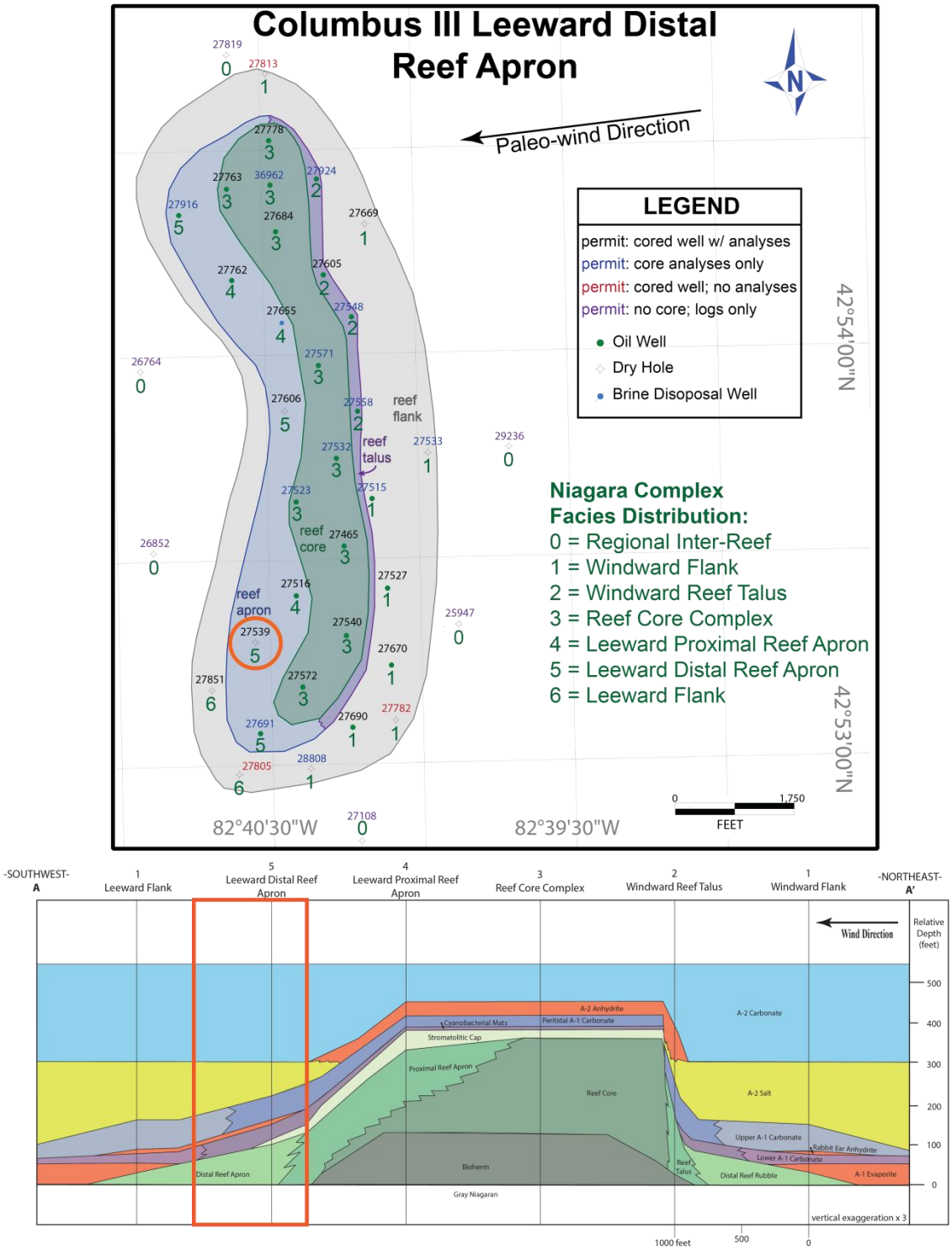

Figure 3.7. The Leeward Distal Reef Apron type section location highlighted on the Columbus III Field map (upper) and reef complex cross-section (lower).

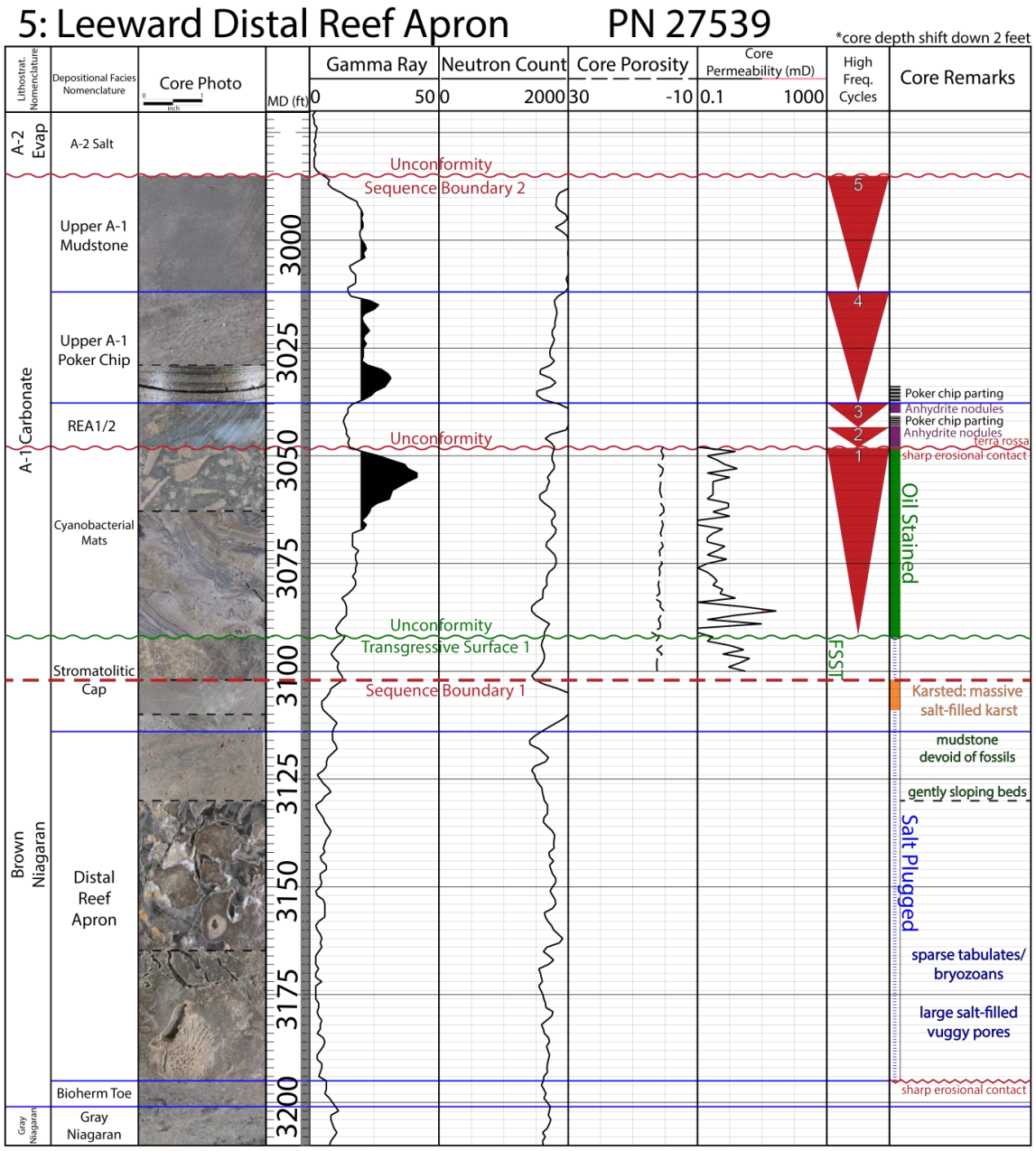

Figure 3.8. A single well cross-section of the 27539 well which illustrates the stack of facies for a leeward distal reef apron location within the Niagara-lower Salina reef complex. Core depths were shifted down 2 feet to match wire-line log depths.

The base of the Leeward Distal Reef Apron type section begins with the Gray Niagaran, which is directly overlain by the bioherm toe (see Fig. 3.8). The bioherm,

which is over 100 feet (30 m) thick in the windward direction of type section 4, is not present in this location. The reef core is also not present in this location, which gives horizontal control for the spatial distribution of both the organic bioherm and reef core facies in the leeward direction. The bioherm toe is interpreted to be contemporaneous with the deposition of the bioherm cap, as they have similar thicknesses and textures (massively bedded crystalline dolomites). The overlying distal reef apron facies is composed of the same lithofacies as in type section 4, with the lithofacies alternating between *skeletal mudstone* to *skeletal wackestone*. Minor tabulate corals are present but typically not intact, nor in growth position. There is no evidence of stromatoporoids, fewer tabulate corals than observed in type section 4, with the majority of fossil fragments consisting of bryozoans and crinoids (see Plate 6, Fig. 1). The top of the distal reef apron in this core is capped by a 5 foot (2 m) interval of massive halite, which exists in the stromatolitic cap facies and is interpreted to be a salt-filled karst surface. This massive salt is directly overlain by stromatolitic cap facies, which are unconformably overlain by the (white) cyanobacterial mat facies of the A-1 Carbonate (see Fig. 3.8).

The cyanobacterial mat facies are very thick (44 feet or 13 m) in this locality and are unconformably overlain by the first rabbit ear anhydrite (REA1). These two facies are separated by a sharp erosional contact, which is lined with orange terra rossa. (see Plate 7, Figure 3). Terra rossa is a red clay soil which is produced by the weathering of limestone, under oxidizing conditions while the soils are above the water table. Iron oxide forms in the clay, resulting in the reddish-orange color (Kerans and Tinker, 1997). This stratigraphic surface is important for environmental interpretations and will be further discussed in the reef growth model. Directly overlying the REA1 facies is a thin interval of thinly-laminated mudstone (poker-chips), which is overlain by the second rabbit ear anhydrite (REA2). The REA2 facies is overlain by the upper A-1 poker chip and upper A-1 mudstone facies. These depositional facies, their associated lithofacies, and preliminary interpretations will be further discussed for the type section 1 location of

the windward flank.

Plate 6

core depth: 3136′ log depth: 3138′
Distal Reef Apron

core depth: 3104′ log depth: 3106′
Salt - Filled Karst (5ft interval)

core depth: 3093′ log depth: 3095′
Stromatolitic Cap

core depth: 3078′ log depth: 3080′
Cyanobacterial Mats

Plate 6. PN 27539 - Leeward Distal Reef Apron Rock Types:

Fig. 1. Distal reef apron – *skeletal wackestone***.** Disarticulated bryozoan fossils within a microcrystalline dolomite matrix.

Fig. 2. Salt-filled karst – A massively bedded halite interval with very small carbonate lenses.

Fig. 3. Stromatolitic cap – *hemispheroid stromatolitic bindstone* and *skeletal wackestone***.** Laterally-linked hemispheroid stromatolites (bottom left) with a skeletal wackestone consisting of very fine skeletal debris in a microcrystalline dolomite matrix (top right).

Fig. 4. Cyanobacterial mats – *crinkly stromatolitic bindstone* and *stromatolitic conglomerate***.** White to gray, thin, crinkly-laminated cyanobacterial stromatolites. Conglomerate of elongated pebbles composed exclusively of stromatolite fragments.

Plate 7

core depth: 3056′ log depth: 3058′
Cyanobacterial Mats

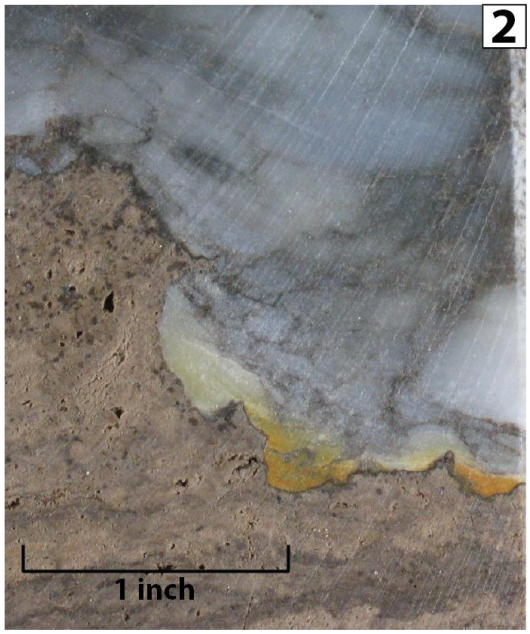

core depth: 3041′ log depth: 3043′
Cyanobacterial Mats - REA1 Contact
Unconformity

core depth: 3026′ log depth: 3028′
Upper A-1 Poker Chip

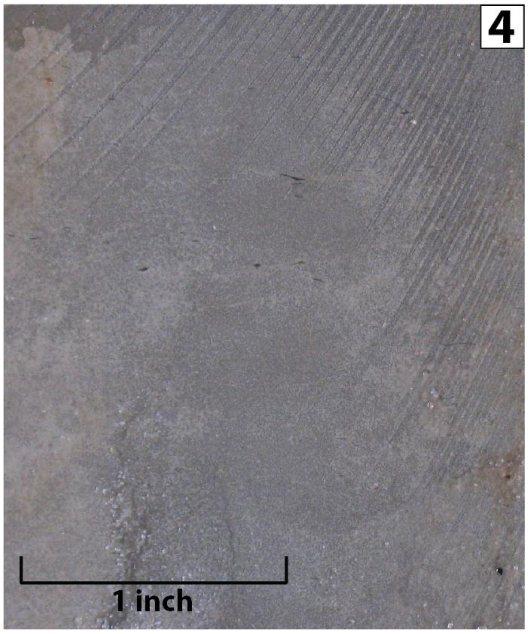

core depth: 3005′ log depth: 3007′
Upper A-1 Mudstone

Plate 7. PN 27539 - Leeward Distal Reef Apron Rock Types:

Fig. 1. Cyanobacterial mats – *stromatolitic conglomerate***.** Conglomerate of thin, elongated pebbles composed exclusively of stromatolite fragments in a gray lime-mud matrix.

Fig. 2. Cyanobacterial mats – Rabbit ear anhydrite 1 contact (unconformity). Sharp contact between underlying *crinkly-laminated stromatolites* and overlying *nodular anhydrite* with orange terra rossa lining the contact.

Fig. 3. Upper A-1 poker chip – *thinly-laminated mudstone*. Thin carbonate mudstone laminations with carbonaceous films.

Fig. 4. Upper A-1 mudstone – Massively bedded, gray mudstone. Mottled texture between gray and brown intervals.

Leeward Distal Reef Apron Wire-Line Log Signatures

This well is most interesting due to its inverted relationship between salt plugging and oil staining in comparison to the previously described localities. In all type section 3 and 4 locations where salt plugging is present, the salt plugged interval ranges from the top of the stromatolitic cap down into the reef core and typically into the bioherm. Where the salt plugging terminates, downward, oil staining is prevalent. However, in this type section location, the oil stained interval occurs above the stromatolitic cap and salt plugged interval of the distal reef apron (see Fig. 3.8). Structurally, this is near the same sub-sea elevation where oil staining is observed in the bioherm and reef core of type sections 3 and 4, but not in the same depositional facies. This is good evidence that oil migration in the reef complex was partially controlled by a combination of salt plugging, structure, and depositional facies.

The wire-line logs for this type section began in the Gray Niagaran, which exhibits a higher gamma ray log intensity than the overlying bioherm toe and distal reef

apron. The gamma ray log signature for the distal reef apron is low and generally increases upward into the stromatolitic cap, with the highest gamma ray intensities in the overlying cyanobacterial mats. The cyanobacterial mats are overlain by a lower gamma ray signature in the rabbit ear anhydrites, with higher gamma ray log signatures in the overlying upper A-1 poker chip and upper A-1 mudstone facies. The highest neutron count intervals (lowest porosity) exist in the salt-filled karst interval within the stromatolitic Cap, as well as the rabbit ear anhydrites interval. These evaporite intervals also contain low gamma ray log intensities.

Type Section 2: Windward Reef Talus

Type section 2 is represented by a distinctly different stack of facies than those previously described. This type section is located very close to the Reef Core Complex in the proximal windward direction, and exhibits internal stratification within the reef talus deposits (see Fig. 3.10). The horizontal extent of this type section's spatial distribution is very limited (less than 250 ft or 76 m) which is illustrated in Figure 3.9. Because of this type sections' close proximity to the Reef Core Complex and the conglomeratic nature of each facies in the vertical section, the windward reef talus is interpreted to be the result of sediments being transported short distances down steep gradients in the windward direction.

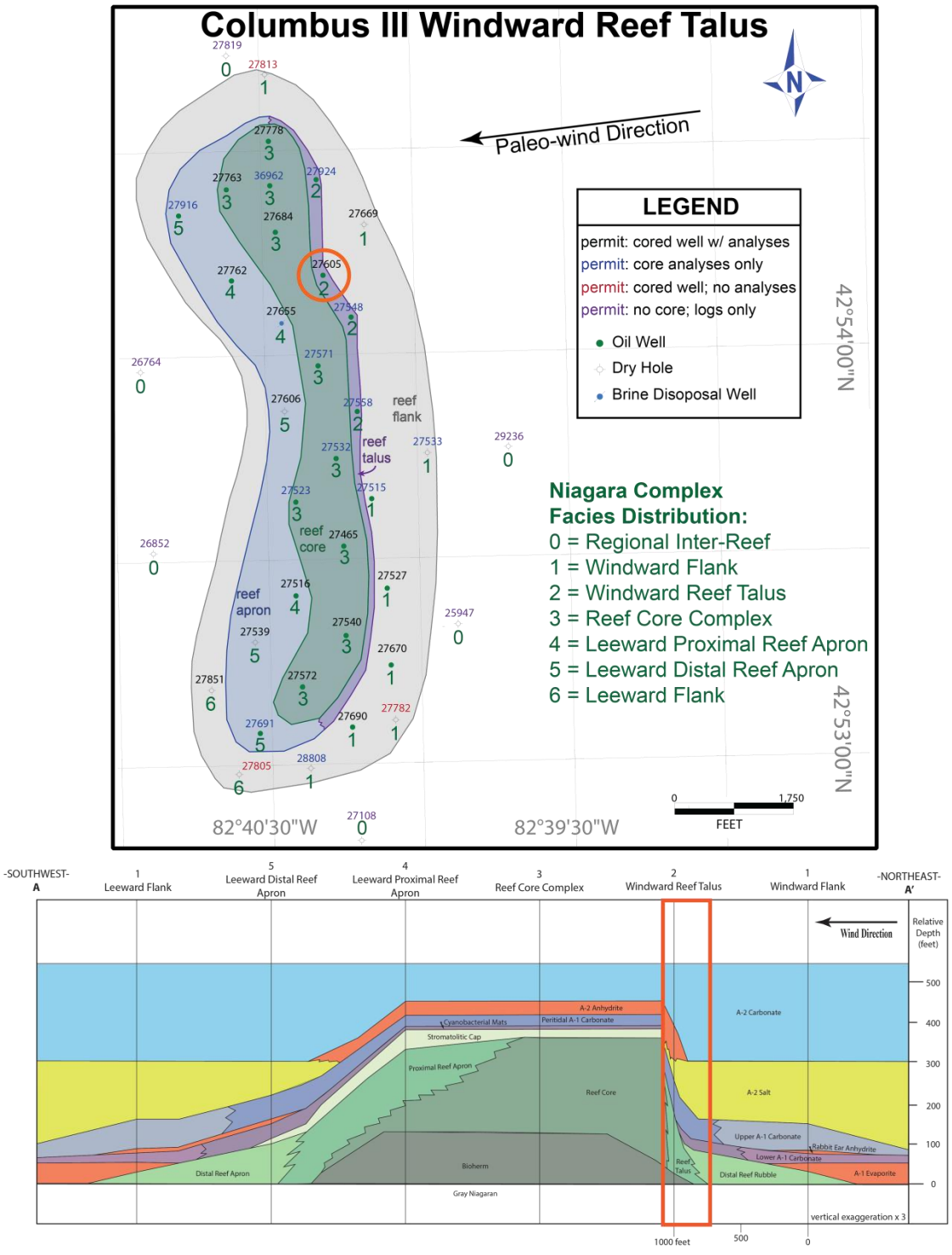

Figure 3.9. The Windward Reef Talus type section location highlighted on the Columbus III Field map (upper) and reef complex cross-section (lower).

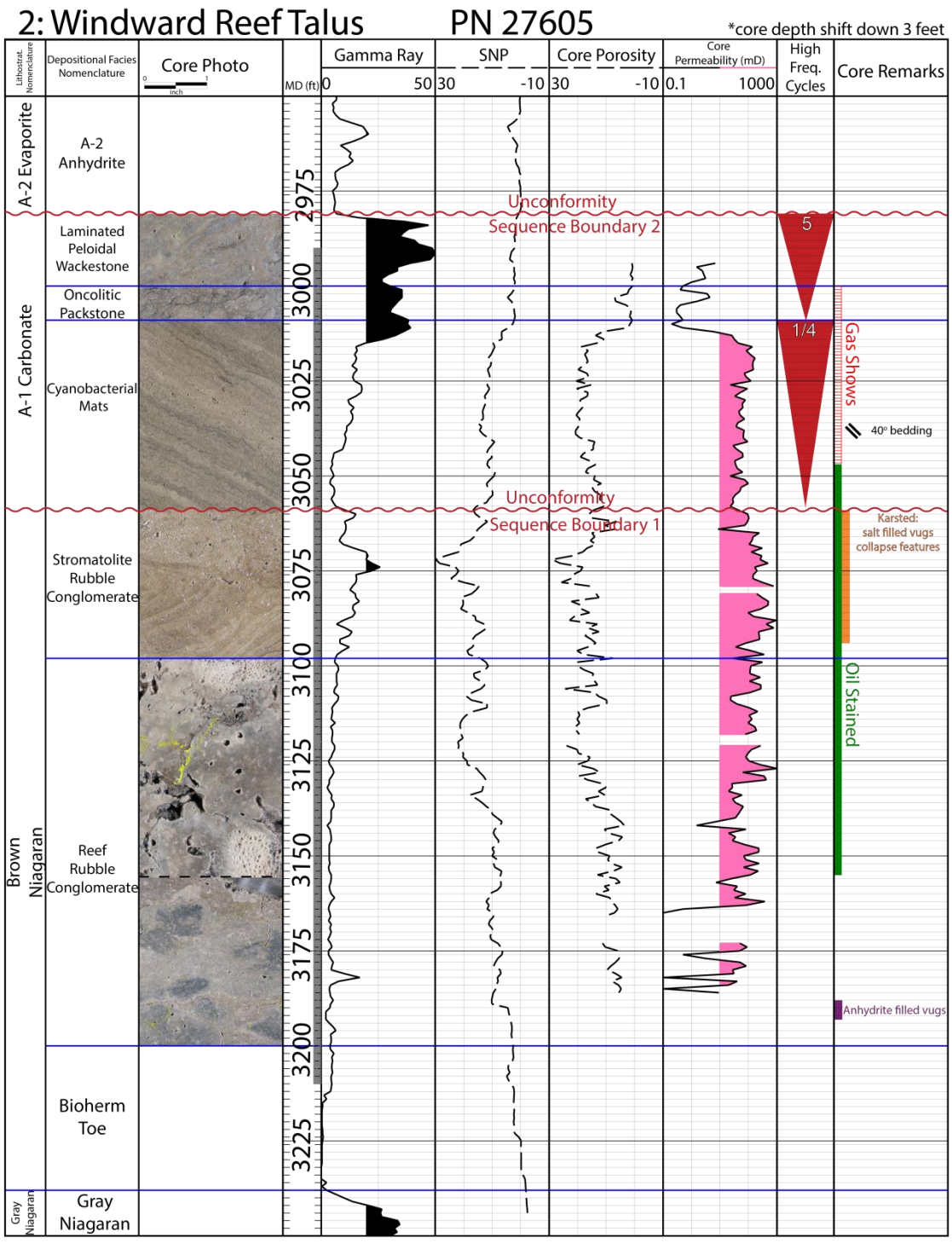

Figure 3.10. A single well cross-section of the 27605 well which illustrates the stack of facies for a windward reef talus location within the Niagara-lower Salina reef complex. Core depths were shifted down 3 feet to match wire-line log depths.

The base of the Windward Reef Talus type section begins in the Gray Niagaran, which is directly overlain by the bioherm toe (see Fig. 3.10). The reef rubble conglomerate facies directly overlies the bioherm toe and is discussed below. Overlying the reef rubble conglomerate is the stromatolite rubble conglomerate, which consists of lithoclasts of distinctly different provenance. The stromatolite rubble conglomerate is unconformably overlain by the cyanobacterial mat facies of the A-1 Carbonate, which are steeply inclined at angles up to 40 degrees. The upper 25 feet (8 m) of the stromatolite rubble conglomerate is heavily karsted, further evidence to support a third-order sequence boundary at this contact. Atop the cyanobacterial mats is a facies very similar called the oncolitic packstone, which contains rounded oncolites of cyanobacterial mat clasts. At this location almost every facies is conglomeratic and appears to have been transported short distances.

Reef Rubble Conglomerate

General Description: The reef rubble conglomerate consists of two main lithofacies: *coarse lithoclastic conglomerate* and *skeletal lithoclastic conglomerate*. These two lithofacies were also identified by Huh (1973) in the Northern Niagaran Reef Trend. The *coarse lithoclastic conglomerate* is always below the *skeletal lithoclastic conglomerate*, which is overlain by the stromatolite rubble conglomerate facies. In this well, the *coarse lithoclastic conglomerate* is only 10 feet (3 m) thick, whereas the overlying *skeletal lithoclastic conglomerate* is 102 feet (31 m) thick. The main difference between the two lithofacies is the presence of large tabulate corals in the *skeletal lithoclast conglomerate*.

The *coarse lithoclastic conglomerate* is composed of large clasts which range in size from 1 to 5 cm in length and 1 to 3 cm in width, and are a darker gray color compared to the surrounding light gray microcrystalline dolomite matrix (see Plate 8, Fig.

1). The large clasts are angular to sub rounded and contain crinoid ossicles within. Large vugs are present throughout this lithofacies, which exist as similar shapes and sizes as the clasts and are always filled with halite.

The *skeletal lithoclastic conglomerate* lithofacies is characterized by its abundance of tabulate corals, brachiopods, and crinoids. Favosites sp. corals (intraclasts) are observed scattered throughout this lithofacies and exist alongside lithoclasts of varying sizes (see Plate 8, Fig. 4). Moldic pores are common and are rarely filled with halite. Salt plugging is mostly present near the bottom 20 feet (6 m) of this lithofacies and occurs in intervals as large as 5 inches (13 cm) in thickness (see Plate 8, Fig 3.).

Preliminary Interpretation: The internal stratification of the reef rubble conglomerate coincides with the internal stack of facies observed in the nearby Reef Core Complex. The lower *coarse lithoclastic conglomerate* contains crinoids that belong to the lower reef core and upper bioherm facies. The mottled texture, consisting of light gray microcrystalline dolomite with dark gray lithoclasts, also corresponds to the mottled appearance of the bioherm. The overlying *skeletal lithoclastic conglomerate* contains tabulate corals and brachiopods, which correlate to the middle and upper reef core facies. This succession of lithoclast types supports an interpretation that reef rubble conglomerate deposition was contemporaneous with both the bioherm and the reef core. Well locations show that the talus slope is located less than 250 feet (76 m) from a Reef Core Complex type section in the windward direction, suggesting short transport distances of the large reef core lithoclasts. Because the reef core is interpreted to have existed above FWB, large storm events would likely result in the destruction and transport of reefal material. The slope of the reef complex is much steeper on the windward versus the leeward side because there is no reef apron on the windward side. Also, the package of conglomerate containing reef-building organisms in the windward direction of the Reef Core Complex is much thinner than the leeward reef apron. Therefore the talus facies would have been deposited in a deeper water environment

compared to the syndepositional reef core facies.

Stromatolite Rubble Conglomerate

General Description: The stromatolite rubble conglomerate is composed of a *stromatolitic lithoclast conglomerate*. This lithofacies has been identified in both Northern and Southern Trend Reefs (Huh, 1973; Gill, 1973). This conglomerate is different than the reef rubble because the clasts are almost completely composed of stromatolites. The clasts are poorly sorted with no preferred orientation. The original internal laminations of the stromatolites are easily observed (see Plate 9, Figs. 1 and 2). The stromatolite rubble conglomerate directly overlies the reef rubble conglomerate in this location and is 39 feet (12 m) thick.

Preliminary Interpretation: Due to the stromatolitic composition of the stromatolite rubble conglomerate, it is interpreted to have been deposited contemporaneously with the stromatolitic cap facies observed in the Reef Core Complex location. Similar to that of the underlying reef rubble conglomerate, this facies is interpreted to be a deeper water deposit rather than the intertidal environment of the stromatolitic cap in the Reef Core Complex location. It was most likely formed by storm events and higher wave energy breaking off pieces of semi-lithified stromatolites at the crest of the reef complex and depositing them in the windward direction as they traveled down the steep windward flanks short distances (less than 250 feet or 76 m).

Plate 8

core depth: 3205′ log depth: 3208′
Reef Rubble Conglomerate

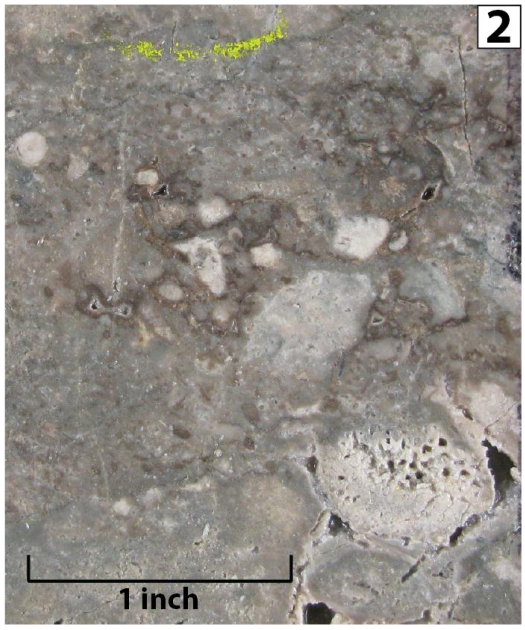

core depth: 3196′ log depth: 3199′
Reef Rubble Conglomerate

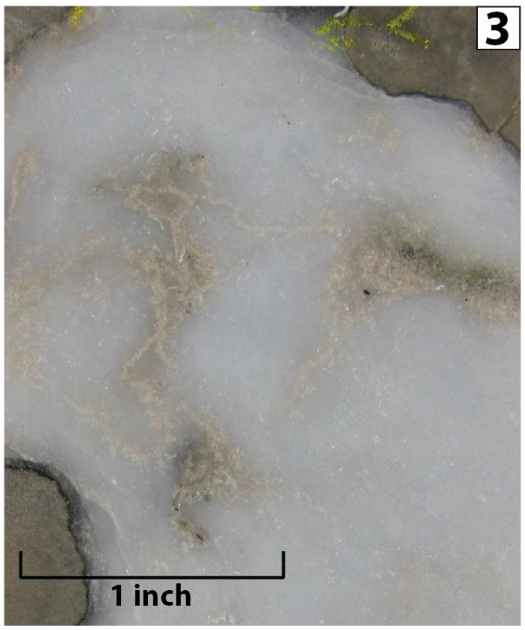

core depth: 3188′ log depth: 3191′
Anhydrite-Filled Vug
Reef Rubble Conglomerate

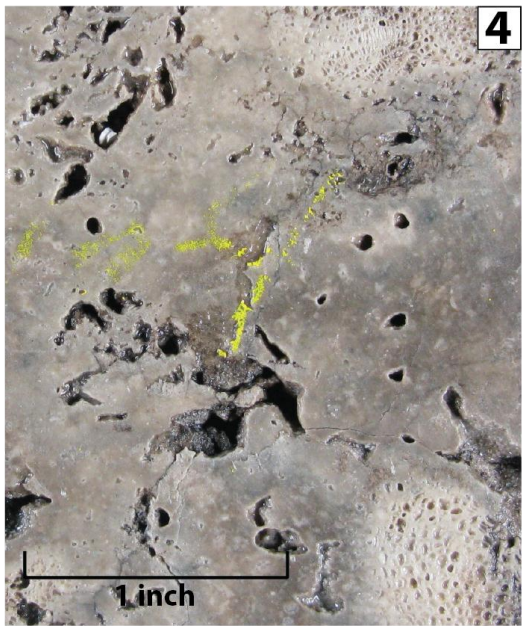

core depth: 3146′ log depth: 3149′
Reef Rubble Conglomerate

Plate 8. PN 27605 – Windward Reef Talus Rock Types:

Fig. 1. Reef rubble conglomerate – *coarse lithoclastic conglomerate***.** Light gray microcrystalline dolomite matrix with dark gray, large, angular crinoidal wackestone lithoclasts and salt filled vugs.

Fig. 2. Reef rubble conglomerate – *skeletal lithoclastic conglomerate***.** Favosites sp. corals and disarticulated brachiopods in a microcrystalline dolomite matrix. Large touching vugs present throughout.

Fig. 3. Reef rubble conglomerate. Anhydrite-filled vug 3 inches (8 cm) wide and 5 inches (13 cm) tall.

Fig. 4. Reef rubble conglomerate – *skeletal lithoclastic conglomerate***.** Favosites sp. corals and abundance of touching, moldic pores.

Plate 9

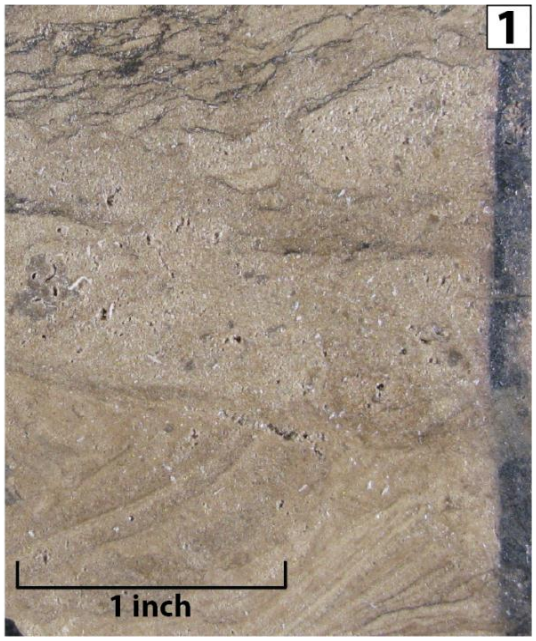

core depth: 3091′ log depth: 3094′
Stromatolite Rubble Conglomerate

core depth: 3064′ log depth: 3067′
Stromatolite Rubble Conglomerate

core depth: 3056′ log depth: 3059′
Cyanobacterial Mats

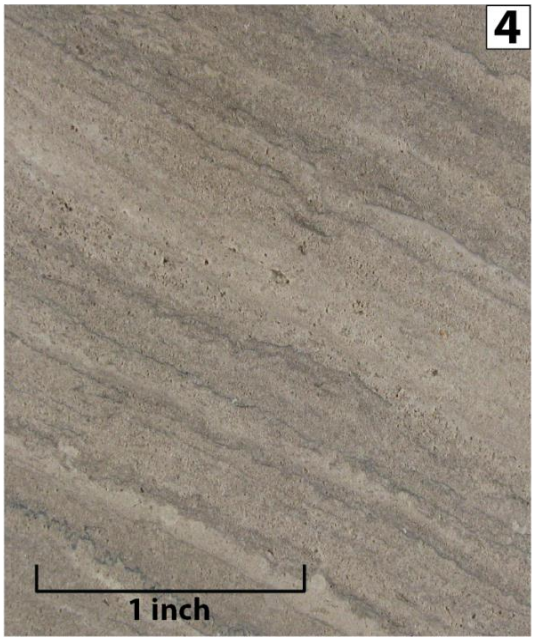

core depth: 3033′ log depth: 3036′
Cyanobacterial Mats

Plate 9. PN 27605 – Windward Reef Talus Rock Types:

Fig. 1. Stromatolite rubble conglomerate – *stromatolitic lithoclastic conglomerate***.** Fragments of stromatolitic bindstone. Brown color due to oil staining.

Fig. 2. Stromatolite rubble conglomerate – *stromatolitic lithoclastic conglomerate***.** Fragments of stromatolitic bindstone. Brown color due to oil staining.

Fig. 3. Cyanobacterial mats – *stromatolitic bindstone***.** Inclined beds composed of thinly-laminated crinkly stromatolites and small peloidal grains.

Fig. 4. Cyanobacterial mats – *stromatolitic bindstone***.** Inclined beds (up to 40 degrees) composed of alternating cyanobacterial mat laminations and stylolites.

Windward Reef Talus Wire-Line Log Signatures

The wire-line logs for this type section begin in the Gray Niagaran, represented by the high gamma ray log signature below the bioherm toe (see Fig. 3.10). The overlying reef rubble conglomerate exhibits relatively low gamma ray log intensities, similar to that of the reef core facies, which are interpreted to be the provenance of this conglomerate. Salt plugged intervals are present near the base of the reef rubble conglomerate and exhibit lower gamma ray log signatures with lower neutron porosity values. The upper 80 feet (24 m) of the reef rubble conglomerate is devoid of salt plugging and exhibits very good reservoir quality and oil staining. The major pore types present are touching vugs. The stromatolite rubble conglomerate exhibits much higher gamma ray log intensities than the underlying reef rubble conglomerate, which is similar to the higher gamma ray signature of the stromatolitic cap facies in the Reef Core Complex location. This stromatolite rubble conglomerate also exhibits the best reservoir quality, with porosity reaching 30% and permeabilities over 1000 mD. This is most likely a product of

the intense karsting observed at the top of this facies, which likely formed during a third-order sea-level drawdown and subsequent exposure. This interval is heavily oil stained.

The other three wells that belong to this type section location in the Columbus III field also have very similar petrophysical properties within the reef rubble and stromatolite conglomerates and are considered the best conventional reservoirs within the entire reef complex. The overlying cyanobacterial mat facies in this location has a gradational increase in gamma ray log response and also reaches permeability values upward of 100 mD. The cyanobacterial mat facies is composed almost entirely of intercrystalline porosity with little to no vugs, very different than the underlying conglomerate facies. Conventional whole core analysis data shows that the cyanobacterial mats interval was gas filled. The overlying oncolitic packstone and laminated peloidal wackestone facies all have significantly higher gamma ray log signatures than the underlying rocks, as well as much poorer reservoir quality. The A-2 Anhydrite overlies the laminated peloidal wackestone and is easily identified by its relatively low gamma ray log intensities.

Type Section 1: Windward Flank

Type section 1 is represented by a completely different stack of facies from any of the type sections previously described. However, this type section location is still greatly influenced by the processes that created the nearby Reef Core Complex, as well as subsequent deposition of the A-1 Carbonate. This type section is critical to a sequence stratigraphic interpretation of the reef complex because this location contains facies which were deposited during hiatus in deposition and erosion in other locations on the reef complex. Some depositional facies, such as the bioherm toe and distal reef rubble are very similar to those observed in the Windward Reef Talus location. However, the stacking pattern that follows, beginning with the deposition of the A-1 Anhydrite, is quite

different and therefore difficult to correlate to stratigraphic surfaces observed in the Reef Core Complex location. The cored interval for this type section spans 151 feet (46 m) of interbedded carbonate and anhydrite interpreted to have been deposited quasi-contemporaneously with depositional facies previously described in other reef complex locations.

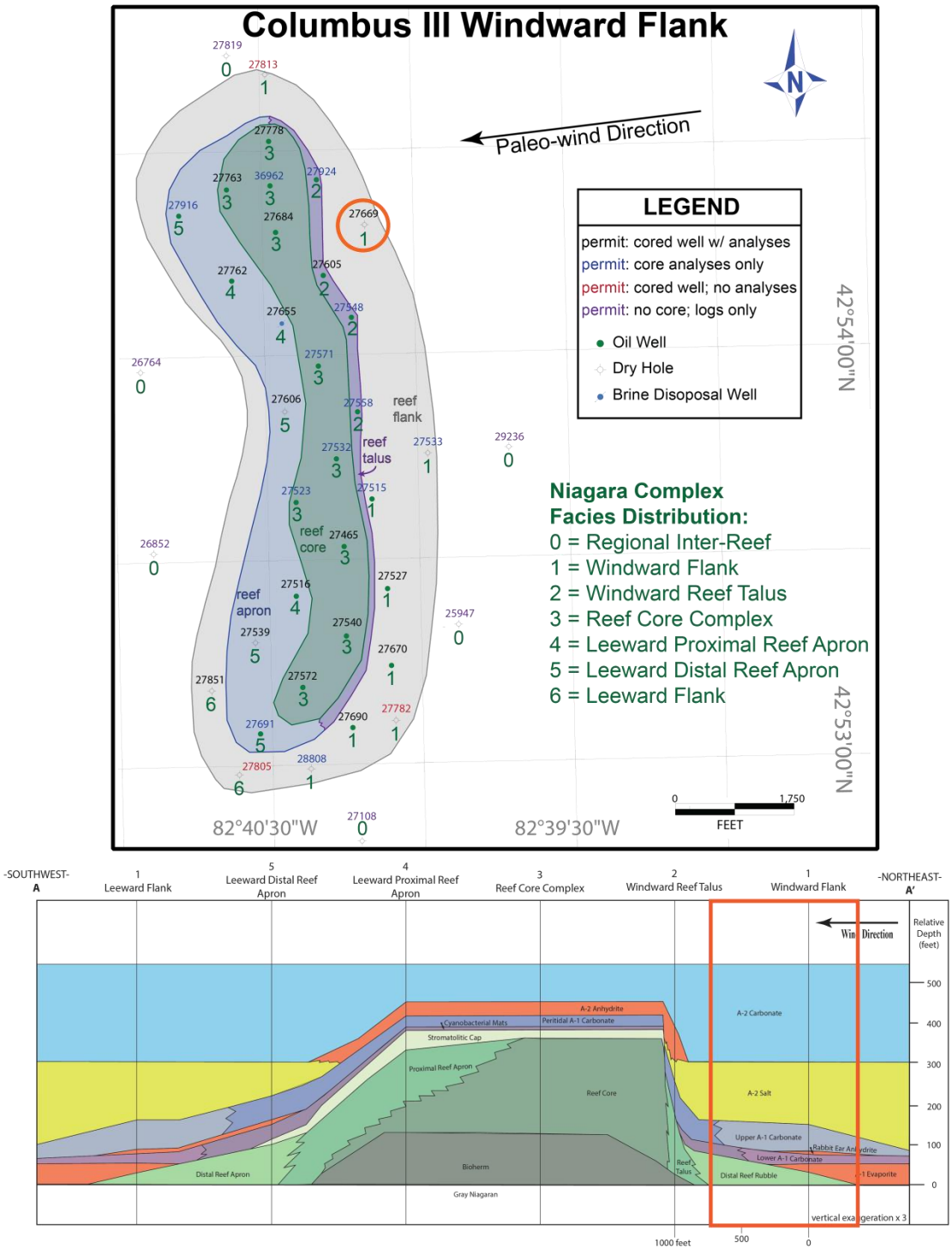

Figure 3.11. The Windward Flank type section location highlighted on the Columbus III Field map (upper) and reef complex cross-section (lower).

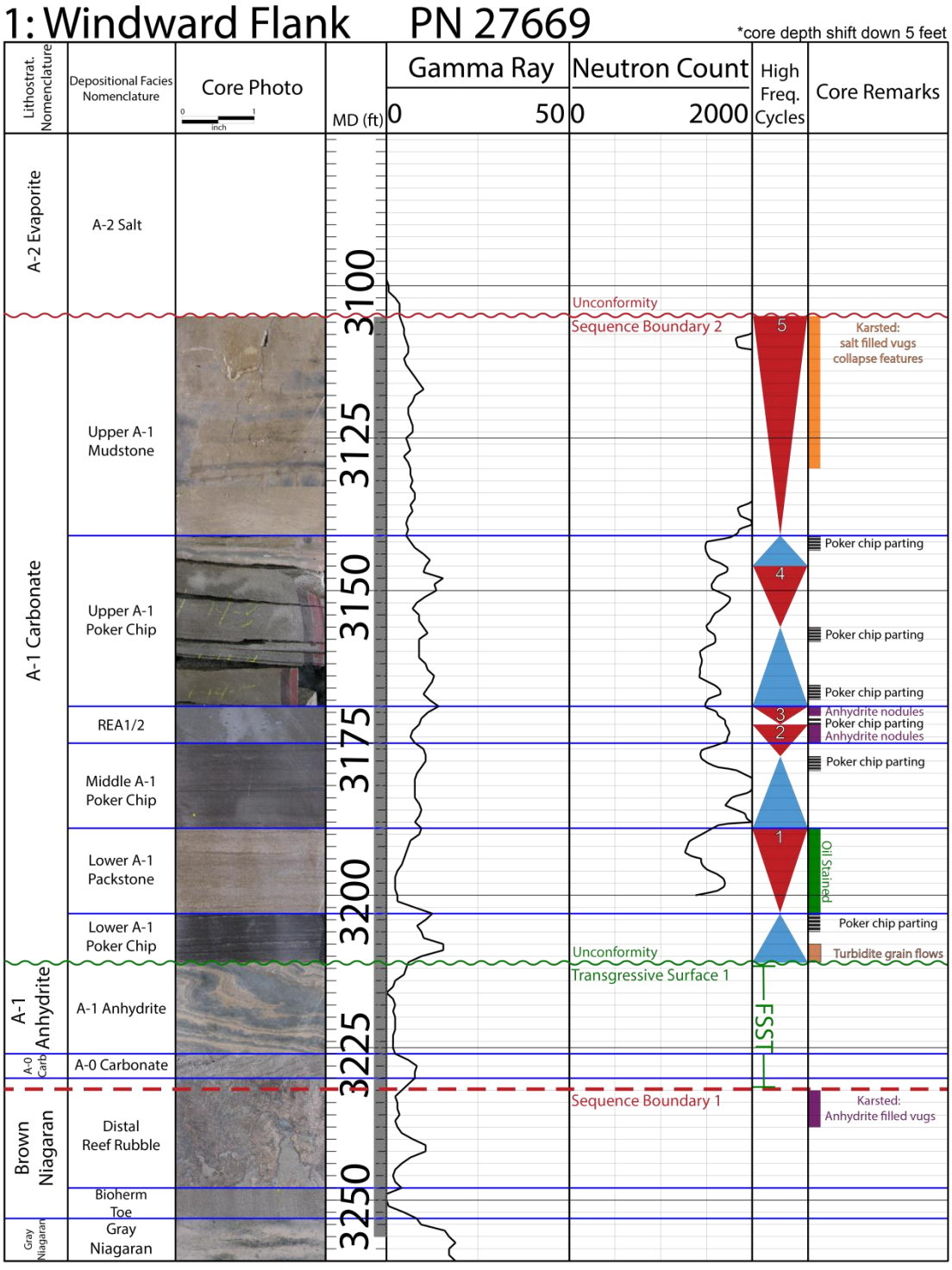

Figure 3.12. A single well cross-section of the 27669 well which illustrates the stack of facies for a windward flank location within the Niagara-lower Salina reef complex. Core depths were shifted down 5 feet to match wire-line log depths.

Type section 1 is represented by a stacking pattern most similar to that of the previously described Windward Reef Talus type section. However, the distal reef rubble in this location is much thinner (18 feet or 5 m) and the distinct internal stratification identified in the Windward Reef Talus location is not easily observed (see Fig. 3.12). The distal reef rubble is directly overlain by the A-0 Carbonate, which is only 4 feet (1 m) thick at this location, and gradationally transitions into the A-1 Anhydrite. The A-1 Anhydrite is unconformably overlain by the A-1 Carbonate lithostratigraphic unit composed of various lithofacies, which will be described in more detail below.

Distal Reef Rubble

General Description: The distal reef rubble is composed of a *skeletal lithoclastic conglomerate*. The lithoclasts are much smaller (1 mm to 1 cm in diameter) than the lithoclasts observed in the more proximal, Windward Reef Talus type section. No tabulate corals or stromatolite fragments are present. Vugs are prevalent and range in size from 1 mm to 2 cm in diameter. Most large vugs are filled with anhydrite cements. Light brown calcite cements are common and are destructive of the original rock fabric. The entire distal reef rubble is composed of dolomite with anhydrite cements throughout, making it difficult to identify original depositional textures. The distal reef rubble in the Windward Flank position ranges from 15 to 20 feet (5 to 6 m) in thickness.

Preliminary Interpretation: The Windward Flank location varies from 750 to 1500 feet (229 to 457 m) away from the Reef Core Complex location in the windward direction. As a result, the distal reef rubble at this location is composed of mostly smaller skeletal lithoclasts than the more proximal Windward Reef Talus location. The unit is also much thinner with an absence of large tabulate corals or stromatolite fragments as further evidence of the more distal location relative to the reef core. The rubble is interpreted to have been deposited in a slightly deeper water setting than the windward

talus reef rubble, as well as contemporaneous with the deposition of the bioherm, reef core, and stromatolitic cap. Because the bioherm is absent in this location, the bioherm toe is interpreted to be a product of eroding semi-lithified skeletal clasts from the nearby bioherm. This distal reef rubble is also interpreted to wedge out within a short distance away from the reef complex (1,500 feet or 457 m) in the windward direction and pass laterally into the "Regional Brown Niagaran" depositional facies (as described by Porcher, 1985). The distal reef rubble facies and the overlying A-0 Carbonate represent the most distal, reef complex-related carbonate deposition in the windward direction during Niagaran time.

A-0 Carbonate

General Description: The A-0 Carbonate is a laminated *crystalline dolomite*, most notable for its inclined laminations. The A-0 Carbonate directly overlies the distal reef rubble and gradationally transitions into the overlying A-1 Anhydrite. Original depositional textures are difficult to identify in this facies as it is composed almost entirely of dolomite rhombs. Laminations are thicker near the base (2-10 mm) and thin towards the contact with the overlying A-1 Anhydrite (less than 2 mm; see Plate 16, Fig. 1). These laminations are also inclined at angles up to 20 degrees and are often separated by jagged stylolites. The majority of pore types are separate vugs (see Plate 10, Fig. 4).

Preliminary Interpretation: Previous studies (Huh, 1973; Gill, 1973) have interpreted the undulating laminations of the A-0 Carbonate to be algal in origin, and therefore be indicative of a shallow, intertidal environment. These studies have also interpreted the A-0 Carbonate to unconformably overlie the distal reef rubble, placing it at the beginning of a transgressive systems tract, prior to the deposition of the A-1 Anhydrite. This interpretation implies that the transition from the A-0 Carbonate to the A-1 Anhydrite is merely a result of a gradual increase in salinity while remaining in a

shallow water environment (Huh, 1973).

While laminations are evident, the binding textures previously observed in the cyanobacterial mat facies are not present. Furthermore, when this facies is evaluated in the context of the underlying and overlying facies and the nature of their contacts, an alternative hypothesis may better fit the textures observed within this thin carbonate unit. Both contacts between the underlying distal reef rubble and overlying A-1 Anhydrite are gradational. As the distal reef rubble marks the end of sea level rise and deposition of the stromatolitic cap increasingly lower on the reef flank, the A-0 Carbonate is most likely the result of lithoclastic grain flows as a drop in sea level exposed the reef. As the reef complex was more extensively exposed, erosion would have continued and the further distance from the Reef Core Complex at this flank position would have resulted in the cyclic deposition of grain flows, interrupted by quiet periods of little to no deposition. As sea level dropped due to increasing restriction of normal marine water input and evaporation in the basin, salinities would have continued to increase near the base of the reef complex.. This important event would have resulted in inclined beds, composed of grain flows of the A-0 Carbonate, gradationally transitioning into the laminated sulfate deposition of the A-1 Anhydrite (see Plate 11, Figs. 1 and 2). The textures observed at the base of the A-1 Anhydrite facies are indicative of deeper water environments, which further disputes the interpretation of the A-0 Carbonate being an intertidal transgressive deposit. This interpretation suggests that the A-0 Carbonate is a low stand deposit transitional from the deepest water environments at its base (gradational contact with the underlying distal reef rubble) to intermediate depths upwards to the overlying contact with the A-1 Anhydrite.

Plate 10

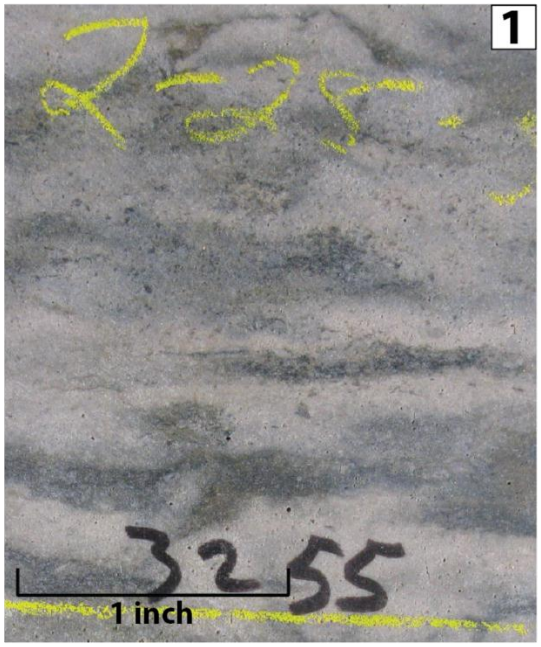

core depth: 3255′ log depth: 3260′
Gray Niagaran

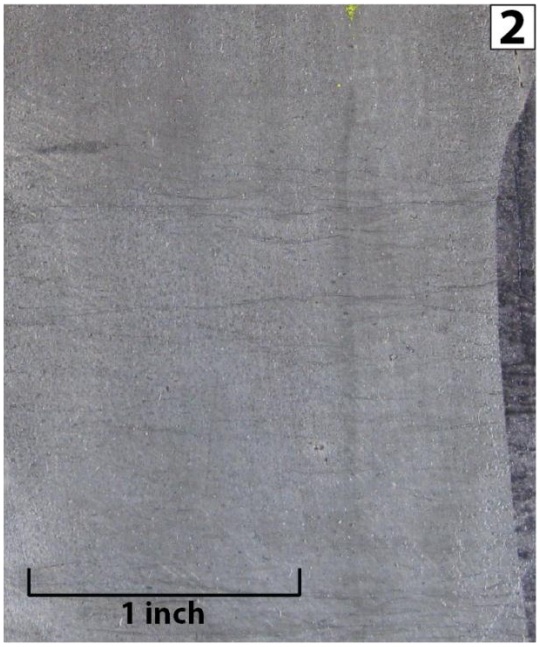

core depth: 3247′ log depth: 3252′
Bioherm Toe

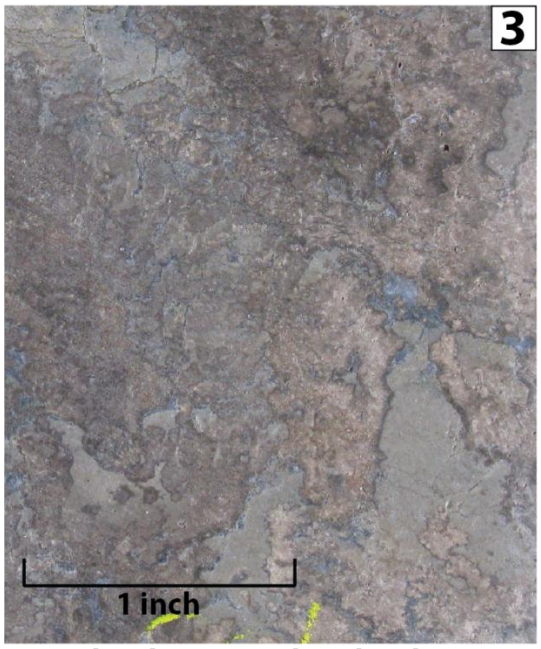

core depth: 3231′ log depth: 3236′
Distal Reef Rubble

core depth: 3224′ log depth: 3229′
A-0 Carbonate

Plate 10. PN 27669 – Windward Flank Rock Types:

Fig. 1. Gray Niagaran – *skeletal mudstone***.** Light to dark gray mottled appearance with small amounts of crinoid ossicles.

Fig. 2. Bioherm toe – *crystalline dolomite***.** Composed entirely of dolomite rhombs with intercrystalline porosity and wispy stylolites.

Fig. 3. Reef rubble conglomerate – *skeletal lithoclastic conglomerate***.** Fine-grained skeletal clasts with abundance of salt-filled vugs. Light brown calcite cement throughout.

Fig. 4. A-0 Carbonate – *crystalline dolomite***.** Steeply inclined beds composed of dolomite rhombs with abundance of small vugs and jagged stylolites.

A-1 Anhydrite

General Description: The A-1 Anhydrite is composed of a variety of different anhydrite fabrics which commonly transition from one fabric to another throughout the facies. The anhydrite fabrics observed have a pale gray color with a bluish hue. The very base of the A-1 Anhydrite is thinly laminated with dolomitic carbonate grains and anhydrite laminae (mm-scale laminites). Thin dolomicrite laminae and anhydrite are highly contorted. The anhydrite laminations are composed of tightly packed coalescing nodules (see Plate 11, Fig. 3). This basal section is the gradational transition with the underlying A-0 Carbonate.

The middle section of the A-1 Anhydrite contains a lower abundance of dolomicrite laminae and the anhydrite exists as a distorted mosaic fabric. The upper section of the A-1 Anhydrite consists of a *crystalline dolomite* composed of subrounded dolomite grains with both anhydrite laths and small nodular fabrics (see Plate 12, Fig. 1). The upper contact with the overlying lower A-1 poker chip facies is sharp, marked by thin, dark carbonate layers (see Plate 12, Fig. 2). The bottom 6 inches (15 cm) of the

overlying A-1 poker chip facies has small anhydrite crystals (less than .5 mm) throughout the dolomicrite matrix, as identified in thin section.

Preliminary Interpretation: The A-1 Anhydrite facies is interpreted to be an overall shallowing upward package from the gradational basal contact with the underlying A-0 Carbonate to the sharp contact with the overlying A-1 Carbonate. The lowermost anhydrite-dolomicrite laminations are thin (1-2 mm) and flat, and are representative of deeper water sulfate laminites compared to the more irregular laminations of shallow-water laminites (Kendall, 2010). While deeper water laminar sulfates often accumulate as pelagic rain (cumulate deposits), it is also possible that these thin, planar laminites represent evaporite turbidites which occur on basin slopes (Kendall, 2010). These thin, planar laminites grade into highly contorted dolomicrite and anhydrite layers. The highly contorted laminations are thus interpreted to be slightly shallower than the underlying flat laminites, but are still indicative of bottom-grown gypsum crystal crusts. Kendall (2010) shows very similar sluggy to flaser-like anhydrite deposits with well-preserved pseudomorphs of gypsum crusts in the Castile Evaporite of the Delaware Basin. This suggests that the basal section of the A-1 Anhydrite is a deep water sulfate deposit formed as bottom-growth gypsum crusts, rather than as sabkha deposits.

These deeper water gypsum-dolomicrite deposits grade into shallower water gypsum deposits, represented by anhydrite with distorted nodular-mosaic fabrics. This middle section of the A-1 Anhydrite is also interpreted to be a shallow-water (subtidal) gypsum deposit as opposed to a sabkha setting. Kendall (2010) states that various 'nodular' anhydrites constitute part of basin-wide, millennial cycles, either forming i) tops of incomplete cycles, or ii) transitions between laminated anhydrite below and halite above. Their position indicates the gypsum precursors formed when bottom basin brines were at the stage just prior to halite net accumulation (Kendall, 2010). This is an ideal analog for the A-1 Anhydrite as it marks the transition between thinly laminated anhydrite below, as well as the top of an incomplete cycle which culminates in the lateral

deposition of halite (A-1 Evaporite) in the basin center as sea-level continued to fall. Other examples of these restricted basin shallow-water gypsum deposits have been recorded in the Zechstein of northern Europe (Kendall, 2010).

The upper section of the A-1 Anhydrite consists of a *crystalline dolomite* that contains an abundance of anhydrite laths and small nodular fabrics. The anhydrite observed in this section is interpreted to be both displacive and intra-sediment precipitates. Both of these anhydrite textures are indicative of a sabkha environment, completing the shallowing upward sequence of the A-1 Anhydrite facies. The full shallowing upward sequence consists of: 1) the basal section characterized by deeper water (tens of meters) thin laminites, 2) the middle section characterized by shallower water (less than 10 meters) bottom-grown crusts, and 3) the upper section characterized by subaerial sabkha environments. The top of the A-1 Anhydrite is bounded by a transgressive flood back surface, which marks the transition to the overlying A-1 Carbonate facies (see Plate 12, Fig. 2).

Plate 11

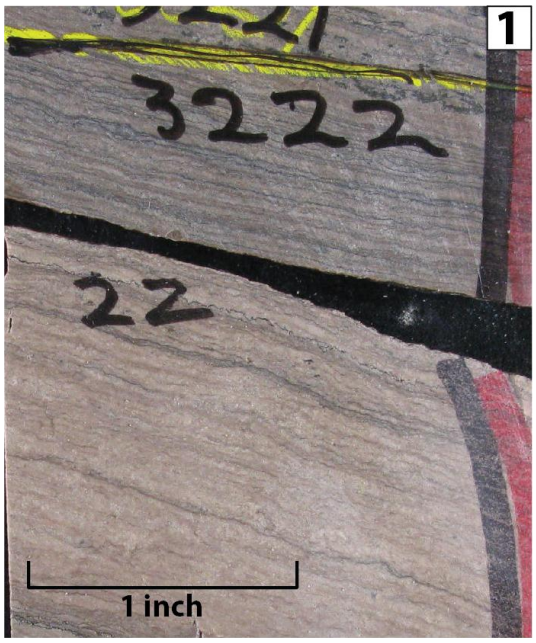

core depth: 3222′ log depth: 3227′
A-0 Carbonate

core depth: 3220′ log depth: 3225′
A-1 Anhydrite - A-0 Carbonate
Gradational Transition

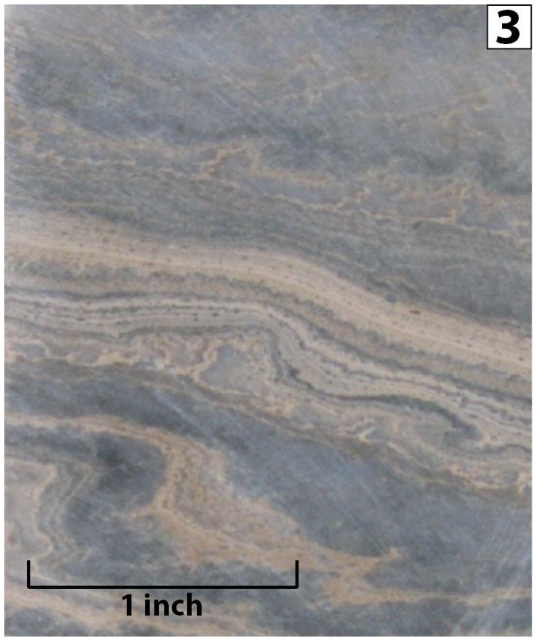

core depth: 3217′ log depth: 3222′
A-1 Anhydrite

core depth: 3208′ log depth: 3213′
A-1 Anhydrite

Plate 11. PN 27669 – Windward Flank Rock Types:

Fig. 1. A-0 Carbonate – *crystalline dolomite***.** Steeply inclined beds composed of dolomite rhombs transitioning from thicker (base) to thinner (top) laminations.

Fig. 2. A-1 Anhydrite – A-0 Carbonate contact. Gradational transition from the steeply inclined crystalline dolomite beds of the A-0 Carbonate to the thinly-laminated A-1 Anhydrite.

Fig. 3. A-1 Anhydrite – Dolomicrite and anhydrite laminae with tightly packed coalescing nodules; highly contorted laminae.

Fig. 4. A-1 Anhydrite – Nodular-mosaic anhydrite fabric at the base; dolomicrite with very small anhydrite nodules at the top.

Lower A-1 Poker Chip

General Description: The lower A-1 poker chip is composed of a *thinly-laminated mudstone*. This lithofacies consists of brown to gray carbonate mudstone laminae alternating with dark brown to black carbonaceous films. Parting typically occurs along the laminations, which has been termed "poker-chip" parting in Michigan. These shaley, carbonaceous laminations are planar and are less than 1mm in thickness. The carbonaceous streaks have small scale undulations with random spacing. Typically the carbonaceous films are so densely packed that they overlie one another without any intervening carbonate sediment. Thin, cm-scale beds of tan carbonate mudstone with an abundance of scattered carbonaceous mat chips exhibit graded bedding, with a higher abundance of chips towards the base of the interval (see Plate 12, Fig. 3).

Preliminary Interpretation: The *thinly-laminated mudstone* lithofacies is characterized by its thin, alternating laminations of carbonate mudstone and carbonaceous films. Previous studies (Gill, 1973; Huh, 1973) have interpreted the carbonaceous films to be remains of planar cyanobacterial stromatolitic mats. Gill (1973)

ruled out the possibility that these planar films could be subtidal deposits based on work by Bathurst (1971), who proposed that grazing and burrowing organisms digested and left no trace of subtidal mats in Berry Island, Bahamas. Therefore, Gill (1973) interpreted these cyanobacterial mats to form in the intertidal zone of a hot, arid tidal flat environment similar to the present Persian Gulf. However, more recent studies have shown that planar microbial films, laminae, and stromatolites produced by photosynthetic microbes can form anywhere in the photic zone, including tranquil lagoon settings (Pratt, 2010). These deeper water, planar microbial laminae can be explained as either the onset of elevated salinity or elevated temperature while remaining submerged (Pratt and Haidl, 2008). Famous examples of these tranquil, restricted subtidal, microbially laminated carbonates include the Late Jurassic Solnhofen Limestone of southern Germany, as well as the Early Silurian of the Eramosa Formation of southern Ontario (Pratt, 2010).

Another study by Elrick and Snider (2002) showed similar sedimentological features of deep-water cyclic deposits observed in the Middle Cambrian Marjun Formation of Nevada and Utah. Petrographic evidence in this study indicated that the thin carbonaceous films were precipitated *in situ* from the activity of benthic microbial communities which thrived in a deep-water, below storm wave-base setting. These benthic microbial communities thrived during periods of decreased input of fine detrital carbonate transported from nearby shallow-water carbonate factories, and struggled during periods of increased detrital carbonate input as sea-level fell and the carbonate factory prograded (Elrick and Snider, 2002). This same cyclicity is observed in the poker chip facies throughout the A-1 Carbonate as the thickness between microbial films varies throughout the thinly-laminated mudstone, as well as throughout the overlying micro-laminated mudstone lithofacies. Therefore, the depositional environment of the more densely packed the carbonaceous films, is interpreted to be further away from the up-slope carbonate factory, which actively sheds detrital carbonate downslope.

Further evidence that supports a subtidal environment of deposition for the *thinly laminated mudstone* lithofacies is the presence of graded deposits, interpreted as storm or gravity induced turbidites. These turbidite deposits (see Plate 12, Fig. 3) are characterized by thicker beds (1 to 3 inches, or 3 to 8 cm) of tan dolomite with an abundance of scattered black mat chips throughout. The dolomite grains appear to be peloidal in origin, however dolomitization has resulted in the lack of conclusive evidence. Whether peloids or not, these carbonate grains were most likely derived from a nearby carbonate factory, upslope on the reef complex where shallower water environments existed. The black mat chips are most likely ripped up from underlying microbial laminations, and are most dense near the base of the bed. Therefore, these beds are interpreted to be the result of single storm events, which resulted in the grading of rip-up mat chips in a grain flow of detrital carbonate grains derived from a nearby, shallower water location on the complex. These turbidite deposits also only exist in flank locations proximal to the reef complex (less than 1,500 feet, 457 m), while only thinly-laminated poker-chips are observed in more basinal and inter-reef locations. Also, in basin center cores, the entire A-1 Carbonate unit exists as thinly-laminated poker chips, bounded by the A-1 Evaporite (halite) below and the A-2 Evaporite (halite) above.

Lower A-1 Packstone

General Description: The lower A-1 packstone ranges from 6 to 16 feet (2 to 5 m) in thickness, and is a crystalline dolomite composed of tan dolomite rhombs. This facies has the best porosity and permeability of the A-1 Carbonate unit, with intercrystalline porosity being the dominant pore type. The dolomite rhombs range from 30 to 50 microns in diameter (as identified in thin section). Stylolites are present and oil staining occurs throughout this interval (see Fig. 3.12).

Preliminary Interpretation: Due to intense dolomitization it is very difficult to identify the original depositional texture of this facies. The carbonate grains present are most likely the result of grain shedding from a nearby upslope carbonate factory in a peritidal environment. Although this facies is a crystalline dolomite, the term packstone has been assigned as an attempt to interpret the original depositional rock type prior to dolomitization. Further observations would be necessary in other fields where this facies has not been dolomitized to identify the true depositional rock fabric. The occurrence of a peloidal wackestone, as observed in the upslope reef core complex position, is evidence that soft-bodied benthos existed in subtidal environments during the deposition of the A-1 Carbonate, which could have resulted in abundant peloidal grains shed downslope. In any case, this facies is interpreted to be subtidal and the result of carbonate grain production and down slope transport.

Plate 12

core depth: 3207′ log depth: 3212′
A-1 Anhydrite

core depth: 3206′ log depth: 3211′
Lower A-1 Poker Chip - A-1 Anhydrite Contact
Transgressive Surface

core depth: 3201′ log depth: 3206′
Lower A-1 Poker Chips

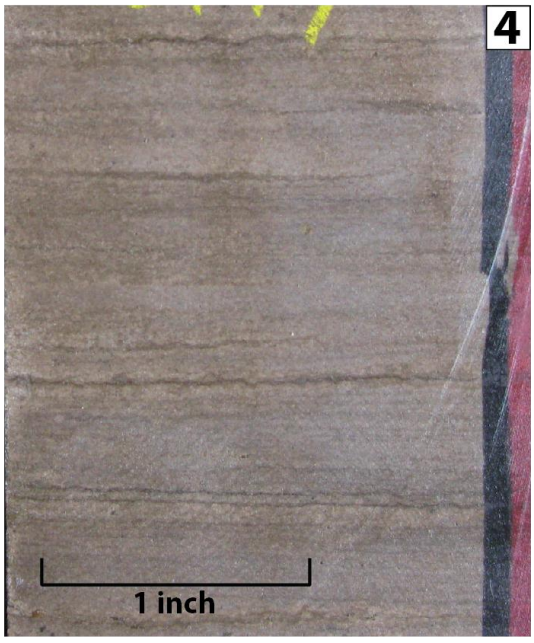

core depth: 3196′ log depth: 3201′
Lower A-1 Packstone

Plate 12. PN 27669 – Windward Flank Rock Types:

Fig. 1. A-1 Anhydrite – *crystalline dolomite***.** Subrounded dolomite grains with an abundance of anhydrite laths throughout.

Fig. 2. Lower A-1 poker chip – A-1 Anhydrite contact (transgressive surface). Sharp contact marked by dark, thin carbonate layers which separates the underlying A-1 Anhydrite and the overlying lower A-1 poker chip facies.

Fig. 3. Lower A-1 poker chips – *thinly-laminated carbonaceous mudstone*. Thin carbonate mudstone laminations with carbonaceous films. Turbidite bed deposit in middle with graded bedding.

Fig. 4. Lower A-1 packstone – *crystalline dolomite*. Tan, massively bedded *crystalline dolomite* composed of dolomite rhombs with stylolites and oil staining.

Middle and Upper A-1 Poker Chips

General Description: The middle and upper A-1 poker chips are composed of a *thinly-laminated carbonaceous mudstone*, as well as a *micro-laminated mudstone*. The *thinly-laminated carbonaceous mudstone* is very similar to that described in the lower A-1 poker chip facies, with slight variations in color and laminae thickness. There are also no turbidite deposits observed in these facies. The *micro-laminated mudstone* is composed of microcrystalline dolomite and has less abundant carbonaceous seams than the *thinly-laminated carbonaceous mudstone*. Carbonaceous mat chips occur, scattered throughout the mudstone. Little to no porosity exists in the *micro-laminated mudstone*, as the microcrystalline dolomite crystals are very tightly packed. The main differentiating factor between the two lithofacies is the presence of alternating carbonaceous films in the *thinly-laminated carbonaceous mudstone*, which is also usually accompanied by poker-chip parting. The *micro-laminated mudstone* is massively

bedded with little to no carbonaceous material.

Preliminary Interpretation: The *thinly-laminated carbonaceous mudstone* within this depositional facies is interpreted to be an identical deposit to that of the lower A-1 poker chip facies. Rather than intertidal to supratidal cyanobacterial mats, these *thinly-laminated carbonaceous mudstones* are believed to be deeper water, planar microbial films which formed at deeper depths due to benthic microbial communities thriving in elevated temperatures during this time in the Michigan Basin. The *micro-laminated mudstone* lithofacies is most likely deposited in a subtidal environment, but is interpreted to be a shallower water environment than the *thinly-laminated carbonaceous mudstone*. As a small relative sea-level fall or slow-down of sea-level rise would have resulted in the progradation of the carbonate factory down the slope of the reef complex, this would increase the detrital carbonate input in the flank location. The presence of carbonaceous mat chips possibly represents incipient microbial film formation that never coalesced into continuous mat surfaces. Possible explanations for these discontinuous carbonaceous films could be: 1) an increase in mat grazing and burrowing organisms during this time, or 2) unfavorable conditions for continuous microbial mat growth, such as less sunlight. A third explanation could simply be an increase in detrital carbonate input and more energetic conditions, resulting in the microbial films to never fully coalesce. Whichever mechanism is responsible, the *micro-laminated mudstone* lithofacies only occurs in close proximity to the reef complex, while basin-center cores exhibit densely packed carbonaceous films with little to no detrital carbonate.

Rabbit Ear Anhydrite 1 and 2

General Description: The rabbit ear anhydrite facies is composed of *nodular anhydrite* in a groundmass of micro-laminated carbonate mudstone. The rabbit ear anhydrite exists in two intervals (REA1 and REA2) in many flank well locations. The

anhydrite is composed of white to bluish nodules of varying sizes, ranging from 1 to 5 mm in diameter and are flattened parallel to bedding (see Plate 11, Fig.2). Adjacent nodules also coalesce in some intervals, resulting in distorted nodular or nodular mosaic fabrics.

Preliminary Interpretation: The nodular anhydrite fabrics observed in this depositional facies are indicative of subaqueous gypsum deposits. Nodular anhydrite has often been interpreted to form as an early diagenetic product within the capillary zone of unconsolidated sediments in the exposed parts of supratidal flats of arid regions (Kendall, 2010). However, these nodular fabrics do not display a typical stacking pattern of a sabkha deposit (as described by Schreiber and Tabakh, 2000), which is often capped by an erosional surface (as observed in the A-1 Anhydrite). Therefore, the rabbit ear anhydrites are interpreted to be subaqueous gypsum deposits which have been diagenetically altered to anhydrite via dehydration.

Upper A-1 Mudstone

General Description: The upper A-1 mudstone is composed of a *micro-laminated mudstone*. This mudstone lithofacies has a variety of colors ranging from tan, to gray, to dark brown, and is composed mostly of limestone. Vertical fractures lined with halite and blocky anhydrite are abundant towards the upper contact of this facies, which is directly overlain by the A-2 Evaporite unit. This very fine crystalline carbonate facies has the lowest porosity and permeability of any of the facies belonging to the A-1 Carbonate unit, and it is also the only facies that has not undergone complete dolomitization. The few laminations observed in this facies are discontinuous parallel to sub-parallel. Anhydrite occurs as small, isolated laths scattered within the surrounding micritic limestone matrix.

Preliminary Interpretation: The *micro-laminated mudstone* in this depositional

facies is interpreted as a subtidal deposit, identical to that of the previously described *micro-laminated mudstone* of the poker chip facies. The vertical fractures and halite filling observed near the top of this lithofacies is interpreted to be a product of secondary alteration (karsting), with the overlying A-2 Evaporite unit as the source of halite saturated connate fluids. The high content of carbonate mud and lack of microbial mats in this facies is evidence for unfavorable conditions for microbial mat growth.

Plate 13

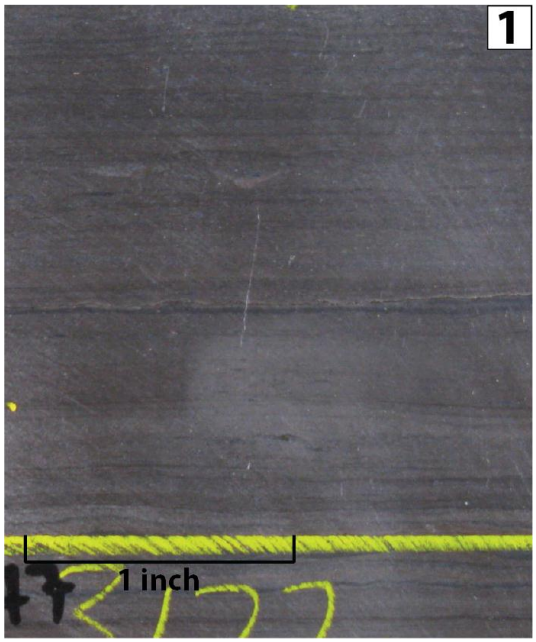

core depth: 3177′ log depth: 3182′
Middle A-1 Poker Chips

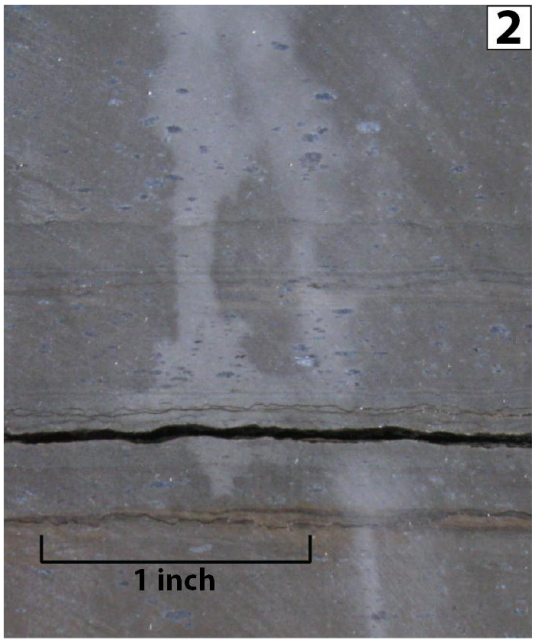

core depth: 3169′ log depth: 3174′
Rabbit Ear Anhydrite 1

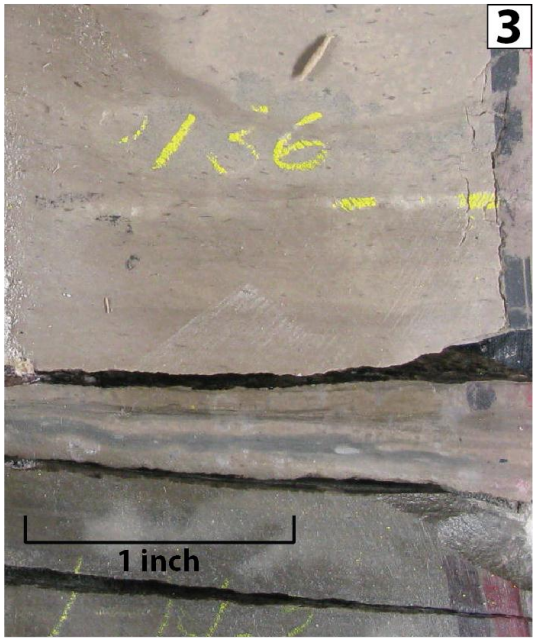

core depth: 3136′ log depth: 3141′
Upper A-1 Mudstone - Upper A-1 Poker Chip Contact

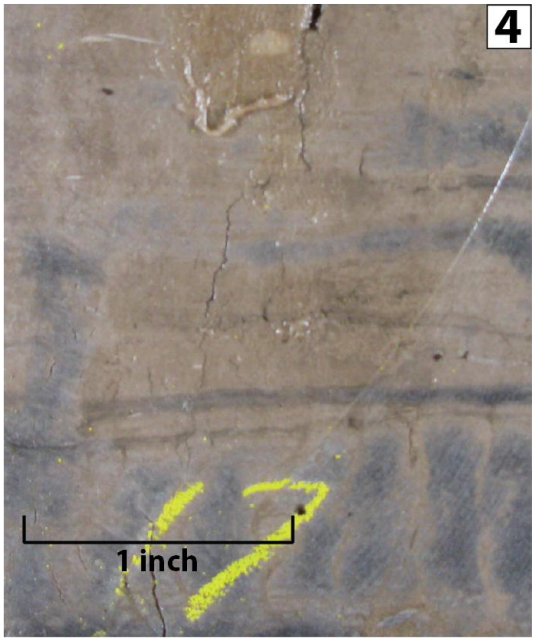

core depth: 3116′ log depth: 3121′
Upper A-1 Mudstone

Plate 13. PN 27669 – Windward Flank Rock Types:

Fig. 1. Middle A-1 poker chips – *thinly-laminated mudstone*. Laminated microcrystalline dolomite with mm-scale carbonaceous seams and scattered mat chips.

Fig. 2. Rabbit ear anhydrite 1 – *nodular anhydrite*. 1 to 5 mm in length nodules of bluish anhydrite, flattened parallel to bedding. Nodules exist within a micro-laminated microcrystalline dolomite groundmass.

Fig. 3. Upper A-1 mudstone – Upper A-1 poker chip contact – Gradational contact between the underlying *thinly-laminated mudstone* with the overlying *micro-laminated mudstone*.

Fig. 4. Upper A-1 mudstone – *micro-laminated mudstone*. Tan and gray micro-laminated mudstone with vertical fractures lined with halite.

Windward Flank Wire-Line Log Signatures

The wire-line logs for this type section begin in the Gray Niagaran, represented by the high gamma ray log signature below the bioherm toe (see Fig. 3.12). The overlying bioherm toe has low gamma ray log intensities, overlain by the fluctuating signature of the distal reef rubble. The gamma ray through the upper section of the distal reef rubble is relatively low, and is gradationally transitional into a slightly higher gamma ray log signature as the facies transitions into the inclined beds of the A-0 Carbonate. The gamma ray log signature abruptly transitions into lower intensities within the A-1 Anhydrite unit, and has slightly higher intensities in the upper portion of the shallow sabkha, *crystalline dolomite* lithofacies of the A-1 Anhydrite.

The A-1 Anhydrite is directly overlain by the lower A-1 poker chip facies, which is carbonaceous and exhibits a much higher gamma ray log signature (15-25 API units). The lower A-1 poker chip is overlain by the lower A-1 packstone, which is bounded by

the middle A-1 poker chip at the top. The lower A-1 packstone has the best reservoir quality of the A-1 Carbonate unit and is oil stained in every location. It is also stratigraphically bounded above and below by the carbonaceous poker chip facies, which are most likely the source of hydrocarbons. The lower A-1 packstone can be identified in wire-line logs by a well-defined low gamma ray shoulder, as well as an increase in neutron porosity (decrease in neutron counts). The lower A-1 packstone gradationally increases in gamma ray intensity into the overlying middle A-1 poker chip facies, which is more readily identified by the increase in neutron count. A slight decrease in gamma ray response is observed for the rabbit ear anhydrite facies, which increases again into the upper A-1 poker chip facies.

The upper-most interval of the non-carbonaceous *thinly-laminated mudstone* lithofacies within the upper A-1 poker chip facies marks the end of the highest gamma ray log intensities in this type section. The overlying upper A-1 mudstone has slightly lower gamma ray intensities (~10 API units). The upper A-1 mudstone is abruptly capped by the A-2 Evaporite unit, which has gamma ray log values nearing 0 API units. Although the gamma ray log never reaches 20 API units in this type section location, small variations and gradational gamma ray transitions are observable and useful for identifying the depositional facies stacking pattern and for correlation. For this reason it is very useful to display the gamma ray log track scale from 0 to 50 API units in order to better observe these small fluctuations.

Type Section 6: Leeward Flank

Type section 6 is represented by very similar depositional facies to the Windward Flank location of type section 1. The depositional facies observed in the A-1 Carbonate unit are completely controlled by inherited paleo-topography developed during the growth of the Niagaran reef complex. That is why very similar stacking of A-0 and A-1

facies are observed in the Windward and Leeward Flank positions, as they both overlie Niagaran sediments less than 20 feet (6 m) thick in the bioherm toe and distal reef rubble facies. The cored interval for this type section spans 152 feet (46 m) and represents the Gray Niagaran, Brown Niagaran, A-0 Carbonate, A-1 Anhydrite, and A-1 Carbonate lithostratigraphic units. The cored section tops out in the upper A-1 mudstone depositional facies of the A-1 Carbonate, 16 feet (5 m) below the contact with the A-2 Evaporite unit.

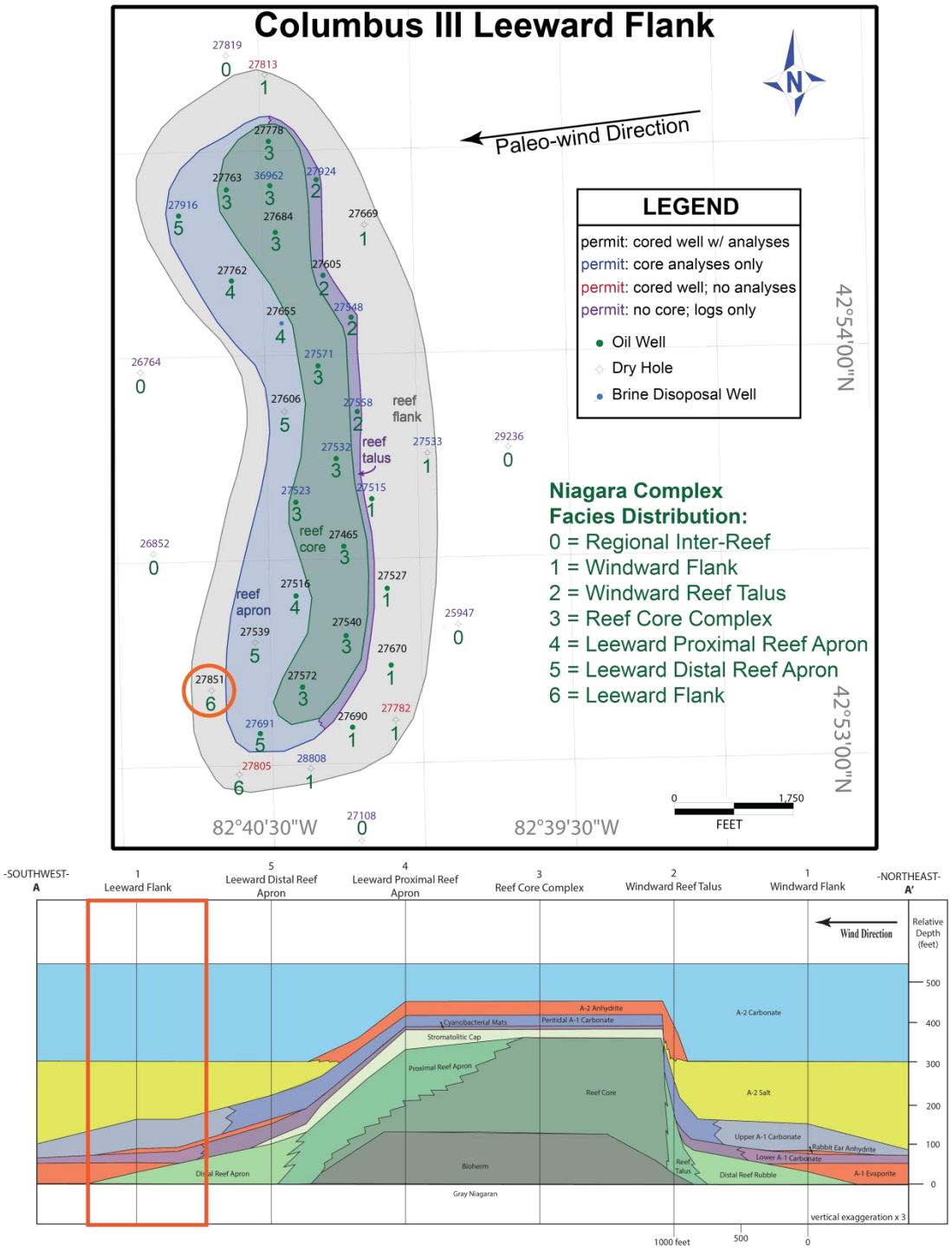

Figure 3.13. The Leeward Flank type section location highlighted on the Columbus III Field map (upper) and reef complex cross-section (lower).

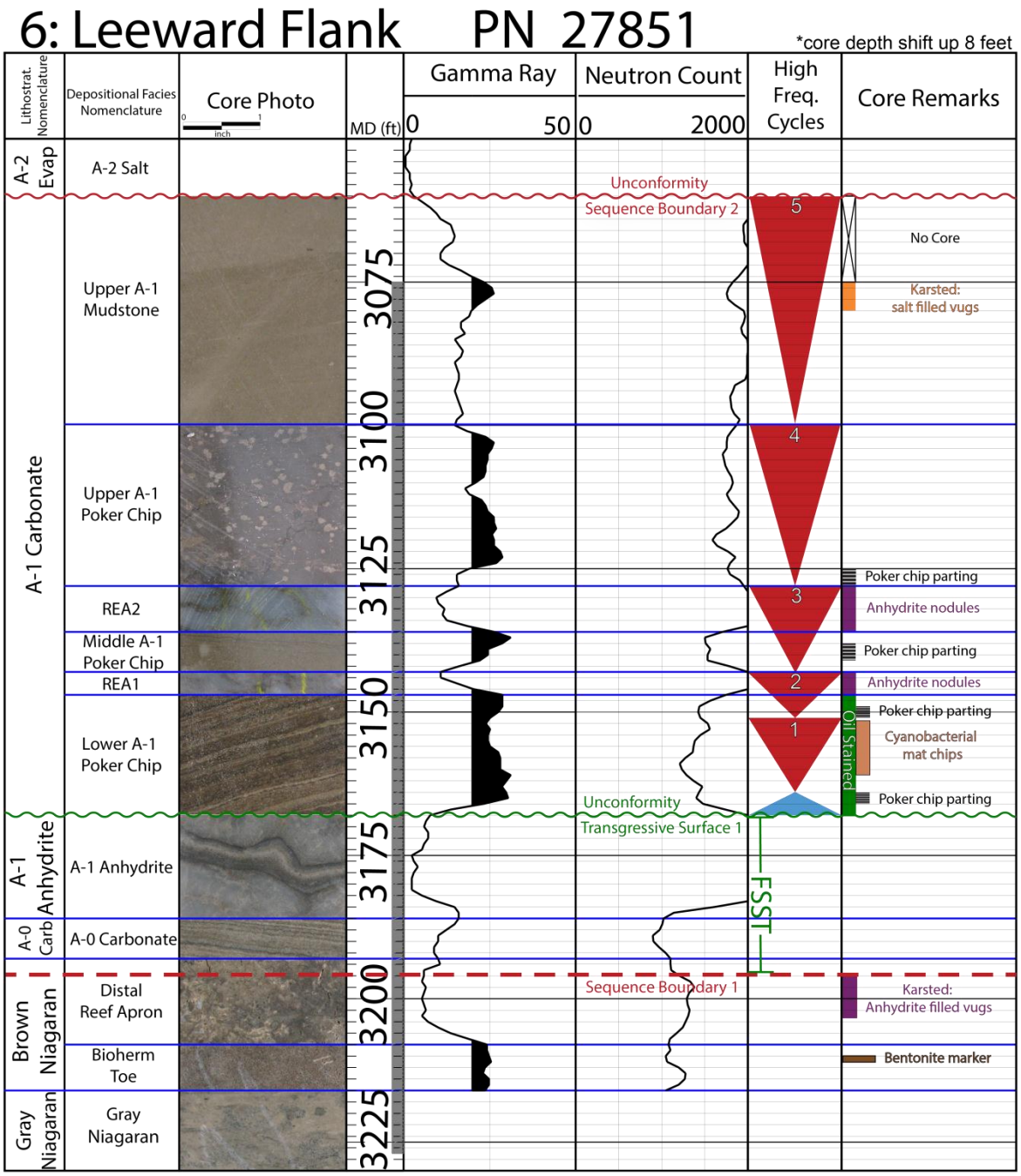

Figure 3.14. A single well cross-section of the 27851 well which illustrates the stack of facies for a leeward flank location within the Niagara-lower Salina reef complex. Core depths were shifted up 8 feet to match wire-line log depths.

The stack of depositional facies in Leeward Flank only varies slightly from that of the Windward Flank. The first major difference is that the lower A-1 poker chip facies is more inclined in this location, with more grainy laminae alternating with carbonaceous mats (see Plate 14, Fig. 2). It appears to look more like the A-0 Carbonate facies, which is interpreted as inclined grain flows, versus the deeper water microbial mats that constructed the *thinly-laminated carbonaceous mudstone* facies observed in the Windward Flank. This lower A-1 poker chip facies is also oil stained in this location, with much higher porosity values than the lower A-1 poker chip facies of the Windward Flank (see Fig. 3.14). This facies is also directly overlain by the first rabbit ear anhydrite, which means that the lower A-1 packstone facies is not present in this location. The lower A-1 packstone facies in type Section 1 is bounded on either side by the carbonaceous poker chip facies, and therefore oil stained in that location. This could mean that the lower A-1 poker chip facies in this location is better correlated to the lower A-1 packstone facies in the Windward Flank location, or be a combination of both the lower A-1 poker chip and lower A-1 packstone at that location.

This type section also exhibits both rabbit ear anhydrites, with much larger anhydrite nodules than are observed in the Windward Flank location. The "rabbit ears" were given their name because they are expressed as two prominent, closely-spaced "kicks" in both the neutron and gamma ray logs, representing the shape of rabbit ears (see Fig. 3.14). The rabbit ear anhydrite facies in this location also exhibit different fabrics, with much larger anhydrite nodules coalescing into nodular-mosaic fabrics (see Plate 14, Fig. 3). The nodules in these facies range from 3 to 6 cm in diameter, which is much different than in the Windward Flank location where they were much smaller in size (1 to 5 mm in diameter). The last major difference is that the middle and upper poker chip facies in this location do not exhibit poker-chip parting, as the lithofacies comprising these depositional facies lack the carbonaceous layers, and are micro-laminated and massively bedded mudstones (see Plate 14, Fig. 4).

Plate 14

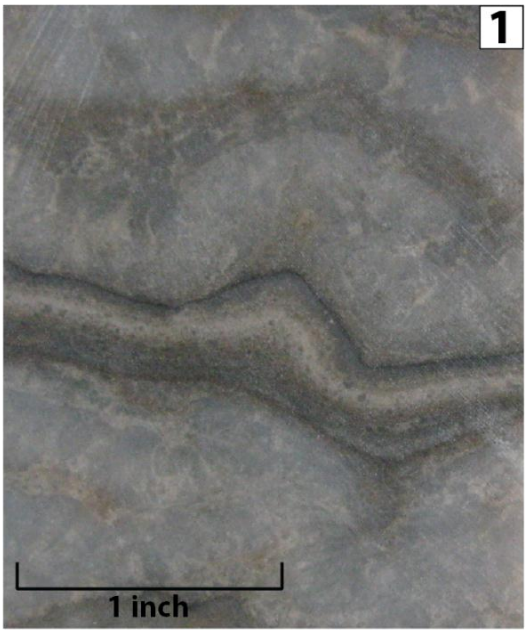

core depth: 3192′ log depth: 3184′
A-1 Anhydrite

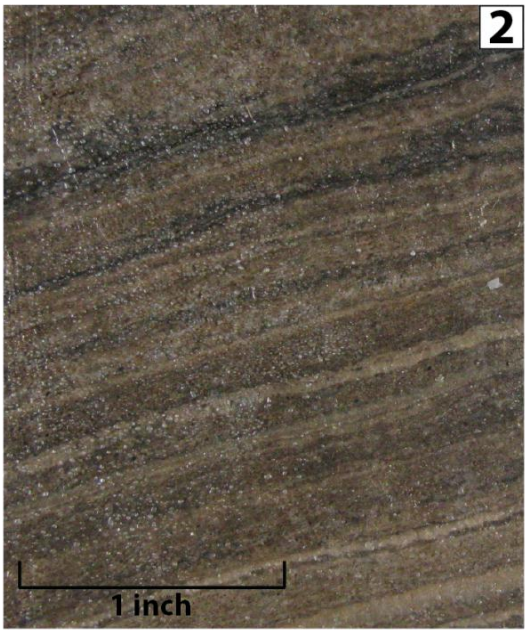

core depth: 3175′ log depth: 3167′
Lower A-1 Poker Chips

core depth: 3154′ log depth: 3146′
Rabbit Ear Anhydrite 1

core depth: 3149′ log depth: 3141′
Middle A-1 Poker Chips

Plate 14. PN 27851 – Leeward Flank Rock Types:

Fig. 1. A-1 Anhydrite – Laminated dolomicrite laminae with anhydrite consisting of tightly packed coalescing nodules; laminations are highly contorted.

Fig. 2. Lower A-1 poker chip – *thinly-laminated mudstone*. Laminated brown dolomitic mudstone with mm-scale black carbonaceous seams.

Fig. 3. Rabbit ear anhydrite 1 – *nodular anhydrite*. Nodular-mosaic anhydrite fabric with coalescing nodules ranging from 3 to 6 cm in diameter.

Fig. 4. Middle A-1 poker chip – *micro-laminated mudstone*. Tan, massively bedded microcrystalline dolomite with thin, black carbonaceous layers and scattered mat chips.

Leeward Flank Wire-Line Log Signatures

The wire-line log signatures observed in type section 6 are very similar to those of type section 1, with some minor differences. One main difference is that the overall gamma ray log signatures show higher intensities for this facies. In type section 1, none of the higher gamma ray log signature facies are higher than 20 API units, whereas all of the higher gamma ray log signature facies in type section 6 exceed 20 API units (as highlighted in black, Fig. 3.14). The evaporite units in both type sections have relatively low gamma ray log signatures and can be easily identified (A-1 Anhydrite, REA1, REA2, and A-2 Evaporite). The rabbit ear anhydrite facies exhibit two closely-spaced kicks in both the neutron and gamma ray logs and are easily identified in un-cored wells. Oil staining occurs within the lower A-1 poker chip facies in this location, as the oil stained lower A-1 packstone facies in type section 1 is not present here. The lower A-1 poker chip facies in this location, however does not exhibit poker-chip partings along laminations, and there is a greater abundance of grainy beds between carbonaceous laminations.

Facies Analysis Summary

Six type sections from cored wells were used to describe the vertical stack of facies throughout the Columbus III Niagara-lower Salina reef complex. Depositional facies were based on a variety of interpreted depositional environments from observations such as rock type, faunal assemblages, and sedimentary structures. The major depositional facies were further sub-divided into lithofacies (e.g. *coral/stromatoporoid boundstone*, *skeletal wackestone*), which are based on Dunham's (1962) classification scheme for carbonates. Each lithofacies has significant implications on both relative water depth and spatial positioning on the reef complex. The depositional facies have been assigned to their correct lithostratigraphic unit (Niagara, Salina) and are summarized in the following tables:

Niagara Facies Classification

Depositional Facies	Lithofacies	Lithologic Attributes	Depositional Environment	Reef Complex Location
Bioherm	*crinoidal mudstone*	Mottled gray and white; micritic mud matrix; crinoid ossicles; abundant stromatactis	Below SWB	3, 4
	skeletal wackestone	Mottled gray and white; micritic mud matrix; crionid ossicles, bryozoans, tabulate corals, rugose corals; abundant stromatactis	Between SWB and FWB	3, 4
Bioherm toe/cap	*crystalline dolomite*	Devoid of fossils; composed of dolomite rhombs; intercrystalline porosity	Above FWB	1, 2, 3, 4, 5, 6
Reef core	*coral/stromatoporoid boundstone*	Frame-building organisms (tabulate corals, stromatoporoids)	Above FWB	3, 4
	skeletal wackestone	Intra-reef faunal assemblages (bryozoans, brachiopods, crinoids, rugose corals); 50-75% micritic mud matrix	Between SWB and FWB	3, 4
Stromatolitic cap	*hemispheroid stromatolitic bindstone*	Dark brown; laterally-linked hemispheroid stromatolites	Above FWB to Intertidal	3, 4, 5
	skeletal wackestone	Skeletal fragments composed of reef core organisms (tabulate corals, brachiopods, bryozoan); abundant cements	Above FWB to Intertidal	3, 4, 5
Proximal reef apron	*skeletal mudstone*	Minor skeletal fragments; abundance of drusy calcite spar cement lining vuggy porosity	Between SWB and FWB	4
	skeletal wackestone	Transported fossils (tabulate corals, brachiopods, bryozoans, crinoids)	Above FWB	4
Distal reef apron	*skeletal mudstone*	Minor skeletal fragments; abundance of drusy calcite spar cement lining vuggy porosity	Below SWB	5, 6
Reef rubble conglomerate	*coarse lithoclastic conglomerate*	Large, dark gray angular clasts in light gray micritic mud matrix; crinoids present	Below SWB	2
	skeletal lithoclastic conglomerate	Abundant tabulate corals, brachiopods, crinoids; moldic porosity	Below SWB	2
Stromatolite rubble conglomerate	*stromatolitic lithoclastic conglomerate*	Clasts composed of stromatolites; poorly sorted	Below SWB	2
Distal reef rubble	*skeletal mudstone*	Minor skeletal fragments; abundance of drusy calcite spar cement lining vuggy porosity	Below SWB	1
A-0 Carbonate	*crystalline dolomite*	Steeply inclined (20 to 40 degrees) crystalline dolomite beds composed of dolomite rhombs; jagged stylolites	Below SWB	1, 6
A-1 Anhydrite	*laminated anhydrite*	Thin laminations of dolomitic carbonate grains and anhydrite laminae; parallel laminations at base, highly contourted at top	Between SWB and FWB; restricted	1, 6
	nodular anhydrite	Pale gray color with a bluish hue; tightly packed coalescing anhydrite nodules; distorted mosaic fabric	Above FWB to Intertidal; restricted	1, 6
	crystalline dolomite	Subrounded dolomite crystals with anhydritic laths and small nodular fabrics	Intertidal to Supratidal; restricted	1, 6

*SWB: 60 feet (18 m) FWB: 30 feet (9 m) Subtidal: 10 feet (3 m) Intertidal: 3 feet (1 m) Supratidal: <3 feet (1 m)

Table 1. Facies classification table for the Niagara lithostratigraphic unit identifying lithofacies, lithologic attributes, depositional environments, and reef complex locations. Colors correspond to the depositional facies model (see Fig. 3.2).

Salina Facies Classification

Depositional Facies	Lithofacies	Lithologic Attributes	Depositional Environment	Reef Complex Location
Cyanobacterial mats	*crinkly stomatolitic bindstone*	White to gray; thin, crinkly laminated cyanobacterial mats; devoid of mud	Supratidal; restricted	2, 3, 4, 5
	stromatolitic conglomerate	White to gray; broken fragments of crinkly stromatolitic bindstone	Supratidal; restricted	2, 3, 4, 5
Thrombolitic bindstone	*thrombolitic bindstone*	Mottled dark brown micrite with light tan sparry cement; irregular patchy mesoclots	Subtidal to Intertidal; restricted to normal	3, 4
Oncolitic packstone	*oncolitic packstone*	Abundance of spherical, cyanobacterial mat encrusted clasts	Intertidal; restricted to normal	2
Laminated peloidal wackestone	*peloidal wackestone*	Wavy parallel laminations of spherical to eliptical peloidal grains	Subtidal to Intertidal; restricted to normal	2, 3, 4
Poker chips (lower, middle, upper)	*thinly-laminated mudstone*	Brown to gray carbonate mudstone laminae with black carbonaceous films; "poker-chip" parting along laminations	Below SWB; restricted	1, 6
	micro-laminated mudstone	Dolomitic mud; carbonaceous mat chips; massively bedded	Between SWB and FWB; restricted	1, 6
A-1 packstone	*crystalline dolomite*	Massively bedded crystalline dolomite composed of dolomite rhombs; ghosts of peloidal packstone fabric; often oil stained	Above FWB to Subtidal; restricted	1, 6
Rabbit ear anhydrite (1, 2)	*nodular anhydrite*	Nodular anhydrite in a micro-laminated carbonate mudstone; white to bluish nodules flattened parallel to bedding	Intertidal to Supratidal; restricted	1, 5, 6
Upper A-1 mudstone	*micro-laminated mudstone*	Mottled tan, to gray, to dark brown; vertical fractures lined with halite; lime mud	Above FWB to Subtidal; restricted	1, 5, 6

*SWB: 60 feet (18 m) FWB: 30 feet (9 m) Subtidal: 10 feet (3 m) Intertidal: 3 feet (1 m) Supratidal: <3 feet (1 m)

Table 2. Facies classification table for the Salina lithostratigraphic unit identifying lithofacies, lithologic attributes, depositional environments, and reef complex locations. Colors correspond to the depositional facies model (see Fig. 3.2).

CHAPTER IV

SEQUENCE STRATIGRAPHIC ANALYSIS

Silurian Sea Level

The Silurian deposits in the Michigan Basin are interpreted to represent a second-order sea level rise and fall, containing seven third-order eustatic sea-level cycles (1-3 Ma) that record sea level change on the order of 50 meters (Johnson and McKerrow, 1991). The third-order cycles coincide with the periodic advance and retreat of ice caps in South America during polar glacial conditions (Crowell et al, 1981). Concomitant fluctuations in seawater temperature have also been suggested to occur throughout the Silurian based on paleothermometry data from conodonts (Lehnert et al., 2010). Conodonts deposited at a slightly lower latitude (10° south) than the Michigan Basin (20-25° south) suggest warm seawater temperatures with pronounced cooling events in the early-Telychian and early-Sheinwoodian (Lehnert et al., 2010). Sea level fluctuations continued throughout the Silurian with three main fluctuations during the Sheinwoodian, Homerian, Gorstian, and Ludfordian. Basin wide sea level fluctuations were further evaluated in this study using the stratigraphy of the Silurian Pinnacle Reefs and related off-reef strata (see Fig. 4.1).

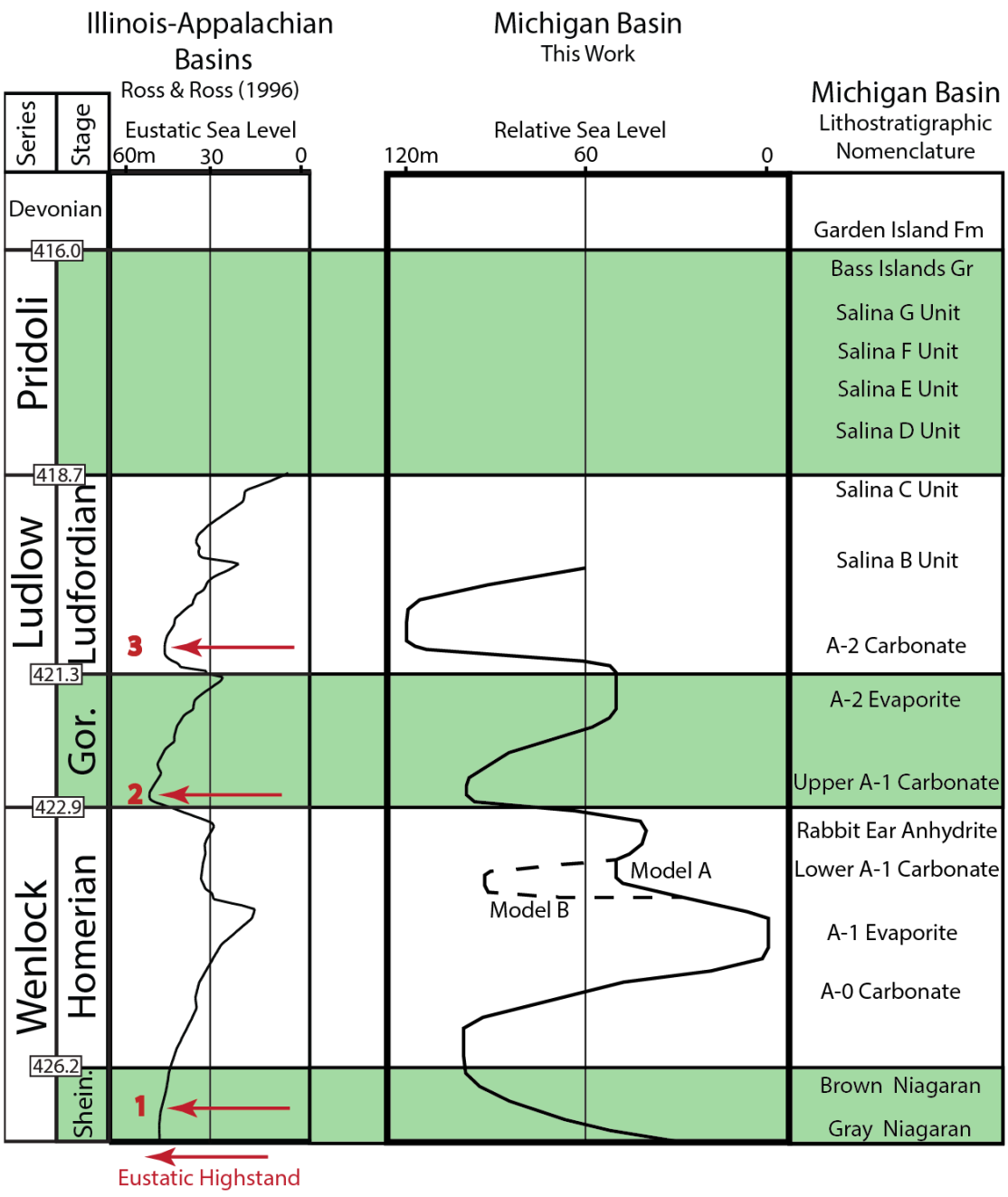

Figure 4.1. Comparison of Global and Michigan Basin sea level fluctuations. Global eustatic sea-level was determined by Ross and Ross (1996) using biostratigraphy in the Illinois and Appalachian Basins. Michigan Basin sea level fluctuations were interpreted in this study based on sequence stratigraphic observations in Niagara-lower Salina units.

Relative sea-level was interpreted here based on a combination of the eustatic sea-level curve by Ross and Ross (1996) and the observed response of the Niagara-lower Salina sediments and their sequence stratigraphic stacking patterns. The assignment of systems tracts (e.g., lowstand, transgressive, and highstand) was subsequently based on the interpreted relative sea-level for the Michigan Basin, using the top of the Gray Niagaran as the datum.

Columbus III Reef Growth Model

A reef growth model was constructed for the Columbus III reef complex to better understand the spatial and temporal distribution of reef complex-related facies that resulted from the complex history of basin dynamics during deposition of the Niagaran-lower Salina succession in the Michigan Basin. Seven reef complex growth stages illustrate unique facies relationships during distinct periods of reef complex development. The reef growth model was constructed using stratigraphic cross sections, both true to scale to better grasp the true geometries of the entire complex, and vertically exaggerated (3X) for better visualization of the thinner reef complex units. The structural cross section (Fig. 4.2) is oriented northeast to southwest parallel to inferred paleo-wind direction. The wells used for the cross section are roughly 1000 feet (305 m) apart. The wells used for the cross section are as follows (see Fig. 4.2 for locations): 6) leeward flank - 27851, 5) leeward grain apron - 27539, 4) reef core + grain apron - 27516, 3) reef proper – 27465, 2) windward reef rubble – 27558, 1) windward flank – 27533. Unit thicknesses and bedding angles observed in these vertical cores were also used for the creation of the true to scale cross-section.

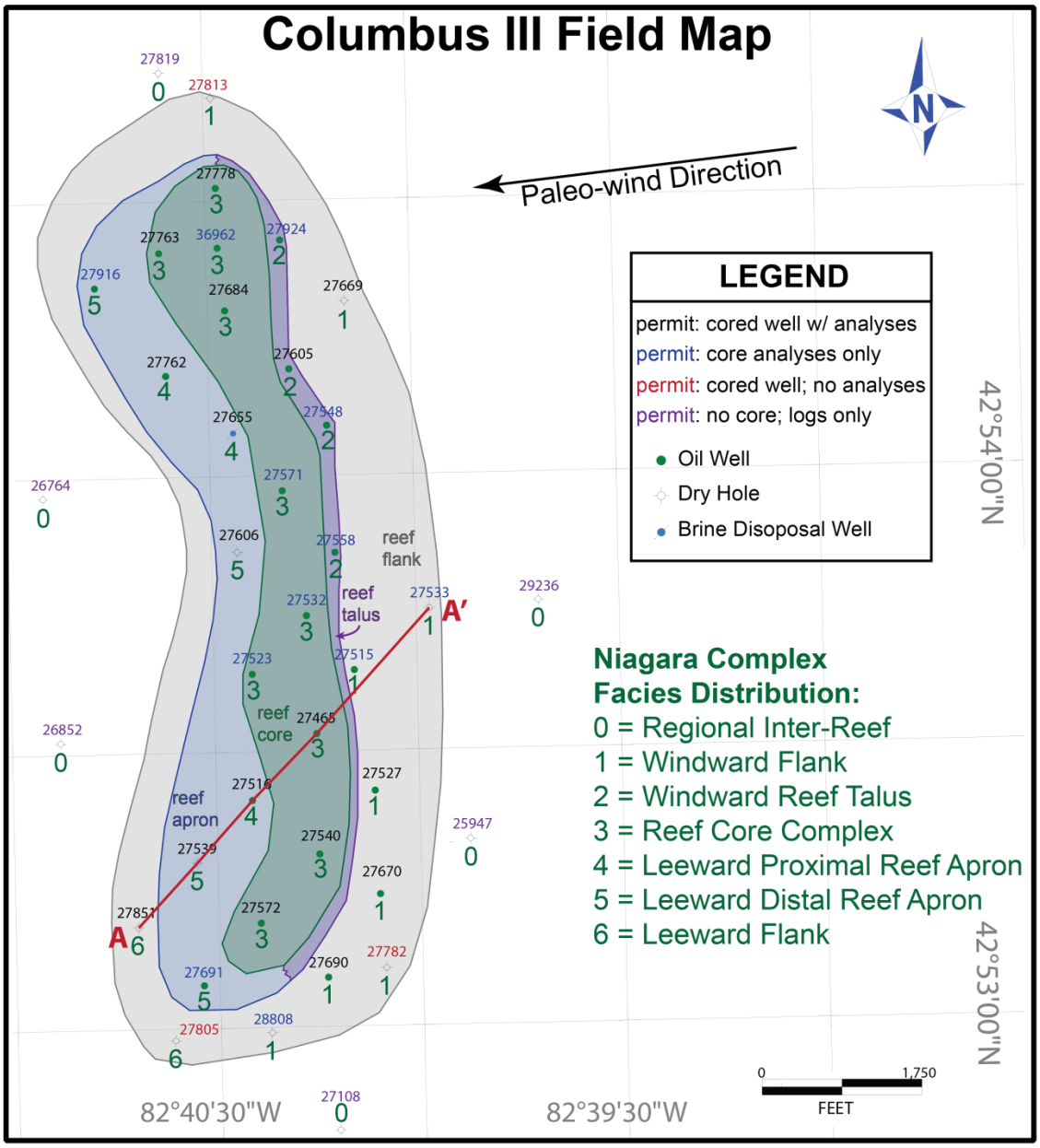

Figure 4.2. Map displaying the A-A' cross-section line of the Columbus III reef complex.

Stages 1 and 2 (Sea Level): Mid- to late-Sheinwoodian (427–426.2 Ma)

The base of the stratigraphic section examined in this study begins in the upper part of the Gray Niagaran lithostratigraphic unit, which is interpreted to be deposited

during the middle of the Sheinwoodian. The mid-Sheinwoodian is marked by a short eustatic lowstand (not shown in Fig. 4.1), followed by a eustatic high (eustatic highstand 1 in Fig. 4.1; Ross and Ross, 1996), which coincides with the initiation of the bioherm. The bioherm is capped by the Niagaran reef, which is referred to as the Brown Niagaran lithostratigraphic unit. Although Global eustatic sea-level shows a slight decline in the late-Sheinwoodian, it remains relatively high (above 30 meters) until the Homerian. The combination of a relative global eustatic highstand in addition to basin-centered subsidence throughout the Silurian (Howell and van der Pluijm, 1999) resulted in an observed relative sea-level rise upwards of 100 meters in the Michigan Basin (discussed below).

Stage 1 (Reef Growth Model): Initiation of Bioherm to Growth of Reef Core

Stage 1 represents the initiation of bioherm deposition, evolution and growth of the reef core, and contemporaneous deposition of the reef apron and reef talus in the leeward and windward directions. These deposits are interpreted to have formed during an overall relative sea level rise. The lowermost bioherm directly overlies the Gray Niagaran and underlies the reef core complex. The Gray Niagaran facies are interpreted to be representative of relatively calm water below storm-wave base (SWB, 60 feet or 18 m). Based on the observation that the bioherm consists of abundant stromatactis and deep-water fauna (crinoids and bryozoans), the bioherm was likely initiated in this same calm water environment, and does not mark a change in relative sea-level, but rather an ecological shift to different mound-building organisms.

The sedimentary structures and facies observed in the lower half of the bioherm are indicative of deposition below SWB. This includes mud-dominated facies as well as crinoid and bryozoan thickets, which were not wave-resistant (Wood, 1999). However, during bioherm growth, the biohermal mound is interpreted to have grown upward into

higher-energy conditions, as evidenced by a gradual increase of corals and stromatoporoids towards the upper half of the bioherm.

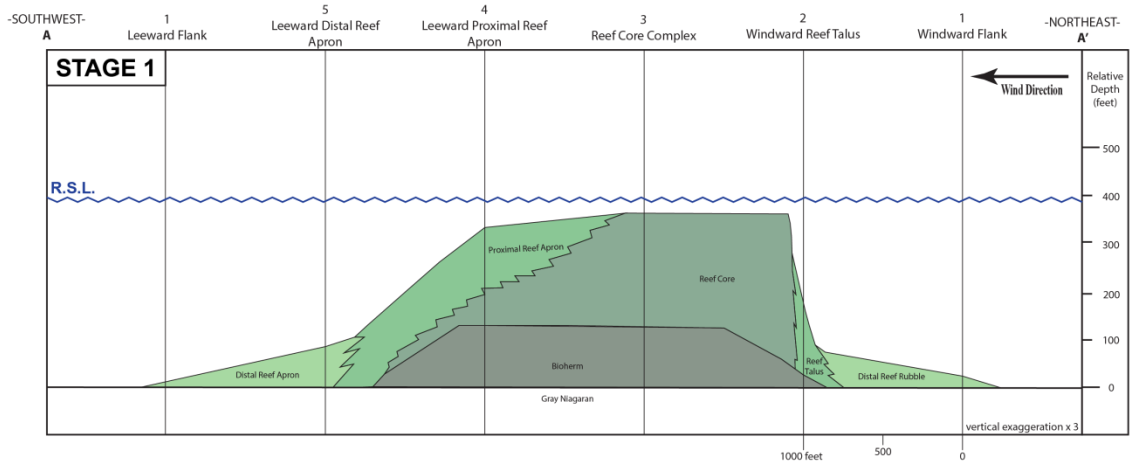

Figure 4.3. Stratigraphic cross-section of the Columbus III reef complex: Stage 1 – Initiation of Bioherm to Growth of Reef Core.

The bioherm is directly overlain in most locations by the reef core, and in others the reef core and bioherm are separated by the thin (< 10 feet or 3 m) bioherm cap facies. The bioherm cap could be a result of either a relative sea-level fall, resulting in a small unconformity, or a small relative sea-level rise and formation of a submarine hardground. The bioherm cap grades laterally on the flanks into the bioherm toe facies, which is also a thin, massively bedded crystalline dolomite and is easily differentiated from the mottled, fossil-rich bioherm core. The bioherm toe is interpreted to be contemporaneous with the bioherm cap, where the facies transition reflects a change in water depth and topography. The top of the bioherm cap marks the transitional boundary between the bioherm and reef core.

The initiation of reef growth represented by the reef core facies is the start of the early highstand deposits. The abundance of wave-resistant, framework building organisms (e.g., corals, stromatoporoids) clearly indicates that the reef core was formed

above FWB for the majority of deposition. As relative sea-level continued to rise, due to a combination of eustatic rise and basin-centered subsidence, the rapid growth rate of the reef core facies allowed it to grow above FWB. As the reef core grew upward concurrent with the relative sea-level rise, carbonate mud and detrital carbonate sediment shed leeward from the carbonate factory, resulting in deposition of the reef apron facies. Over time, shedding and progradation of the leeward reef apron resulted in the stack of facies observed in type section 4 (leeward proximal reef apron above reef core).

The resultant asymmetrical geometry of the Niagara reef complex, as driven by the paleo-wind direction, is a major contribution of this study (see Fig. 4.3). Previous studies (Huh, 1973; Gill, 1973) portrayed these reef complexes as symmetrical, smooth-topped towers, with a random distribution of reef bounding facies in the vertical and lateral directions. An asymmetrical distribution of depositional environments and facies is based in large part from the 27605 core in the windward reef talus location (type section 2). Although this windward reef talus only spans a few hundred feet laterally from the reef core complex, it is a vertically thick package of reef rubble and stromatolite conglomerate. Furthermore, bedding dips nearly 40 degrees, which clearly shows the uniqueness of windward deposition within the reef complex. With abundant core coverage in the leeward direction of the reef complex, it is evident that these high-angle talus beds and thick conglomeratic deposits are confined to the proximal windward reef talus environment. More specifically, the leeward side of the complex has shallow-dipping, finer-grained deposits of both proximal and distal leeward reef apron environments. In the leeward direction, the proximal reef apron grades into the distal reef apron, as marked by the decrease in fossil content and increase in fine-grained, matrix material. A similar gradational facies shift is observed in the windward direction as the windward reef rubble at the reef talus location grades into a fine-grained, distal reef rubble with fewer clasts derived from the reef core. The asymmetrical topography set up during stage 1 deposition also influences subsequent deposition.

Stage 2 (Reef Growth Model): Deposition of Stromatolitic Cap

Stage 2 represents a transition from early to late highstand due to a slowing of relative sea-level rise, which resulted in the deposition of shallower, intertidal facies of the stromatolitic cap. The abundance of laterally-linked hemispheroidal forms of stromatolites in this unit are indicative of high energy conditions, with deposits of up to 30 feet (9 m) thick. Contemporaneous with the growth of intertidal stromatolites in the reef crest position, semi-lithified stromatolites are interpreted to have been ripped up by waves and deposited on the windward reef talus slope (type section 2). The vertical transition up-section from the reef rubble conglomerate facies to the stromatolitic conglomerate facies is a very important time marker as it places the growth of the reef-top stromatolitic cap prior to the following lowstand deposition of the A-1 Evaporite (stage 3).

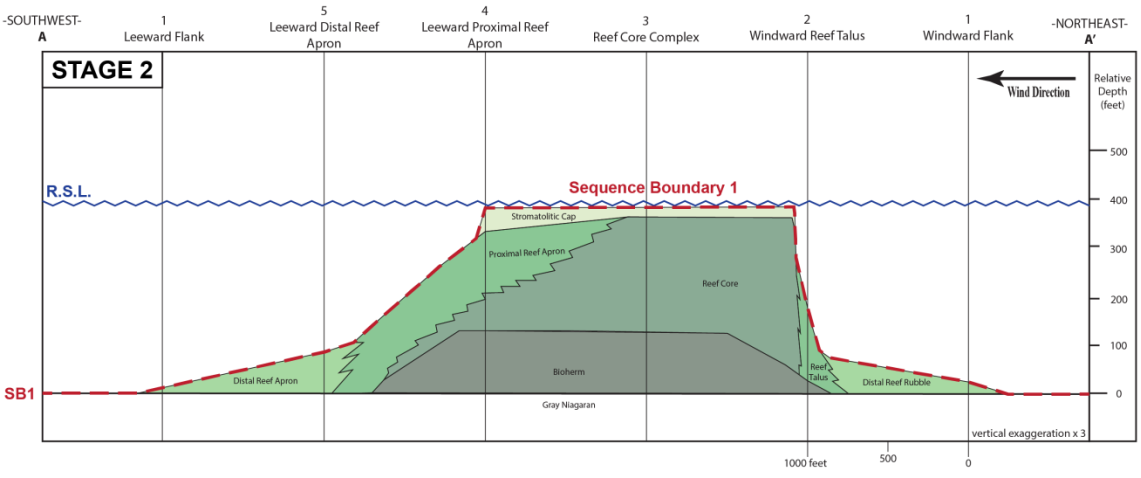

Figure 4.4. Stratigraphic cross-section of the Columbus III reef complex: Stage 2 – Deposition of Stromatolitic Cap.

Based on the significant thickness of the stromatolitic cap facies (9 m), sea-level is interpreted to have risen during deposition of the unit. Although it would be possible to preserve a few feet of intertidal deposits during a sea level fall , 30 feet (9 m) of intertidal, stromatolitic cap deposits is strong evidence that relative sea-level must have continued to rise, thus creating accommodation. An unconformity indicates termination of growth of the stromatolitic cap in the crestal position.

Once relative sea-level dropped below the top of the reef complex, thus exposing the late highstand stromatolitic cap deposits, a third-order sequence boundary developed across the entire reef complex (see Fig. 4.4). However, as sea-level fell, the stromatolitic cap continued depositing on the flanks of the reef complex (Fig. 4.7). Sequence stratigraphically, this would mean that deposition of the stromatolitic cap facies on the flanks of the "dead" reef occurred on top of the sequence boundary. Therefore, the stromatolitic cap is interpreted to be part of the subsequent falling stage systems tract (see Fig. 4.5). This is supported by observations down slope of the reef crest position (type sections 3 and 4) in the leeward distal reef apron location (type section 5) where stromatolitic cap facies exist on the leeward flanks over 200 feet (61 m) lower than those observed in the reef crest position. It is not plausible that these stromatolitic cap facies were contemporaneous with those atop the reef crest since the former would have had to be deposited in water depths greater than 200 feet (61 m). This suggests that as relative sea-level moved down the side of the reef, stromatolitic cap facies continued to be deposited as the intertidal zone moved lower and lower in response to a falling sea level. It is not likely that compaction of the leeward sediments could generate this post-reef-growth geometry.

A-0 Carbonate deposition occurred either contemporaneously or subsequently to the deposition of the stromatolitic cap facies, and is interpreted to belong to the falling stage systems tract above the sequence boundary. The A-0 Carbonate only exists in the reef flank positions (type sections 1 and 6) and has been interpreted to be either: i)

lithoclastic grain flows deposited as sea-level moved down the sides of the reef and extensive erosion of lithified reef complex occurred, or ii) detrital carbonate shed downslope from stromatolitic cap deposition in an intertidal environment. Although the A-0 Carbonate beds are laminated, and were previously interpreted as intertidal cyanobacterial mats (Gill, 1973; Budros, 1974), an alternative interpretation is presented here based on two observations. First, the basal section of the overlying A-1 Anhydrite, which is gradationally in contact with the A-0 Carbonate, is interpreted to be a deep water sulfate deposit. This makes it less likely that the underlying A-0 Carbonate was deposited in a shallow intertidal environment. Secondly, the A-0 Carbonate does not exhibit the same stromatolitic morphologies that were observed in any of the stromatolitic facies within the entire Niagara-lower Salina reef complex. It is simply described as a thinly-laminated crystalline dolomite, with no unequivocal evidence to be characterized as stromatolitic.

Stage 3 (Sea Level): Early- to mid-Homerian (426.2–424.5 Ma)

At the Homerian-Sheinwoodian boundary (426.2 Ma) global eustatic sea-level began to fall (Ross and Ross, 1996), and is also observed in the Michigan Basin. Initiation of this sea level fall ended the period of Niagaran pinnacle reef growth between 427 Ma and 426.2 Ma (see Fig. 4.1). Based on work by Wood (1999), 800 Ka is sufficient time for the construction of 300 feet (91 m) of vertical reef complex, especially with the addition of accommodation from basin-centered subsidence. At the point when eustatic sea-level had dropped 10 to 20 meters, the Michigan Basin likely became isolated from the world ocean as local sea-level dropped below the shelf margin. This resulted in accelerated evaporation and a rapid relative sea-level fall in the basin, which Cercone (1988) called the evaporative drawdown in the Michigan Basin. As eustatic sea-level continued to fall in the early-Homerian (Fig. 4.1), the only normal marine water

entering the basin would have been through small inlets and/or percolation through the porous carbonate margin rocks that separated the basin from the world ocean (see Fig. 4.5). Geologic evidence for this drawdown event includes subaerial exposure of pre-evaporitic carbonates within the Michigan Basin, extensive early dolomitization of Wabash Platform carbonates at the basin margin, and reduced deposition of sulfate and magnesium salts in the basin center (Cercone, 1988). As magnesium was stripped out of the sea-water due to the extensive dolomitization of basin margin carbonates, low-magnesium salts began to deposit in the basin center (Cercone, 1988).

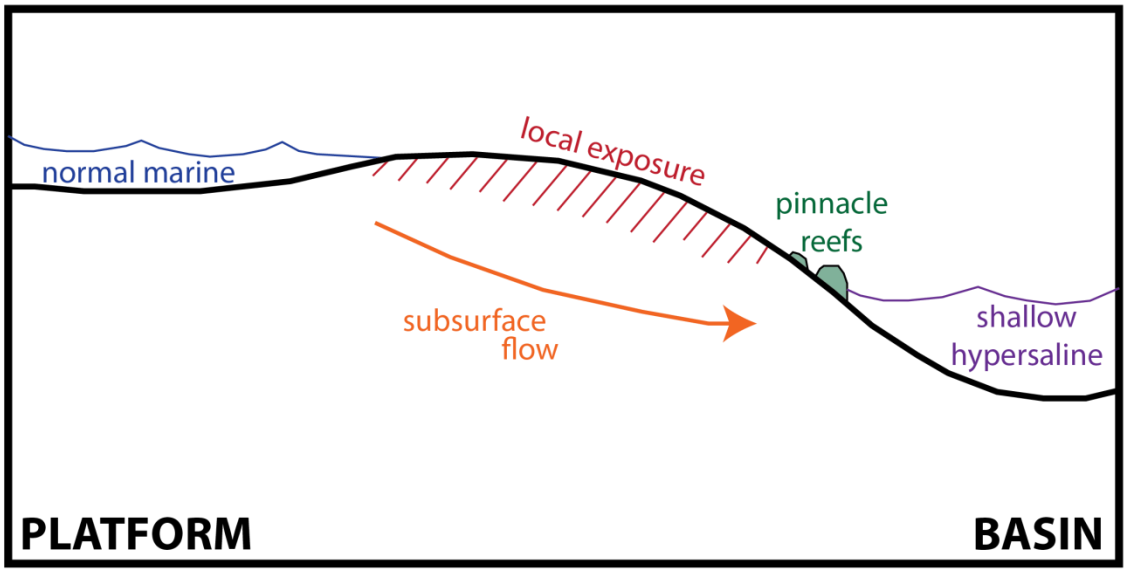

Figure 4.5. A schematic depiction of decoupled sea levels between the Michigan Basin and the Wabash Platform with the exposed basin margins serving as a barrier between normal and hypersaline seas (modified from Cercone, 1988).

During the initial stages of the early Homerian relative sea-level fall in the Michigan Basin, the Niagaran pinnacle reefs were exposed. This exposure resulted in widespread karsting, as well as the erosion of the reefs and subsequent deposition of the A-0 carbonate in the flank positions of reef complexes. These flank deposits are

composed of steeply dipping grain flows with primary dips of up to 40 degrees. These deposits are thickest closer to the reef complex. In a vertical profile, the grain flow deposits gradually transition into overlying anhydrite (A-1 Anhydrite) as relative sea-level continued to fall and the basin waters became increasingly restricted. As gypsum began to precipitate at 3.8X normal seawater concentration (Kendall, 2010), a subaqueous gypsum-mush formed around the paleo-topographic highs of the reef complex flanks. Isopach maps from Mesolella (1974) also indicate that the A-1 Evaporite transitions from anhydrite to halite deeper in the basin (see Fig. 4.6). This progression of evaporite deposition is also supported by Leibold (1992), who used geochemical methods to place the sulfate and halite deposits into a sequence stratigraphic model (refer to Fig. 1.4).

The A-1 Evaporite in the basin center is upward of 400 feet (122 m) thick and contains potassium-bearing salts at the top of the section. Potash salts need 90X normal seawater concentration to precipitate (Kendall, 2010). Thus, these deposits may mark near or complete desiccation of the basin. The fact that thick, continuous evaporite deposits up to 400 feet (122 m) thick could not possibly have been derived from a static volume of seawater in the basin supports a mechanism of seawater replenishment by normal marine waters that percolated into the basin though the carbonate margin rocks via subsurface flow or narrow ocean inlets (see Fig. 4.5).

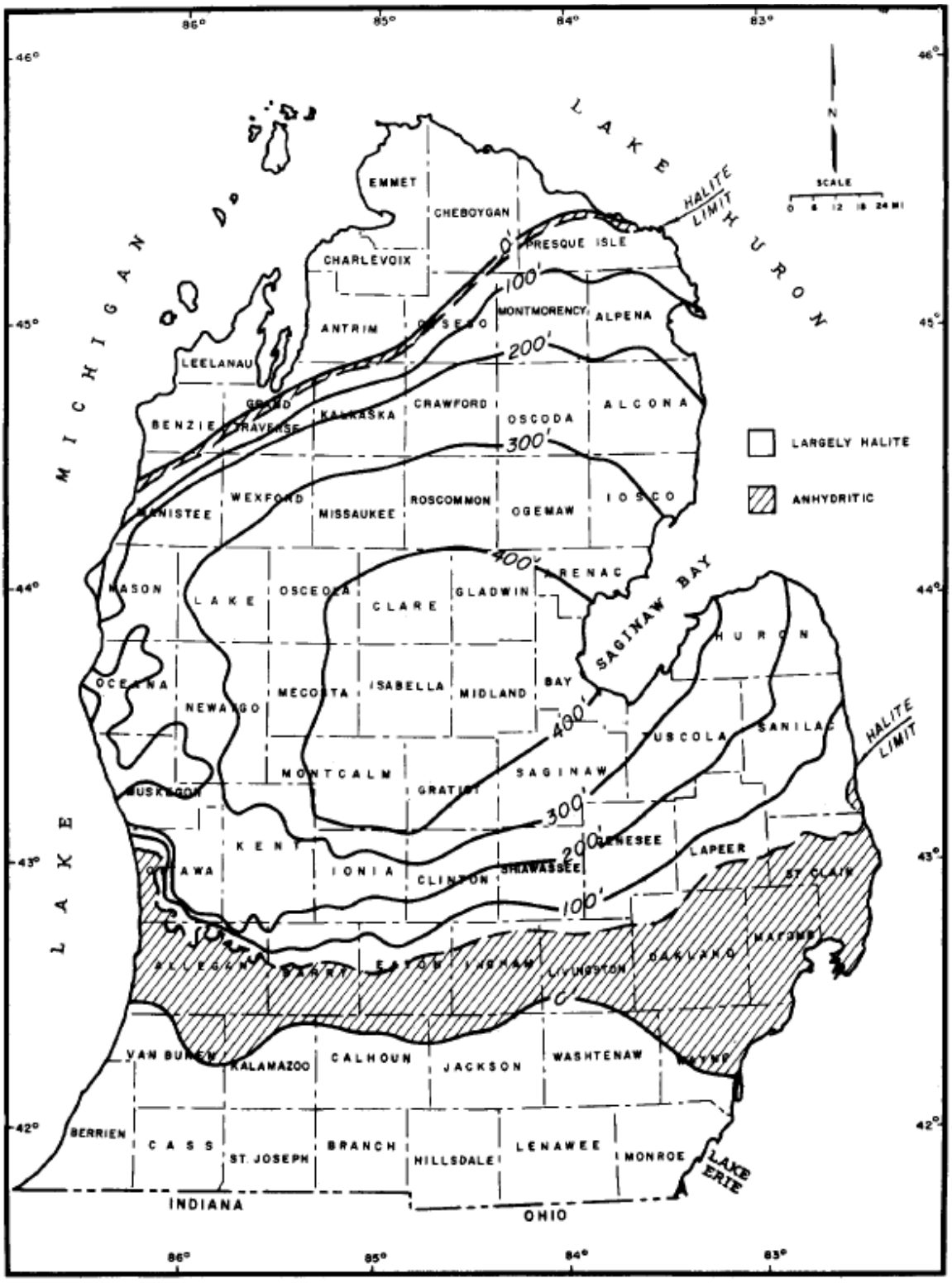

Figure 4.6. Isopach map of the A-1 Evaporite formation from Mesolella (1974).

Stage 3 (Reef Growth Model): Deposition of A-1 Evaporite

Depositional stage 3 is represented by the lowstand and transgressive facies of the A-1 Evaporite. The A-1 Evaporite exists only in reef flank locations (type sections 1 and 6) and exhibits a gradational transition from the underlying A-0 Carbonate. As relative sea-levels dropped over 300 feet (91 m), the reef complex was completely exposed as basin waters grew increasingly restricted due to evaporation and decoupling of the basin from normal marine ocean waters (Cercone, 1988). This drastic sea level fall resulted in extensive karsting at and below the sequence boundary across the entire reef complex, and exposure of the reef flank A-1 Anhydrite that had accumulated during falling sea level.

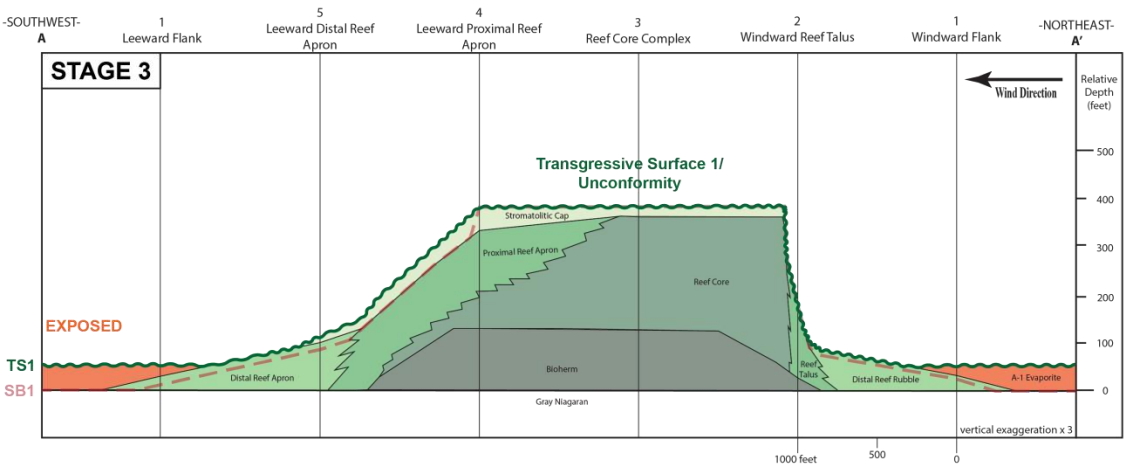

Figure 4.7. Stratigraphic cross-section of the Columbus III reef complex: Stage 3 – Deposition of A-1 Evaporite.

In the reef flank positions, the A-1 Evaporite exists as a thin anhydrite unit (in the Southern Niagaran Pinnacle Reef Trend only; exists as halite in the Northern Trend). This anhydrite was observed by Leibold (1992), in both core and wire-line logs, to transition into halite in the inter-reef locations and basin center. During this stage,

normal marine waters continued to replenish the basin at a rate slower than that of evaporation, resulting in the deposition of thick evaporites. According to Leibold (1992), gypsum was deposited first (A-1 Anhydrite), followed by a regressive stage halite (lower A-1 Evaporite in the basin center), capped by the complete desiccation of the basin and deposition of potash in the basin center. As relative sea-level in the basin began to increase as a result of a eustatic sea-level rise and flooding of the carbonate margin surrounding the basin, evaporite deposition persisted, resulting in transgressive deposition of halite in the basin center (upper A-1 Evaporite). Sequence stratigraphically, this places the A-1 Evaporite as a combination of lowstand and transgressive deposits, with the maximum regressive surface (MRS) existing somewhere in the middle or upper part of the unit in the central part of the basin. As relative sea-level rise in the basin reached the flanks of the reef complexes, basinal evaporite deposition concluded, and carbonate deposition resumed where conditions allowed. This is evidenced by a sharp transgressive surface observed at the top of the A-1 Anhydrite in the flank position, separating anhydrite deposition below and carbonate deposition above (see Fig. 4.7). Huh (1973) reported a similar, sometimes corroded, surface on the top of the A-1 Anhydrite on reef flanks in the Northern Trend.

Stage 4 (Sea Level): Mid- to late-Homerian (424.5–422.9 Ma)

Deposition of the A-1 Evaporite culminated as eustatic sea-level rose during the mid-Homerian (424.5 Ma). This eustatic rise did not reach the magnitude of the previous highstand, and was briefly interrupted by a fourth or fifth-order fall during the late-Homerian (see Fig. 4.1). Because eustatic sea-level rose only about 30 meters in the mid-Homerian, it most likely did not completely submerge the exposed carbonate bank surrounding the Michigan Basin. However, this sea-level increase appears to have

resulted in an increased flux of normal marine waters into the basin, enough to produce a transition from evaporite to carbonate deposition.

The mid-Homerian sea-level rise is interpreted to coincide with deposition of the lower A-1 Carbonate, as a microbialite-dominated carbonate factory was rejuvenated on the flanks of the pinnacle reefs. The re-establishment of a microbialite-dominated carbonate factory resulted in the cyanobacterial stromatolites and thrombolites in the Leeward Distal Reef Apron location (type section 5), which were able to re-establish themselves in the hypersaline basin waters during this time, along with microbial films in slightly deeper water, resulting in poker chip facies. As global sea-level began to drop a few meters as a result of a fourth or fifth-order fluctuation during the late-Homerian, the basin again became more saline, resulting in the deposition of thin subaqueous gypsum beds on the reef flanks (Rabbit Ear Anhydrite). These anhydrite units are very thin (< 10 feet, 3 m) and only exist in the reef flank position in both the northern and southern reef trends. The Rabbit Ears Anhydrite grades into carbonate in deeper marine, inter-reef positions without deposition of halite, suggesting that the basin was never fully desiccated during this drawdown.

Stage 4 (Reef Growth Model): Deposition of Lower A-1 Carbonate and Rabbit Ear Anhydrites

Two models are proposed for stage 4, which represents deposition of the lower A-1 Carbonate and overlying rabbit ear anhydrites (REA). In both models, the lower A-1 Carbonate unconformably overlies the A-1 Anhydrite, which is separated by a transgressive surface (see Fig. 4.8). These alternative models are reflected in the Michigan Basin relative sea-level curve during the mid- to late-Homerian (see Fig. 4.1). The major difference pertains to whether or not relative sea-level reached the crest of the reef complex prior to deposition of the REA. In model A (see Fig. 4.8), relative sea-level

only reaches about half way up the side of the reef complex (150 feet or 46 m) before it is interrupted by a higher-order relative sea-level fall and subsequent deposition of the REA on underlying, inherited paleotopography. In model B, relative sea-level climbs up the side of the reef complex and completely submerges its crest (300 foot or 91 m rise) prior to REA deposition (see Fig. 4.9).

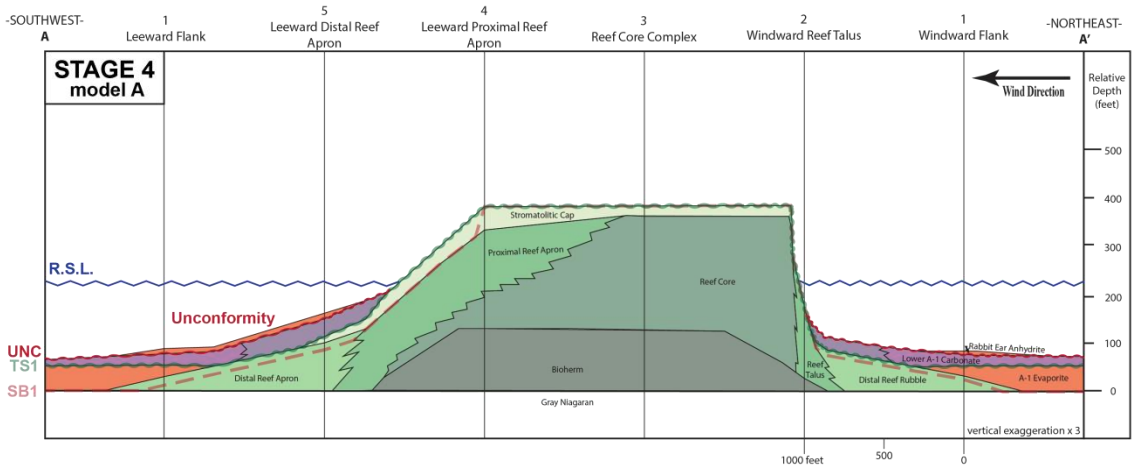

Figure 4.8. Stratigraphic cross-section of the Columbus III reef complex: Stage 4: **Model A** – Deposition of Lower A-1 Carbonate and Rabbit Ear Anhydrites.

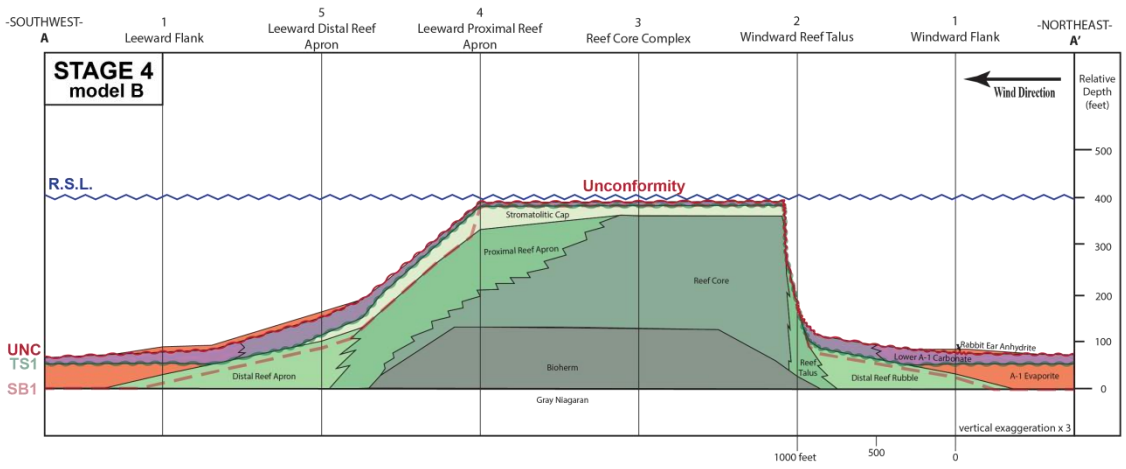

Figure 4.9. Stratigraphic cross-section of the Columbus III reef complex: Stage 4: **Model B** – Deposition of Lower A-1 Carbonate and Rabbit Ear Anhydrites.

Based on the presence of thin turbidites, characterized by sharp erosional bases and undisturbed, non-burrowed normal grading, the depositional facies observed in the lower A-1 Carbonate in the flank positions are interpreted to have formed in deeper water below SWB or low energy environments without normal marine benthos. The majority of this material is interpreted to have derived from a combination of fine detrital carbonate sediments, shed from an upslope carbonate factory, and pelagic settling of carbonate mud and carbonaceous material. The presence of crinkly cyanobacterial facies in the leeward distal reef apron location, above the falling stage stromatolitic cap and the underlying first sequence boundary, is evidence that cyanobacterial organisms had re-established themselves during this relative sea-level rise and freshening of basin waters. The cyanobacterial mats observed in this location (of the A-1 Carbonate) are identical to those observed on top of the reef core complex in the same stratigraphic position (i.e. on the crest and above the sequence boundary). This observation, however, is not unequivocal evidence that the white, crinkly-laminated stromatolites in the two locations were contemporaneous, or even belong within the same depositional sequence. If both cyanobacterial mats in type sections 3, 4, and 5 were deposited during the same transgression and subsequent submergence of the reef complex crest, then model A is more likely. If the cyanobacterial mat facies observed atop the reef complex crest are not deposited until after the REA deposition and continued sea level rise (stage 5), then model B is more likely. Although this sequence stratigraphic conundrum could not be resolved from the cores available in the Columbus III field, further investigation in other fields could potentially resolve this question.

Although no single depositional model for this stage is unequivocal, a few observations have been made that support an overall relative sea-level fall during this stage. In the leeward distal reef apron location (type section 5), an unconformity has

been identified which separates the lower A-1 Carbonate facies from the overlying REA. This unconformity is marked by erosion and deposition of terra rossa at the contact (see Fig. 4.10). This unconformity marks a dramatic shift from transgressive, below SWB deposits of the lower A-1 Carbonate, to subaerial exposure, followed by sea level rise within a still restricted basin and deposition of subaqueous REA gypsum. This observation does not rule out model B as an unconformity is observed atop the cyanobacterial mat facies in type sections 3 and 4. Again, the unconformity on the crest of the reef complex could be equivalent to or post-date the unconformity observed below the REA in type section 5.

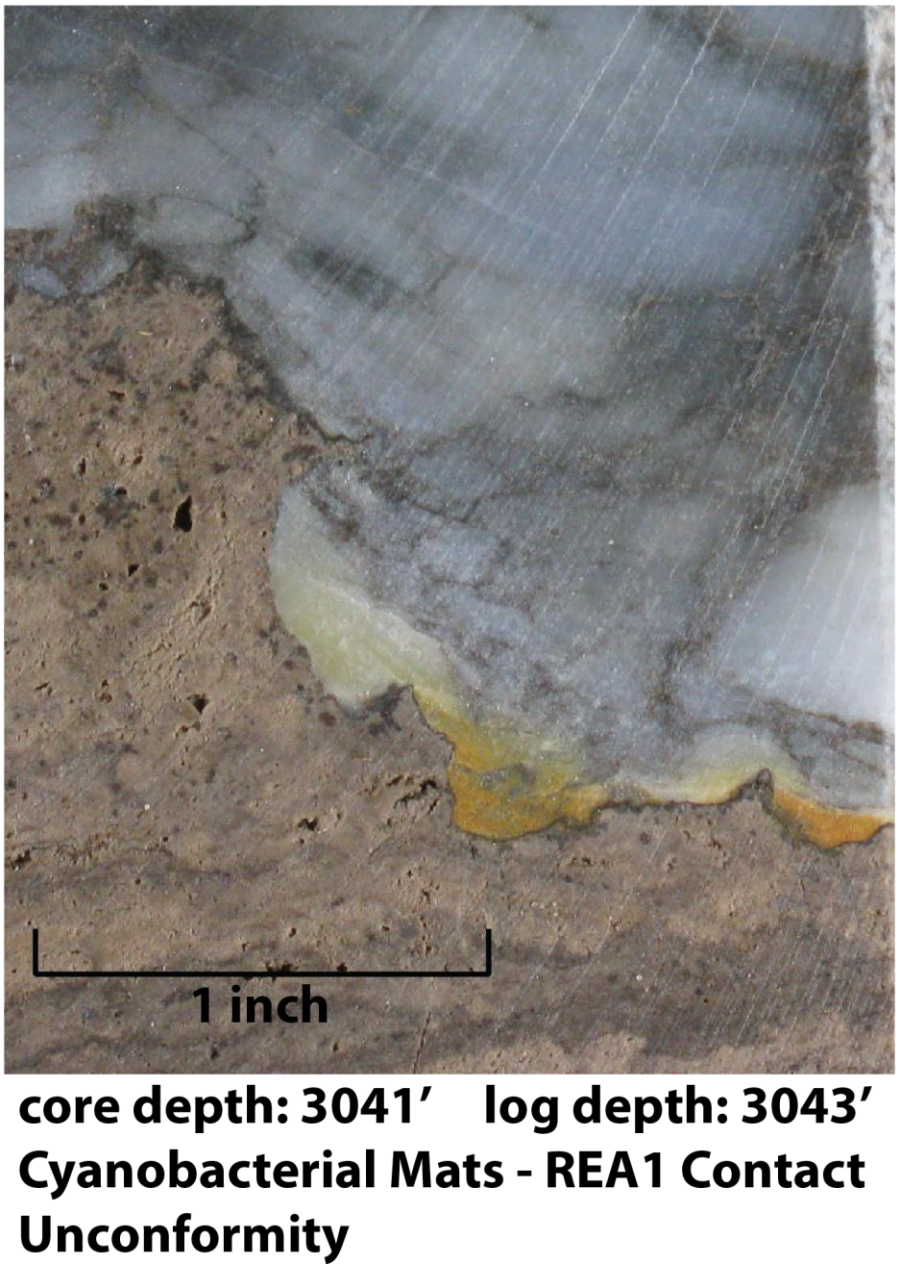

Figure 4.10. Contact lined with terra rossa between the cyanobacterial mat facies of the lower A-1 Carbonate and the overlying Rabbit Ear Anhydrite 1 facies in the PN27539 core.

The reason this particular relative sea-level fall, which corresponds to deposition of the REA, is not interpreted to be of the same magnitude as the first, third-order drawdown (stage 3) is because the Michigan Basin did not appear to completely dry up

during this higher-order drawdown. The REA deposits are only observed in around the flanks of Niagara reef complexes (now paleo-topographic highs), as they grade into continued carbonate deposition (condensed A-1 Carbonate) in the inter-reef and basin center locations. Therefore this particular smaller order sequence boundary is difficult to trace into the basin center, as it separates deeper water deposits of the lower A-1 Carbonate from deeper water deposits of the upper A-1 Carbonate. The smaller magnitude (fourth- of fifth-order) of this sea level fluctuation is also observed in the eustatic sea-level curve during the late-Homerian (Ross and Ross, 1996; see Fig. 4.1).

Stage 5 (Sea Level): Early- to mid-Gorstian (422.9–422.1 Ma)

The Gorstian-Homerian boundary (also Wenlock-Ludlow/Niagaran-Cayugan boundary, 422.9 Ma) marks the second major third-order eustatic sea-level rise (see Fig. 4.1). Based on the observed change from restricted halite deposition of the A-1 Evaporite to more normal marine deposition of the lower A-1 Carbonate, this rise resulted in partial reconnection of the Michigan Basin with normal marine waters of the adjacent world ocean. However, from the Niagaran to the Cayugan, the paleolatitude of the Michigan Basin had shifted to the north by a few degrees, resulting in the transition from humid tropics into an arid tropical belt (Briggs, 1974). Therefore, conditions remained intensely evaporitic and reef growth organisms that thrived during the Niagaran pinnacle reef growth never reappeared. Even as sea level rose above the crest of the paleo-reef complexes (for either the first or second time), the only fauna observed during the highstand are cyanobacterial mats and fecal pellets of soft bodied organisms, suggesting that marine conditions never fully returned to normal. As basinal waters flooded the flanks of the older reef complexes, microbial mat communities existed in peritidal environments. Microbial deposits are observed in places as low as the Leeward Distal Reef Apron location (type section 5), which was over 250 feet (76 m) below the crest of

the paleo-reef complex. If this sea level rise marks the first time marine water rose back above the paleo-reef complex crest, it culminated a depositional hiatus on the reef top of around 3.3 Ma. As microbially-derived sediment was deposited atop the reef crest, this distinct carbonate debris was shed into the flank and inter-reef position (as evidenced by microbial lithoclasts in the upper A-1 Carbonate) until sea-level began to fall in the mid- to late-Gorstian.

Stage 5 (Reef Growth Model): Deposition of the Upper A-1 Carbonate

Stage 5 is represented by the transgressive and highstand deposits of the upper A-1 Carbonate facies in the flank positions and their equivalents in the reef crest position. Following the deposition of the subaqueous REA facies in the flank and leeward distal reef apron positions (type sections 1, 5, and 6), carbonate deposition occurred. As basinal waters flooded the sides of the reef complex for a second time, the carbonate factory migrated up dip as well, resulting in deeper water, low energy carbonate deposition in the lower flank positions. In the leeward distal reef apron position (type section 5), cyanobacterial growth is not observed above the REA, and therefore microbial re-establishment is not believed to have occurred until relative sea-level reached the crest of the reef complex.

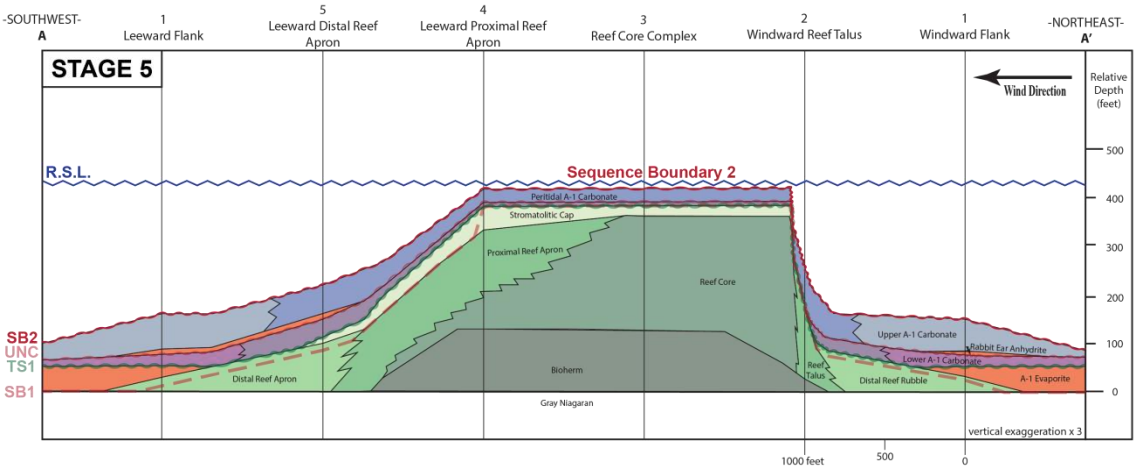

Figure 4.11. Stratigraphic cross-section of the Columbus III reef complex: Stage 5 – Deposition of the Upper A-1 Carbonate.

Once sea-level flooded the reef complex crest for either the first (model A) or second (model B) time since the deposition of the stromatolitic cap (stage 2), highstand, peritidal deposits including cyanobacterial mats, thrombolites, and peloidal wackestones began to accumulate. A re-established carbonate factory on the reef crest shed carbonate sediment down the slope and onto the flanks, resulting in the facies observed in the upper A-1 Carbonate. The lithofacies observed in the reef crest are cyclic, with distinct shallowing upward packages separated by small discontinuity surfaces. These smaller order discontinuities on the reef crest may record carbonate deposition outpacing sea level rise, or may have been a result of much smaller sea-level fluctuations and did not result in a distinct shift in facies in the flank positions, since facies in flank positions remained in deep water for the entire duration of stage 5.

Towards the end of upper A-1 Carbonate deposition, the laminated peloidal wackestone facies is the last carbonate deposition observed prior to the second, third-order sequence boundary. This wackestone facies contains an abundance of cyanobacterial mats, interbedded with peloids, indicative of an active carbonate factory. This carbonate factory most likely prograded off of the reef complex crest and down the slope as relative sea-level rise in the Michigan Basin began to slow. This "last gasp" of the carbonate factory is interpreted to be a major contributor to the detrital carbonate observed down slope in the flank positions of the upper A-1 Carbonate facies. Peloidal wackestone facies have been observed at lateral distances of up to 2,000 feet (610 m) away from the reef margin in flank locations, again indicative of lateral progradation of the carbonate factory during the late highstand or falling stages of the upper A-1 Carbonate.

Stage 6 (Sea Level): Mid- to late-Gorstian (422.1–421.3 Ma)

Following the early-Gorstian high stand a eustatic sea-level fall of over 30 meters occurred until the late-Gorstian (see Fig. 4.1). This sea-level fall resulted in another period of basin restriction and decoupling of the basin from normal marine waters, similar to that of the mid-Homerian, and ultimately the deposition of the A-2 Evaporite (see Fig. 4.2). This third-order drawdown also resulted in exposure of the Niagara-lower Salina reef complexes, resulting in extensive karsting observed at the top of the A-1 Carbonate unit. During the late-Gorstian eustatic drawdown, little to no deposition occurred during sea level fall, as observed by Leibold (1992). This sea level fall is significantly different from the first major third-order sea level drawdown, which resulted in both regressive (falling stage systems tract; part of the stromatolitic cap, A-0 Carbonate, A-1 Anhydrite, lower A-1 Evaporite) and transgressive (lowstand systems tract; upper A-1 Evaporite) deposits prior to the onset of A-1 Carbonate deposition. During this third-order drawdown, Leibold (1992) reported that only transgressive (lowstand systems tract) evaporites were deposited in the Michigan Basin. Similar to the A-1 Evaporite, the A-2 Evaporite transitions from anhydrite to halite in a more basinal direction and reaches thicknesses upward of 400 feet (122 m) in the basin center (see Fig. 4.12). However, according to the interpretation of Leibold (1992), the A-2 Anhydrite post-dates the deposition of the A-2 Evaporite (halite) as a result of relative sea-level rise (during the following Ludfordian) and freshening of the Michigan Basin waters.

Figure 4.12. Isopach map of the A-2 Evaporite formation from Mesolella (1974).

Stage 6 (Reef Growth Model): Deposition of A-2 Evaporite

Stage 6 represents the third-order sea-level drawdown and deposition of the A-2 Evaporite (halite). This stage is similar to that of stage 3 (A-1 Evaporite), with the main difference being that the A-2 Evaporite was not deposited during the falling stage systems tract (Leibold, 1992; determined from sedimentological textures and geochemical analyses). Also different than that of the A-1 Evaporite, the A-2 Evaporite exists as a thick halite deposit in the flank positions (over 200 feet or 61 m thick; see Fig. 4.13). It unconformably overlies the upper A-1 Carbonate in the flank position and marks the second, third-order sequence boundary interpreted in this reef growth model. As eustatic sea-level began to fall during this stage, the basin again became decoupled from normal marine waters, resulting in restricted, hypersaline basin waters. However, anhydrite deposits are not observed in this location because either: i) basin waters were not supersaturated with respect to gypsum until relative sea-level dropped below the exposed reef complex flanks; or ii) gypsum was deposited, but was subsequently eroded/dissolved prior to the following transgression and deposition of 200 feet (or 61 m) of halite (A-2 Evaporite).

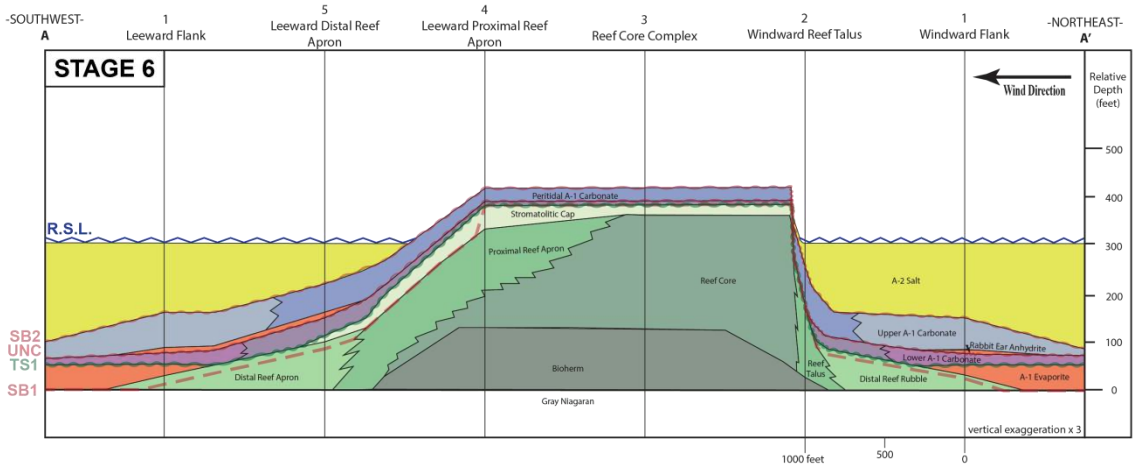

Figure 4.13. Stratigraphic cross-section of the Columbus III reef complex: Stage 6 – Deposition of A-2 Evaporite.

Stage 7 (Sea Level): Early-Ludfordian to late-Pridoli (421.3–416.0 Ma)

The cessation of A-2 Evaporite deposition was the result of the third major third-order eustatic sea-level rise at the beginning of the Ludfordian (421.3 Ma). This sea-level rise resulted in the sequential deposition of the A-2 Evaporite (halite), A-2 Anhydrite, and A-2 Carbonate, until a eustatic sea-level fall in the middle Ludfordian. As relative sea-level had overtopped the crest of the Niagara-lower Salina reef complexes, salinities in the Michigan Basin began to freshen from halite to gypsum saturation. This resulted in the deposition of the A-2 Anhydrite unit on the crest of reef complexes in the form of interbedded anhydrite and cyanobacterial mats. The A-2 Anhydrite then gradationally transitioned into the A-2 Carbonate unit as a result of continued freshening of the Michigan Basin waters and re-coupling to the world ocean.

The A-2 Carbonate is the first unit to onlap the southern margin of the basin and therefore the first unit in this stratigraphic sequence that can be directly correlated outside of the basin (Gill, 1977). Basin-centered subsidence continued through A-2 Carbonate deposition, resulting in the creation of the accommodation necessary to facilitate the continued restriction and subsequent evaporite deposition of the upper Salina Group (Salina B through G units). During early-to mid-Pridoli, eustatic sea-level did not reach the shelf margin and the Michigan Basin became decoupled from the global ocean until the deposition of the Bass Islands Group at the end of the Pridoli. Four fourth or fifth-order sea-level fluctuations throughout the Pridoli resulted in the deposition of the Salina D through G units, which amounted to over 2,000 feet (610 m) of heterolithic evaporite, carbonate, and shale (Leibold, 1992).

Stage 7 (Reef Growth Model): Deposition of the A-2 Anhydrite and A-2 Carbonate

Stage 7 represents the continued transgression of stage 6, resulting in the freshening of Michigan Basin waters and shift from halite deposition to gypsum and

ultimately carbonate. This transition was not observed in core, therefore interpretations are made from lithologies and thicknesses observed in wire-line logs. In the reef crest position, the upper A-1 Carbonate deposits are all shallow, peritidal deposits, capped by an unconformity and third-order sequence boundary. This unconformity is associated with karsting that is observed in all six type section locations, followed by deposition of the overlying A-2 Evaporite (halite) around the Niagara-lower Salina reef complex flanks (see Fig. 4.14). Once relative sea-level had overtopped the reef complex crest, Michigan Basin waters had freshened to sulfate saturation, resulting in the deposition of the A-2 Anhydrite above the second third-order sequence boundary.

Following deposition of the A-2 Anhydrite on the paleo-topographic highs of the reef complex, the basin waters continued to freshen, resulting in the deposition of the A-2 Carbonate. No cores in this field contained either the A-2 Anhydrite or A-2 Carbonate units, making it difficult to interpret a depositional environment. The A-2 Carbonate unit was the first to completely cover the Niagara-lower Salina reef complex. This thick carbonate unit (greater than 200 feet or 61 m) completely entombs the Niagara-Salina reef complex and marks the end of topographic relief related to the reef complex (see Fig. 4.13).

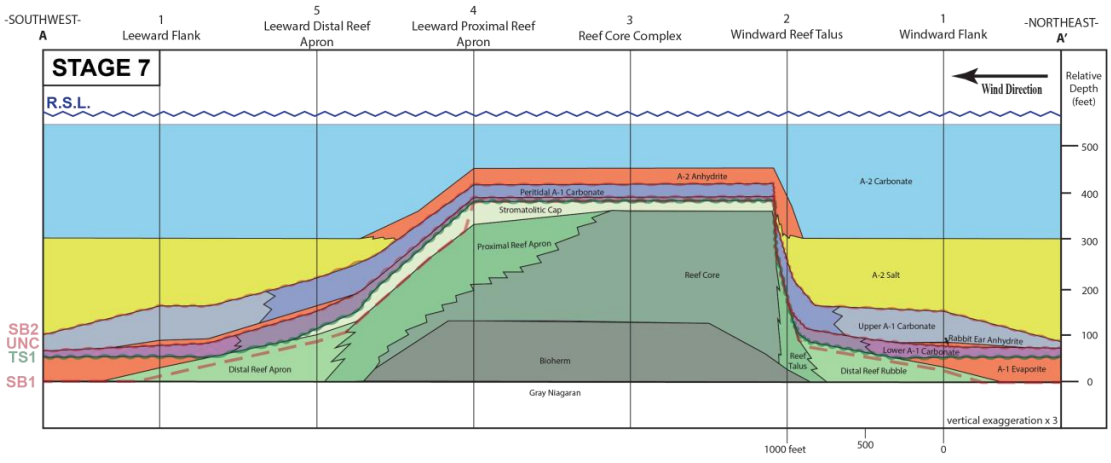

Figure 4.14. Stratigraphic cross-section of the Columbus III reef complex: Stage 7 – Deposition of the A-2 Anhydrite and A-2 Carbonate.

Reef Growth Model Summary

The reef growth model constructed for the Columbus III reef complex is divided into seven stages. These stages were determined based on a combination of distinctly different stacking of facies, sequence stratigraphic surfaces, and relative sea-level interpretations. While some of the interpretations of this model vary from those of previous models, (e.g. the asymmetry of the reef complex; predictability of windward and leeward facies; placement of third-order sequence boundaries) it most closely corresponds to that of model 3 previously described. The seven reef growth stages are summarized in the following table:

Reef Growth Model Summary

Stage	Summary	Systems Tract	R.S.L. (m) Reef Crest	R.S.L. (m) Flank	Lithostratigraphic Unit
1	Initiation of bioherm; evolution and growth of reef core; contemporaneous deposition of reef apron, reef talus, and reef rubble	Transgressive to Early Highstand	30 to 10	30 to 100	Brown Niagaran
2	Deposition of stromatolitic cap; slowing of relative sea-level rise	Late Highstand	10 to 0	100	Brown Niagaran
3	Deposition of A-0 Carbonate and A-1 Evaporite; third-order relative sea-level fall; complete exposure of reef complex; decoupling of basin from normal marine ocean waters	Falling Stage to Lowstand	exposed	20 to exposed	A-0 Carbonate; A-1 Evaporite
4	Deposition of lower A-1 Carbonate and Rabbit Ear Anhydrites; re-establishment of cyanobacterial organisms in the flank position; relative sea-level rise and freshening of basin waters	Transgressive to Highstand; Highstand to Lowstand	exposed (model A); or 10 (model B)	10 to 70; 70 to exposed (model A); or 10 to 100; 100 to exposed (model B)	Lower A-1 Carbonate; Rabbit Ear Anhydrites
5	Deposition of upper A-1 Carbonate; first (model A) or second (model B) time sea-level reached reef complex crest since end of Stage 2; re-establishment of cyanobacterial organisms on reef crest	Transgressive to Highstand	exposed to 3	10 to 100	Upper A-1 Carbonate
6	Deposition of A-2 Evaporite; second third-order sea-level fall; complete exposure of reef complex; decoupling of basin from normal marine ocean waters	Lowstand to Transgressive	exposed	20 to exposed	A-2 Evaporite
7	Deposition of A-2 Anhydrite and A-2 Carbonate; Niagara-lower Salina reef complex physically encompassed	Highstand	3 to 10	3 to 10	A-2 Anhydrite; A-2 Carbonate

Table 3. Table summarizing the Reef Growth stages for the Niagara-lower Salina reef complexes.

Reef Growth Model Comparison

Three contrasting depositional models for pinnacle reef development have been presented. The main point of disagreement is whether the upper parts of pinnacle reef complexes are Niagaran or Cayugan in age. The first model, supported by Gill (1975), Briggs (1978), and Balogh (1981), suggests that the entire pinnacle reef complex (everything below A-2 Anhydrite in the reef core complex location and above Gray Niagaran) is of Niagaran age and was entirely constructed prior to deposition of the A-1 Evaporite and A-1 Carbonate in the inter-reef to flank positions. The second model, supported by Jodry (1969) proposes contemporaneous deposition of the reef complex with the A-1 Evaporite deposits in the inter-reef and basin center areas. The third model, supported by Huh (1973), Sharma (1966), Mesolella (1975), Sears and Lucia (1979), and Shaver (1974), suggests that there were two or three distinct, stratigraphic discontinuity-bounded, episodes of carbonate deposition on the crest of the pinnacle reef complexes. This third model is strongly supported by this work with only small differences in the location of sequence stratigraphic surfaces in the reef proper location.

Strong evidence to refute Model 1, which suggests that the construction of the reef complex was an uninterrupted and continuous process, can be found in the transitional flank –to –crest, reef complex locations. First, in the windward reef talus location (type section 2), the clear transition from the reef rubble conglomerate to the stromatolite rubble conglomerate facies marks the end of Niagaran Reef growth. This is supported by the succession of distal reef rubble gradationally overlain by A-0 Carbonate and A-1 Anhydrite facies in both reef flank locations, and the interpretation that these strata are the lateral equivalent of the A-1 Evaporite in the basin center.

These relationships do not alone refute Model 1. However, in the windward reef talus location, the stromatolite rubble conglomerate facies is overlain by cyanobacterial mats belonging to the A-1 Carbonate, which are separated by a third-order sequence

boundary, evidenced by extensive karsting. These Cayugan-age, cyanobacterial-mat-dominated facies are clearly different than the underlying Niagaran-age deposits in the reef complex location and are separated by an unconformity, interpreted to be a hiatus of at least 3.3 Ma. A second piece of evidence exists in the leeward distal reef apron location of the reef complex (type section 5). A large (5 foot), salt-filled karsted surface lies within the stromatolitic cap facies, which marks the end of Niagara reef complex growth (stage 2). Overlying this karsted surface are A-1 Carbonate facies, including a Rabbit Ear Anhydrite deposit. The stack of facies observed at this type section clearly shows that cyanobacterial facies of the A-1 Carbonate directly overly a third-order sequence boundary and were not continuously deposited.

Following confirmation of at least one third-order sequence boundary within the entire Niagara-lower Salina reef complex, it was necessary to assess whether additional sequence boundaries were present. The presence of the Rabbit Ear Anhydrite facies in the flank position is evidence for a potential third, third-order sequence boundary within the reef complex. If this were the case, after the first major third-order drawdown and subsequent deposition of the A-1 Evaporite, sea-level would have had to rise over 400 feet (122 m) back above the reef crest. This would result in the lower A-1 Carbonate facies in the flank position to be contemporaneous with the cyanobacterial mat facies atop the reef crest (stage 4, model B). If this were the case, then the lower A-1 Carbonate facies would have to be a deep water (greater than 400 feet or 122 m) deposit while the cyanobacterial community thrived in a shallow-water environment on the reef crest. Following this period would be a higher-order sea-level drawdown, smaller magnitude to that of the first, which resulted in the deposition of the Rabbit Ear Anhydrite facies in the flank position.

An alternative hypothesis would be that following the first third-order drawdown, sea-level slowly rose, resulting in the shallow water, lower A-1 Carbonate to be deposited. This third-order rise then may have been interrupted by a smaller fourth or

fifth-order sea-level drop, prior to reaching the reef complex crest (stage 4, model A), which resulted in shifting from shallow water to a sabkha setting and deposition of a thin anhydrite layer (Rabbit Ear Anhydrite 1). This smaller order rise and fall repeated itself one more time for the deposition of second thin anhydrite unit (Rabbit Ear Anhydrite 2). Then sea-level continued its third-order rise to reach its maximum high stand during the deposition of the upper A-1 Carbonate facies in the flank position and shallow water facies in the reef crest position.

CHAPTER V

CONCLUSIONS

In order to most effectively convey the conclusions of this study, it is necessary to re-examine the fundamental research questions. The first question asks: *Can sequence stratigraphic models more effectively constrain and predict the lateral and vertical facies distribution of the Niagaran and Salina Groups in the Michigan Basin?* This question was examined by analyzing the individual stack of facies for six type sections throughout the Columbus III Niagara-lower Salina reef complex and determining depositional environments for the individual facies. These facies relationships were utilized within a sequence stratigraphic model which allowed for the correlation of depositional facies from the reef crest to the inter-reef position by examining the entire complex in synoptic slices. The sequence stratigraphic model was then compared to those which had been previously published and contended, resulting in the creation of a new model.

This new model places emphasis on the asymmetry of the Niagaran-lower Salina reef complex, something that had not been previously observed due to the lack of necessary subsurface core data. This asymmetry is primarily influenced by paleo-wind direction and is important factor in the predictability of depositional facies throughout the reef complex. Also, distinctive wire-line log signatures observed in this study aid in the ability to predict depositional facies where core data is absent. Therefore, a sequence stratigraphic model does effectively constrain, as well as aid in the prediction of lateral and vertical facies distribution of the Niagaran and Salina Groups in the Michigan Basin.

The second fundamental research questions was: *What are the main geological controls on Niagaran pinnacle reef sediment distribution?* This question was assessed by developing a better understanding for the controls on carbonate production, most specifically those related to reef complex development and microbial sediment

production. The depositional facies observed in the Columbus III reef complex reflect a combination of biological factors, hydrologic regimes, sea-water chemistry, and authigenic processes. In order to guide interpretations, it was necessary to gain a better understanding for the Silurian paleogeography of the Michigan Basin, as well as the eustatic sea-level fluctuations throughout the Niagaran and Cayugan which greatly influenced the deposition of the reef complex. The prevailing wind direction, which was interpreted from paleo-trade wind direction during the Niagaran and Cayugan (southeasterlies), had a major influence on the depositional profile and reef complex morphology. Also, incorporating examples from studies outside of the Michigan Basin was essential for aiding in the identification and interpretation of distinct carbonate and evaporite features. Deposits such as microbial laminites of the Early Silurian of the Eramosa Formation of southern Ontario, or deep-water, laminated anhydrites of the Castile Evaporite of the Delaware Basin were key analogs which were representative of inter-reef Salina deposits of the reef complex. All of these factors were equally important in understanding the main geological controls on Niagaran pinnacle reef sediment distribution patterns.

The third fundamental research question was: *How did Niagara and Salina sedimentation record changes in both eustatic sea-level and Michigan Basin subsidence?* This question was examined by correlating the depositional history of the interbedded carbonate and evaporite deposits of the Niagaran and lower Salina units with Silurian eustatic sea-level curves. For example, the thick package of reef core facies observed here reflects increasing accommodation and thus a relative sea-level rise within the Michigan Basin. Combining this observation with previously published observations of variations in reefal geometries (taller reef complexes down depositional slope) allows for the interpretation of relative sea-level fluctuations being a result of basin-centered subsidence, rather than eustatic sea-level fluctuations, which have been shown to not fluctuate more than 40 meters throughout the Silurian. Moreover, eustatic sea-level falls

resulted in the de-coupling and isolation of the Michigan Basin from the world ocean, which is recorded in the deposition of the thick, A-1 and A-2 Evaporite units. These eustatic correlations into the Michigan Basin also aid in the constraint of relative ages of the Niagaran and lower Salina units, resulting in an updated chronostratigraphic chart for these Silurian strata (see Fig. 1.2).

The final fundamental research question was: *What is the general geometry of the reef and how are sediments spatially distributed within the reef complex?* This question is best answered by referring to Figure 3.2, which portrays both the true to scale and vertically exaggerated cross-sections of the Columbus III reef complex. In general, the geometry of the reef is asymmetrical, with a steeply-sloped (40 degrees) windward side and gradual sloping leeward side (20 degrees). In the leeward direction, the reef core gradationally transitions into the proximal reef apron, which then transitions into the distal reef apron in the leeward flank position. The reef core and proximal reef apron is capped by a thin stromatolitic cap facies, which marks the end of Niagara sedimentation atop the reef complex crest. In the opposite direction, a thin windward reef talus deposit exists in close proximity to the steeply-sloped reef core, which gradationally transitions into the distal reef rubble in the windward flank location. Subsequent deposition of the A-0 Carbonate, A-1 Evaporite, A-1 Carbonate, A-2 Evaporite, and A-2 Carbonate is heavily controlled by the geometries imparted during Niagara deposition, with subtle variations controlled by Michigan Basin restriction, paleo-wind direction, and water depths.

BIBLIOGRAPHY

Balogh, R., 1981, A study of the Middle Silurian Belle River Mills, Peters, and Ray Pinnacle Reefs from the Michigan Basin: Master's Thesis, Bowling Green State University, Bowling Green, Ohio.

Bathurst, R., 1971, Carbonate sediments and their diagenesis: Elsevier, Amsterdam, 620 p.

Berry, W., and Boucot, A., 1970, Correlation of the North American Silurian Rocks: GSA Special Paper No. 102.

Briggs, L., and Briggs, D., 1974, Niagara-Salina relationships in the Michigan Basin: in R.V. Kesling, ed., Silurian reef-evaporite relationships: Michigan Basin Geol. Soc. Ann. Field Conf., p. 1-23.

Briggs, L., Briggs, D., Elmore, D., Gill, D., 1978, Stratigraphic facies of carbonate platform and basinal deposits, Late Middle Silurian, Michigan Basin: Field Excursions from the University of Michigan, p. 117-131.

Budros, R., 1974, The stratigraphy and petrogenesis of the Ruff Formation, Salina Group in southeast Michigan: Master's Thesis, University of Michigan, Ann Arbor, Michigan.

Burgess, R., and Benson, A., 1969, Exploration for Niagaran reefs in Michigan: Ont. Petrol. Inst. 8th Ann. Conf. and Oil and Gas Hour, Dec. 22, 1969, p. 80-82; Dec. 29, 1969, p. 180-188; Jan 5, 1970, p. 122-127.

Catacosinos, P., Daniels, P., and Harrison, W., 1991, Structure, stratigraphy, and petroleum geology of the Michigan Basin; interior cratonic basins. AAPG Memoir, v.51, p. 561-601.

Cercone, K., 1988, Evaporative sea-level drawdown in the Silurian Michigan basin: Geology, v.16, p. 397-390.

Charbonneau, S., 1990, Subaerial exposure of Middle Silurian Guelph Formation Pinnacle Reefs of the Michigan Basin, Southwestern Ontario: Master's Thesis, Queen's University, Kingston, Ontario.

Cohee, G., and Landes, K., 1958, Oil in the Michigan basin, in L.G. Weeks (ed.), Habitat of oil: Tulsa, American Association of Petroleum Geologists, p. 473-493.

Cramer, B., Brett, C., Melchin, M., Mannik, P., Kleffner, M., McLaughlin, P., Loydell, D., Munnecke, A., Jeppsson, L., Corradinin, C., Brunton, F., and Saltzman, M., 2011, Revised correlation of Silurian Provincial Series of North America with global and regional chronostratigraphic units and delta (super 13) C (sub carb) chemostratigraphy: Lethia, v. 44, p. 185-202.

Crowell, J., Suarez-Soruco, R., and Rocha-Campos, A., 1981, Silurian glaciation in central South America: Gondwana Five, Proceedings of the Fifth International Gondwana Symposium: Rotterdam. A. A. Balkema, p. 105-110.

Dunham, R., 1962, Classification of carbonate rocks according to depositional texture, Depositional Environments in Carbonate Rocks, Special Publication Social Economic Paleontology and Mineralogy, Houston, Texas, p. 108-121.

Ells, G., 1967, Michigan's Silurian oil and gas pools. G.D. Ells, Geological Survey, Department of Conservation.

Elrick, M., and Snider, A, 2002, Deep-water stratigraphic cyclicity and carbonate mud mound development in the Middle Cambrian Marjum Formation, House Range, Utah, USA: Sedimentology v.49, p. 1021-1047.

Embry, A., 1995, Sequence boundaries and sequence hierarchies: problems and proposals, in: Tectonics and sequence stratigraphy, Williams, G., and Dobb, A. (eds.), Geological Society London Special Publication 71, p. 15-34.

Embry, A., 2001, The six surfaces of sequence stratigraphy: AAPG Hedberg Conference on sequence stratigraphic and allostratigraphic principles and concepts, Dallas, abstract volume, p. 26-27.

Embry, A., 2009, Practical Sequence Stratigraphy. Canadian Society of Petroleum Geologists, Online at www.cspg.org, 79 p.

Felber, B., 1964, Silurian Reefs of Southeastern Michigan: Doctoral Dissertation, Northwestern University, Evanston, Illinois.

Gill, D., 1973, Stratigraphy, facies, evolution and diagenesis of productive Niagaran Guelph reefs and Cayugan sabkha deposits, the Bell River Mills gas field, Michigan Basin: Doctoral Dissertation, University of Michigan, Ann Arbor, Michigan.

Gill, D., 1975, Cyclic deposition of Silurian carbonates and evaporites in the Michigan Basin: Discussion: AAPG Bulletin v.59, p. 535-538.

Gill, D., 1977, Salina A-1 sabkha cycles and the Late Silurian paleogeography of the Michigan Basin: Journal of Sedimentary Petrology v.47, no.3, p. 979-1017.

Gill, D., Briggs, L., Briggs, D., 1978, The Cain Formation: a transitional succession from open marine carbonates to evaporites in a deep water basin, Silurian, Michigan basin (abs): 10th IAS Internat. Cong. Sedimentology Abs., v. 1, p. 244-245.

Grammer, M., Barnes, D., Harrison III, B., Sandomierski, A., and Mannes, R., 2008, Practical synergies for increasing domestic oil production and geological sequestration of anthropogenic CO_2: An example from the Michigan Basin, *in* M. Grobe, J. C. Pashin, and R. L. Dodge, eds., Carbon dioxide sequestration in geological media – State of science: AAPG Studies 59, p. 1-18.

Grammer, M., Noack, A., Qualman, H., Ritter-Varga, A., Wold, J., Sandomierski, A., and Harrison, W.B. III, 2010, Reservoir Characterization of Silurian (Niagaran) "Pinnacle" Reefs in the Michigan Basin: Search and Discovery Article #50286 (2010) Posted July 30, 2010. Adapted from oral presentation at AAPG Annual Convention and Exhibition, New Orleans, Louisiana, April 11-14, 2010.

Haq, B., and Schutter, S., 2008, A chronology of Paleozoic sea-level changes: Science, v.322, p. 64-68.

Howell, P., and van der Pluijm, B., 1999, Structural sequences and styles of subsidence in the Michigan Basin. Geological Society of America Bulletin, v.111, no.7, p. 974-991.

Hubbard, D., Miller, A., and Scatura, D., 1990, Production and cycling of calcium carbonate in a shelf-edge reef system (St. Croix, US Virgin Islands): applications to the nature of reef systems in the fossil record. Journal of Sedimentology v. 56, p. 848-861.

Huh, J., 1973, Geology and diagenesis of the Niagaran pinnacle reefs in the northern shelf of the Michigan Basin: Doctoral Dissertation, University of Michigan, Ann Arbor, Michigan.

James, P., Kendall, A., and Pufahl, P., 2010, 13) Introduction to Biological and Chemical Sedimentary Facies Models, *in* Facies Models 4, Dalrymple, R., & James, N. eds., Geological Association of Canada, p. 323-337.

James, N., and Wood, R., 2010, 17) Reefs, *in* Facies Models 4, Dalrymple, R., & James, N. eds., Geological Association of Canada, p. 421-445.

Jodry, R., 1969, Growth and dolomitization of Silurian reefs, St. Clair County, Michigan: AAPG Bulletin v.53, no.4., p. 957-981.

Johnson, M., and McKerrow, W., 1991, Sea level and faunal changes during the latest Llandovery and earliest Ludlow (Silurian): Historical Biology, v.5, p. 153-169.

Johnson, M., 2010, Tracking Silurian eustasy: Alignment of empirical evidence or pursuit of deductive reasoning: Paleogeography, Paleoclimatology, Paleoecology, v.296, p. 276-284.

Kendall, A., 2010, 20) Marine Evaporites, *in* Facies Models 4, Dalrymple, R., & James, N. eds., Geological Association of Canada, p. 505-538.

Kennard, J., & James, N, 1986. Thrombolites and Stromatolites: Two distinct types of microbial structures. Palaios, 1(5): 492–503.

Kerans, C., and Tinker, S.W., 1997, Sequence Stratigraphy and Characterization of Carbonate Reservoirs: SEPM Short Course Notes #40.

Lehnert, O., Mannik, P., Joachimski, M., Calner, M., Fryda, J., 2010, Paleoclimate perturbations before the Sheinwoodian glaciation: a trigger for extinctions during the 'Ireviken Event'. Paleogeography, Paleoclimatology, Paleoecology 296, p. 320-331.

Leibold, A., 1992, Sedimentological and Geochemical constraints on Niagara/Salina deposition, Michigan Basin: Doctoral Dissertation, University of Michigan, Ann Arbor, Michigan.

Lowenstam, H., 1950, Niagaran reefs of the Great Lakes area. J. Geol., 58: p. 430-487.

Leibold, A., 1992, Sedimentological and Geochemical constraints on Niagara/Salina deposition, Michigan Basin: Doctoral Dissertation, University of Michigan, Ann Arbor, Michigan.

Lucia, J., 2007, Carbonate Reservoir Characterization (2nd Ed., p. 342). New York: Springer.

Mesolella, K., Robinson, J., McCormick, L., and Ormiston, A., 1974, Cyclic deposition of Silurian carbonates and evaporites in the Michigan Basin: AAPG Bulletin v.58, no.1, p. 34-62.

Mesolella, K., Robinson, J., McCormick, L., and Ormiston, A., 1975, Cyclic deposition of Silurian carbonates and evaporites in the Michigan Basin: Reply: AAPG Bulletin v.59, p. 538-542.

Moore, C., & Wade, W., 2013, Carbonate reservoirs porosity and diagenesis in a sequence stratigraphic framework (2nd ed.). Amsterdam: Elsevier Science.

Noack, A., 2008, Analysis of pore architecture and correlations to sonic velocity values in Silurian (Niagaran) Reefs of the Michigan Basin: Master's Thesis, Western Michigan University, Kalamazoo, Michigan.

Porcher, E., 1985, Lithofacies and geochemistry of interreef carbonates, Middle Silurian, Michigan Basin: Master's Thesis, Western Michigan University, Kalamazoo, Michigan.

Pratt, B., 2010, 16) Peritidal Carbonates, *in* Facies Models 4, Dalrymple, R., & James, N. eds., Geological Association of Canada, p. 401- 419.

Pratt, B., and Haidl, F., 2008, Microbial patch reefs in Upper Ordovician Red River strata, Williston Basin, Saskatchewan: signal of heating in a deteriorating epeiric sea, *in* Pratt, B. and Holmden, C., *eds.*, Dynamics of Epeiric Seas: Geological Association of Canada, Special Paper 48, p. 315–352.

Qualman, H., 2009, 3-D Interpretation of reservoir property distribution in the Belle River Mills Silurian (Niagaran) Reef, St. Clair County, Michigan: Master's Thesis, Western Michigan University, Kalamazoo, Michigan.

Ritter, A., 2008, Evaluating the controls on reservoir heterogeneity of Silurian Pinnacle Reefs, Michigan Basin: Master's Thesis, Western Michigan University, Kalamazoo, Michigan.

Ross, C., and Ross, J., 1996, Silurian sea level fluctuations: Paleozoic Sequence Stratigraphy: Views from the North American Craton, Colorado, Geological Society of America Special Paper 306, p. 187-192.

Schreiber, C., and Tabakh, M., 2000, Deposition and early alteration of evaporites: Sedimentology v. 47, p. 215-238.

Scotese, C., 2002, http://www.scotese.com, (PALEOMAP website).

Sears, S., and Lucia, F., 1979, Reef-growth model for Silurian pinnacle reefs, northern Michigan reef trend: Geology v.7, p. 299-302.

Sharma, G., 1966, Geology of Peters Reef, St. Clair County, Michigan: AAPG Bulletin v.50, p. 327-350.

Shaver, R., 1974, Silurian Reefs of Northern Indiana: Reef and Interreef Macrofaunas: AAPG Bulletin v.58, no.6, p. 934-956.

Shaver, R., 1996, Silurian sequence stratigraphy in the North American craton, Great Lakes area, Geological Society of America Special Paper 306, p. 193-202.

Spengler, A., and Read, J., 2010, Sequence development on a sediment-starved, low accommodation epeiric carbonate ramp: Silurian Wabash Platform, USA mid-continent during icehouse to greenhouse transition: Sedimentary Geology, v.224, p. 84-115.

Tang, D., et al., 2013, Environment controls on Mesoproterozoic thrombolite morphogenesis: A case study from the North China Platform. Journal of Palaeogeography, 2(3): 275-296.

Wold, J., 2008, Sequence Stratigraphy and 3-D reservoir characterization of a Silurian (Niagaran) Reef – Ray Gas Storage field, Macomb County, Michigan: Master's Thesis, Western Michigan University, Kalamazoo, Michigan.

Wood, R., 1999, Reef Evolution. Oxford: Oxford University Press.

APPENDIX A

Additional Core Photographs

PN 27516 – Leeward Proximal Reef Apron

Plate 1

core depth: 3135′ log depth: 3141′
Bioherm

core depth: 3125′ log depth: 3131′
Bioherm

core depth: 3116′ log depth: 3122′
Bioherm

core depth: 3085′ log depth: 3091′
Bioherm Cap - Bioherm Contact

PN 27516 – Leeward Proximal Reef Apron

Plate 2

core depth: 3083′ log depth: 3089′
Bioherm Cap

core depth: 3057′ log depth: 3063′
Reef Core

core depth: 3052′ log depth: 3058′
Reef Core

core depth: 3015′ log depth: 3021′
Proximal Reef Apron - Reef Core Contact

PN 27516 – Leeward Proximal Reef Apron

Plate 3

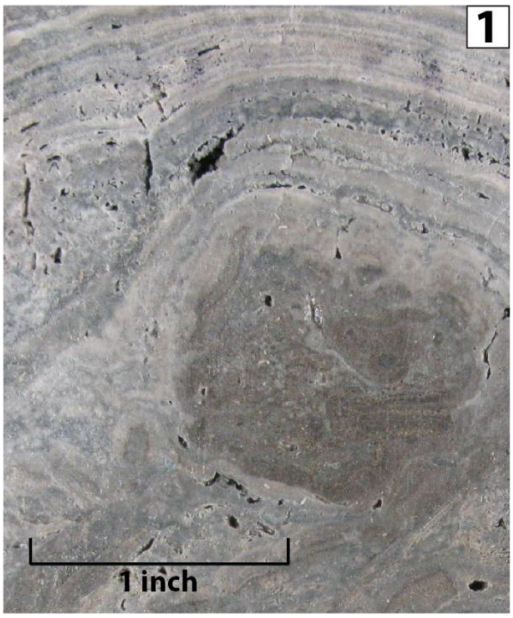

core depth: 2842′ log depth: 2848′
Cyanobacterial Mats - Stromatolitic Cap Contact Sequence Boundary 1

core depth: 2841′ log depth: 2847′
Cyanobacterial Mats

core depth: 2836′ log depth: 2842′
Thrombolitic Bindstone - Cyanobacterial Mats Contact Unconformity

core depth: 2818′ log depth: 2824′
Thrombolitic Bindstone

PN 27539 – Leeward Distal Reef Apron

Plate 4

core depth: 3204′ log depth: 3206′
Gray Niagaran

core depth: 3194′ log depth: 3196′
Bioherm Toe - Gray Niagaran Contact

core depth: 3193′ log depth: 3195′
Distal Reef Apron - Bioherm Toe Contact

core depth: 3161′ log depth: 3163′
Distal Reef Apron

PN 27605 – Windward Reef Talus

Plate 5

core depth: 3011′ log depth: 3014′
Dolopackstone

core depth: 3008′ log depth: 3011′
Cyanobacterial Mats

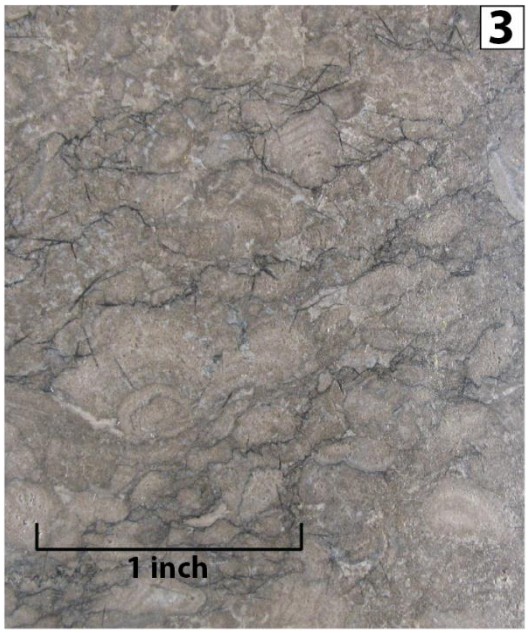

core depth: 3003′ log depth: 3006′
Oncolitic Packstone

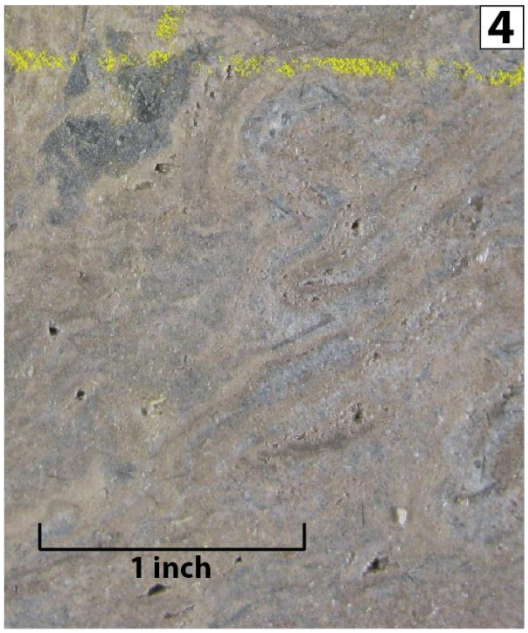

core depth: 2994′ log depth: 2997′
Laminated Peloidal Wackestone

PN 27851 – Leeward Flank

Plate 6

core depth: 3227′ log depth: 3219′
Gray Niagaran

core depth: 3220′ log depth: 3212′
Bioherm Toe

core depth: 3211′ log depth: 3203′
Distal Reef Apron

core depth: 3194′ log depth: 3186′
A-0 Carbonate

PN 27851 – Leeward Flank

Plate 7

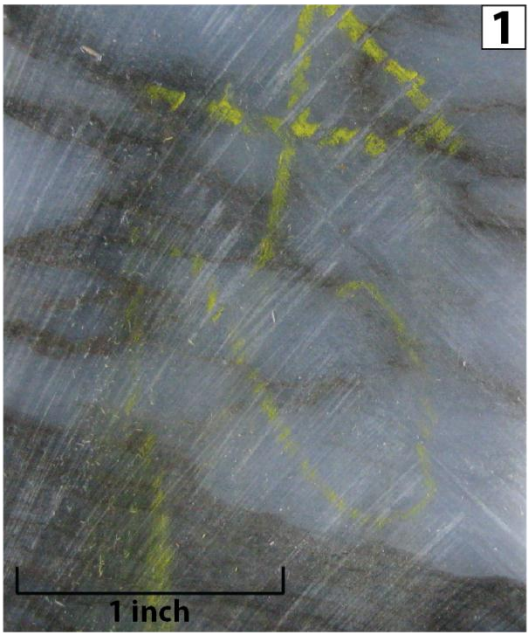

core depth: 3142′ log depth: 3134′
Rabbit Ear Anhydrite 2

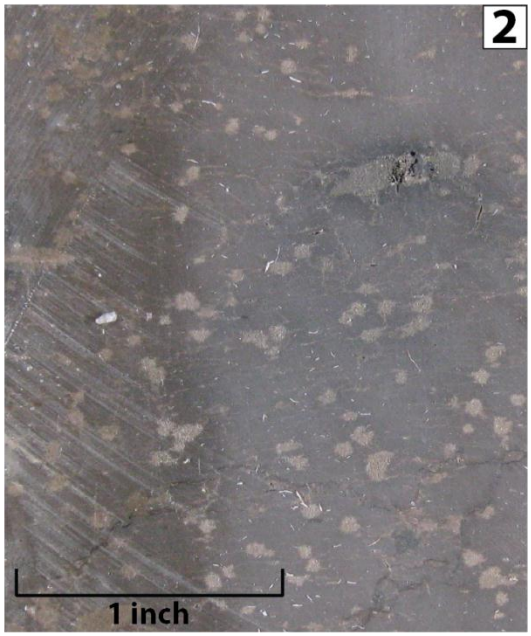

core depth: 3127′ log depth: 3119′
Upper A-1 Poker Chips

core depth: 3107′ log depth: 3099′
Upper A-1 Mudstone

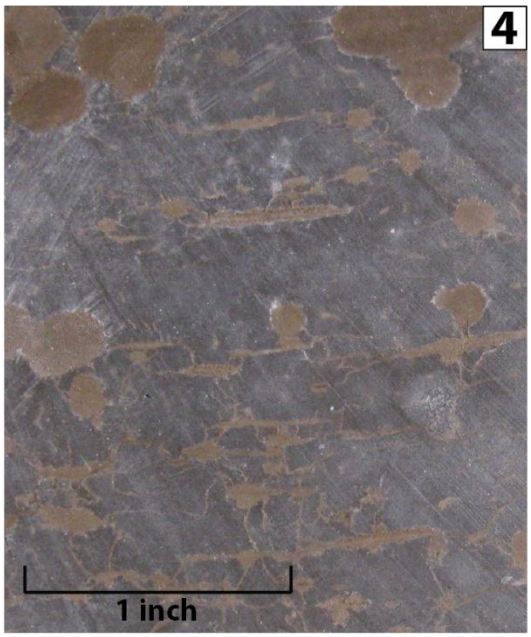

core depth: 3093′ log depth: 3085′
Upper A-1 Mudstone

APPENDIX B

Additional Core Profiles

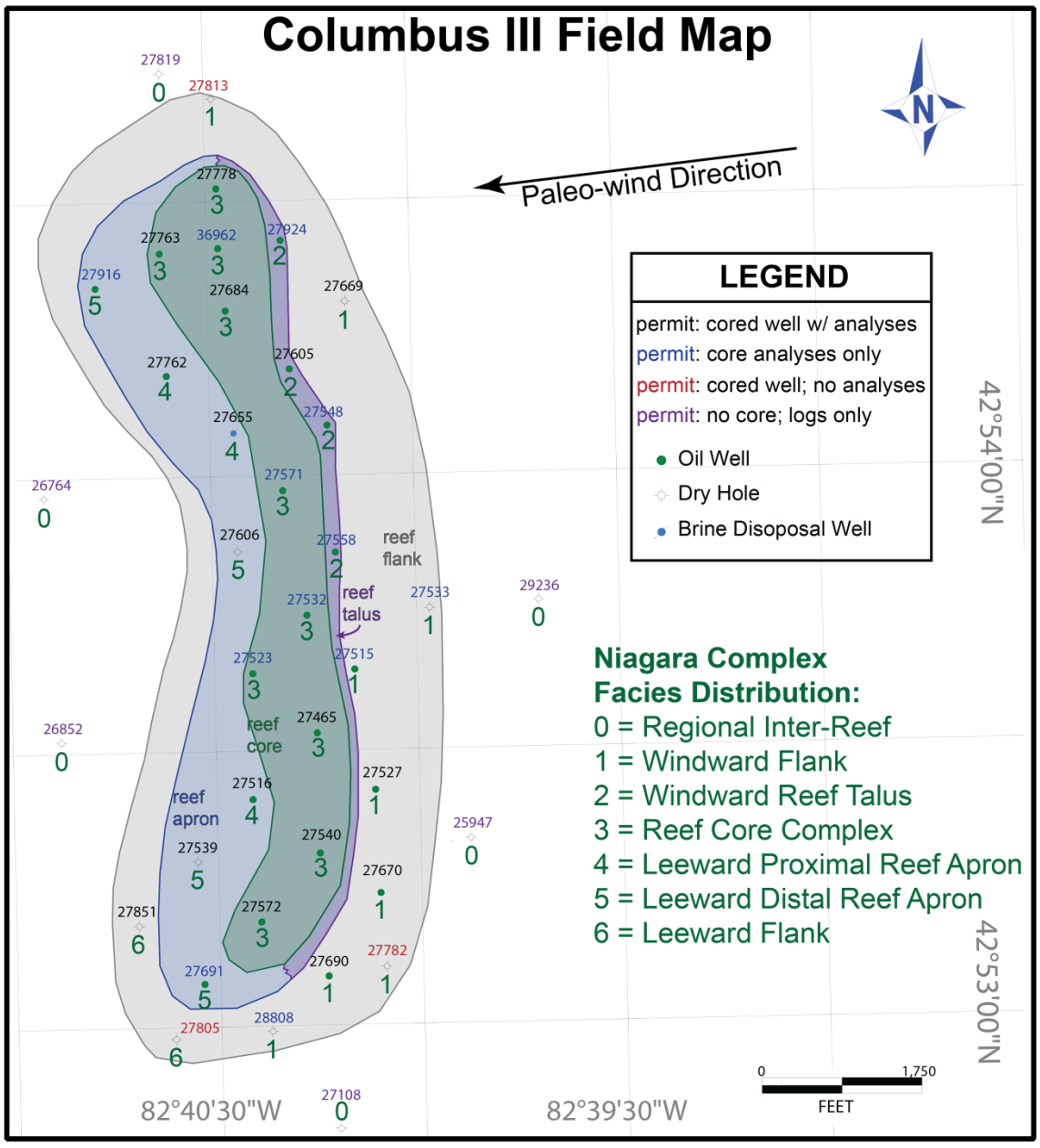
Columbus III Field Map
N
Paleo-wind Direction
LEGEND
permit: cored well w/ analyses
permit: core analyses only
permit: cored well; no analyses
permit: no core; logs only
Oil Well
Dry Hole
Brine Disoposal Well
Niagara Complex
Facies Distribution:
0 = Regional Inter-Reef
1 = Windward Flank
2 = Windward Reef Talus
3 = Reef Core Complex
4 = Leeward Proximal Reef Apron
5 = Leeward Distal Reef Apron
6 = Leeward Flank
reef flank
reef talus
reef core
reef apron
27819
27813
27778
27763
36962
27924
27916
27684
27669
27762
27605
27655
27548
27571
26764
27606
27558
27532
27533
29236
27523
27515
26852
27465
27527
27516
27540
27539
25947
27670
27851
27572
27691
27690
27782
28808
27805
27108
82°40'30"W
82°39'30"W
42°54'00"N
42°53'00"N
0
1,750
FEET

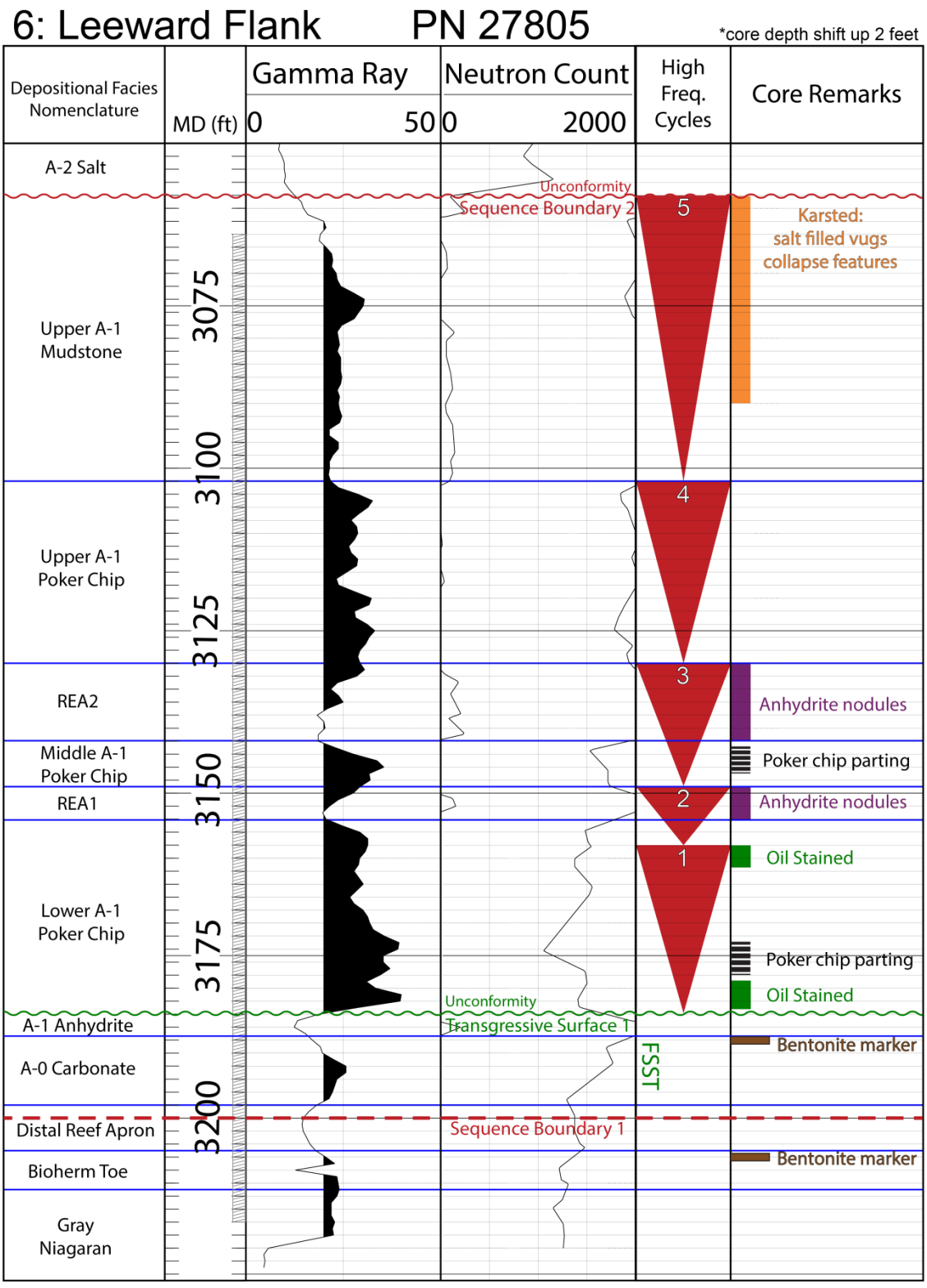
6: Leeward Flank
PN 27805
*core depth shift up 2 feet
Depositional Facies Nomenclature
MD (ft)
Gamma Ray
0
50
Neutron Count
0
2000
High Freq. Cycles
Core Remarks
A-2 Salt
Unconformity
Sequence Boundary 2
5
Karsted:
salt filled vugs
collapse features
Upper A-1 Mudstone
3075
3100
Upper A-1 Poker Chip
4
3125
REA2
3
Anhydrite nodules
Middle A-1 Poker Chip
Poker chip parting
3150
REA1
2
Anhydrite nodules
1
Oil Stained
Lower A-1 Poker Chip
3175
Poker chip parting
Oil Stained
Unconformity
Transgressive Surface 1
A-1 Anhydrite
Bentonite marker
A-0 Carbonate
FSST
3200
Distal Reef Apron
Sequence Boundary 1
Bioherm Toe
Bentonite marker
Gray Niagaran

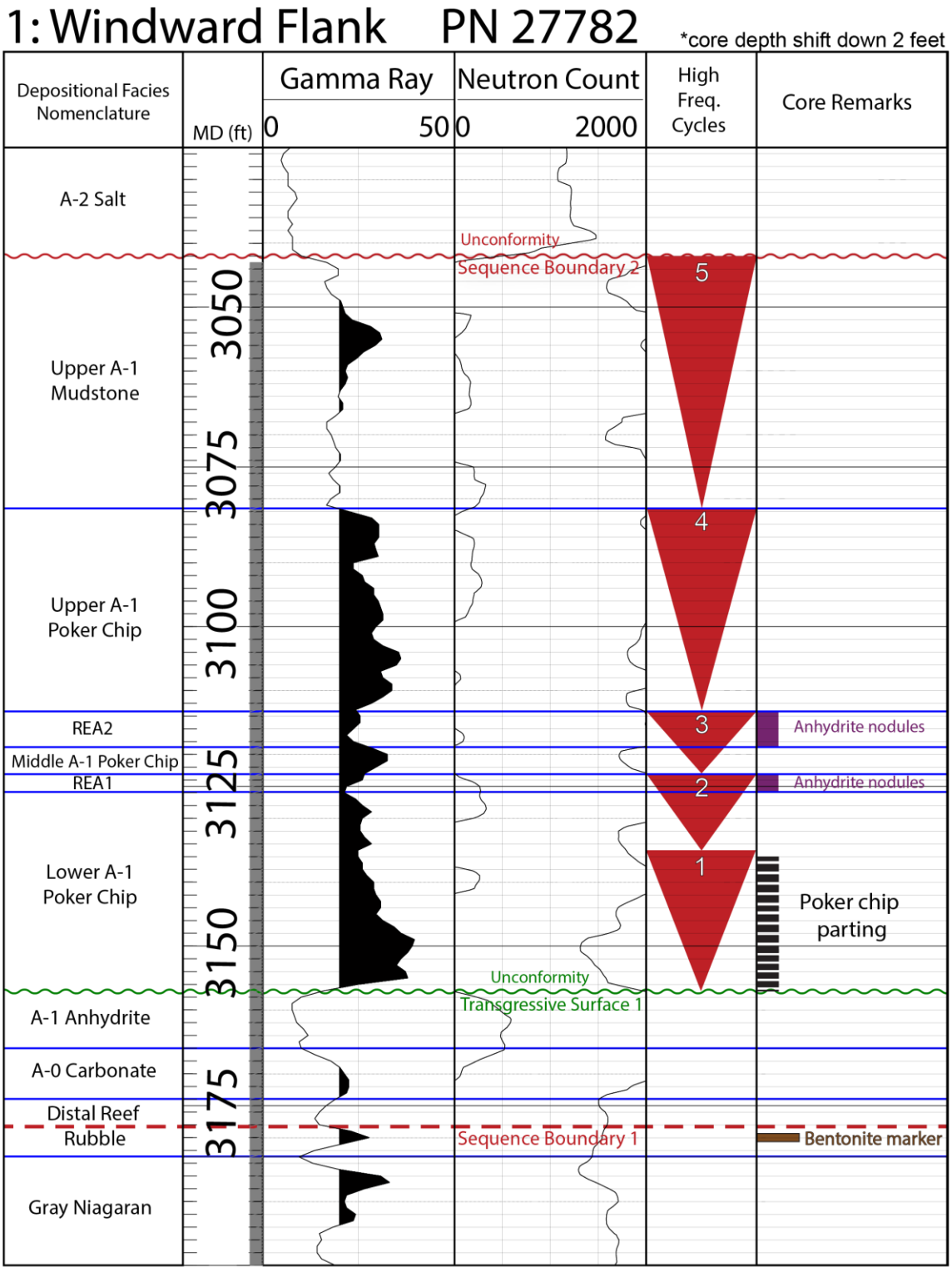
1: Windward Flank PN 27782
*core depth shift down 2 feet
Depositional Facies Nomenclature
MD (ft)
Gamma Ray
0
50
Neutron Count
0
2000
High Freq. Cycles
Core Remarks
A-2 Salt
Unconformity
Sequence Boundary 2
Upper A-1 Mudstone
3050
3075
Upper A-1 Poker Chip
3100
REA2
Middle A-1 Poker Chip
REA1
3125
Lower A-1 Poker Chip
3150
Unconformity
Transgressive Surface 1
A-1 Anhydrite
A-0 Carbonate
Distal Reef Rubble
3175
Sequence Boundary 1
Gray Niagaran
5
4
3
2
1
Anhydrite nodules
Anhydrite nodules
Poker chip parting
Bentonite marker

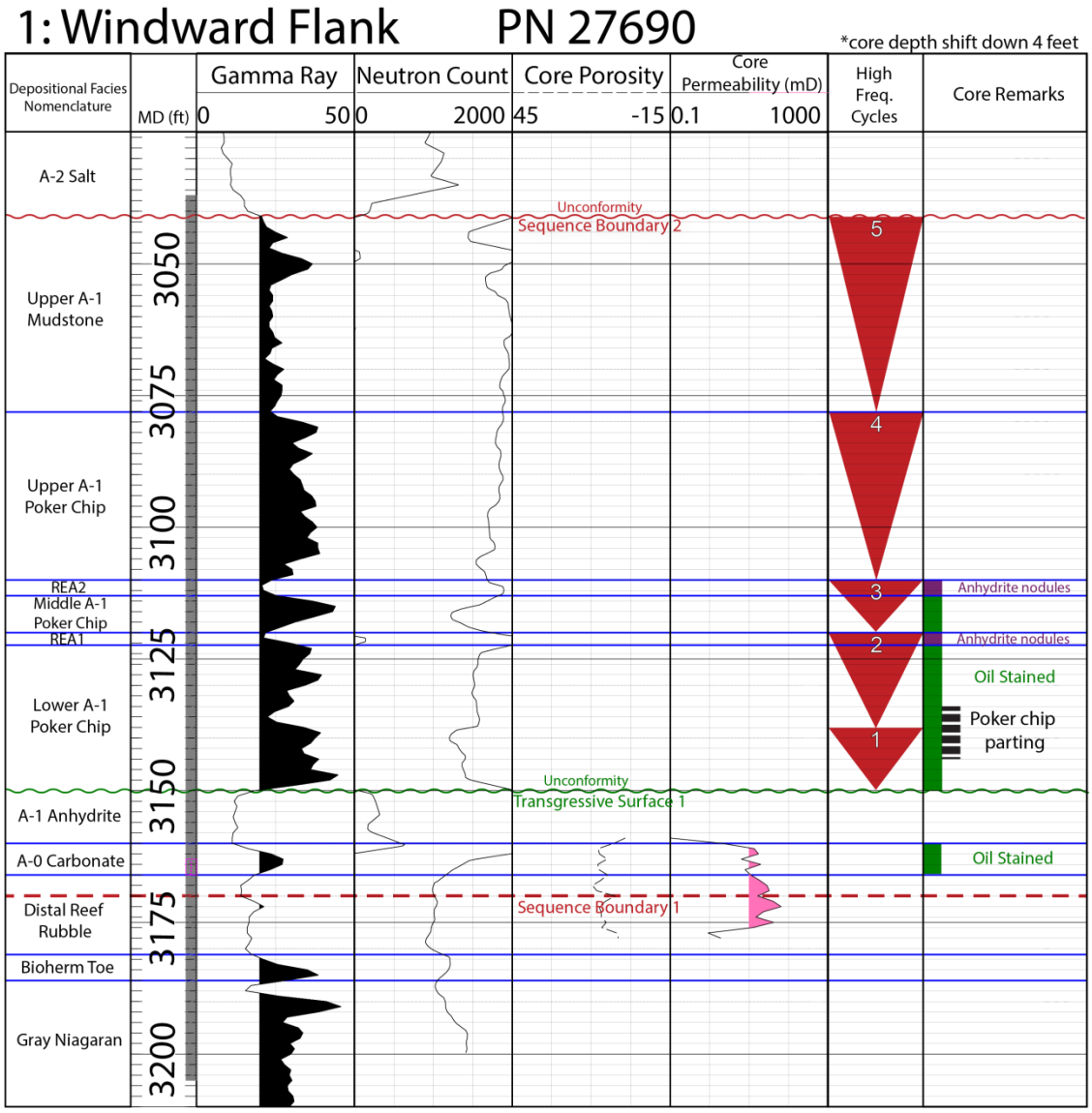
1: Windward Flank PN 27690
*core depth shift down 4 feet
Depositional Facies Nomenclature
MD (ft)
Gamma Ray
0
50
Neutron Count
0
2000
Core Porosity
45
-15
Core Permeability (mD)
0.1
1000
High Freq. Cycles
Core Remarks
A-2 Salt
Unconformity
Sequence Boundary 2
Upper A-1 Mudstone
3050
3075
Upper A-1 Poker Chip
3100
REA2
Middle A-1 Poker Chip
REA1
3125
Lower A-1 Poker Chip
3150
Unconformity
Transgressive Surface 1
A-1 Anhydrite
A-0 Carbonate
Distal Reef Rubble
Sequence Boundary 1
3175
Bioherm Toe
Gray Niagaran
3200
5
4
3
2
1
Anhydrite nodules
Anhydrite nodules
Oil Stained
Poker chip parting
Oil Stained

1: Windward Flank PN 27813

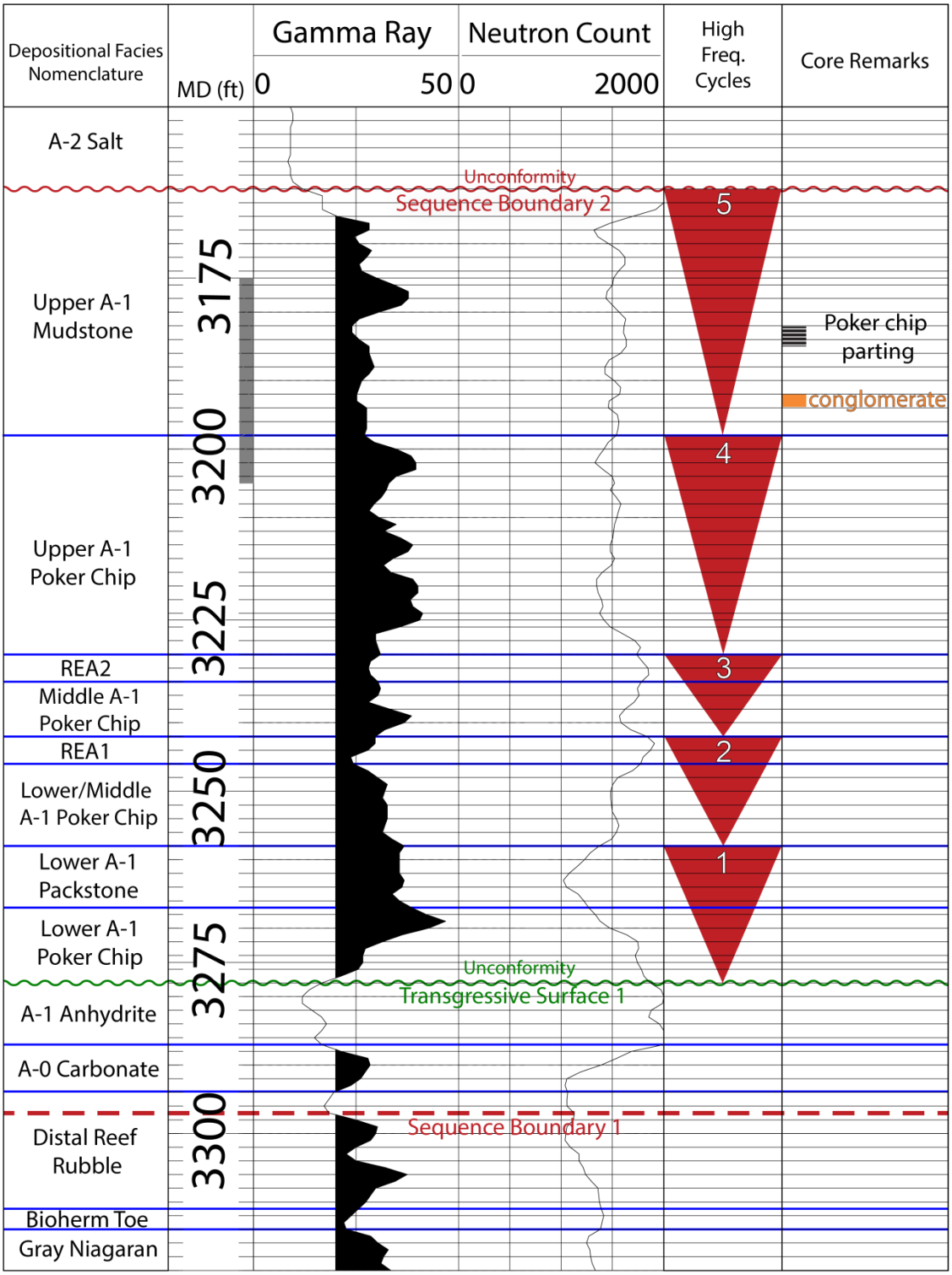

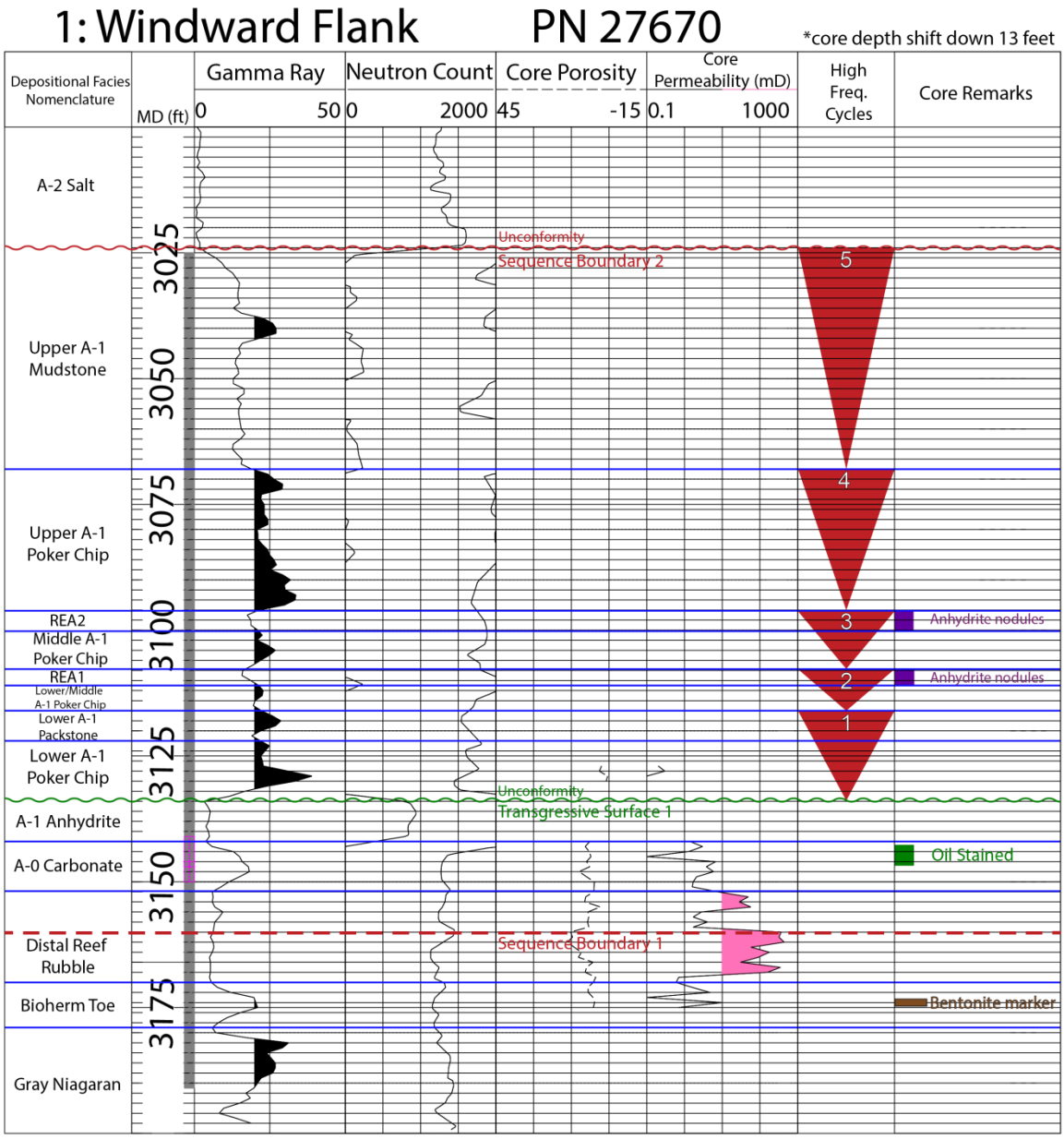
1: Windward Flank
PN 27670
*core depth shift down 13 feet
Depositional Facies Nomenclature
MD (ft)
Gamma Ray
0
50
Neutron Count
0
2000
Core Porosity
45
-15
Core Permeability (mD)
0.1
1000
High Freq. Cycles
Core Remarks
A-2 Salt
Unconformity
Sequence Boundary 2
Upper A-1 Mudstone
3025
3050
Upper A-1 Poker Chip
3075
REA2
Middle A-1 Poker Chip
3100
REA1
Lower/Middle A-1 Poker Chip
Lower A-1 Packstone
Lower A-1 Poker Chip
3125
Unconformity
Transgressive Surface 1
A-1 Anhydrite
A-0 Carbonate
3150
Distal Reef Rubble
Sequence Boundary 1
Bioherm Toe
3175
Gray Niagaran
5
4
3
2
1
Anhydrite nodules
Anhydrite nodules
Oil Stained
Bentonite marker

1: Windward Flank PN 27527

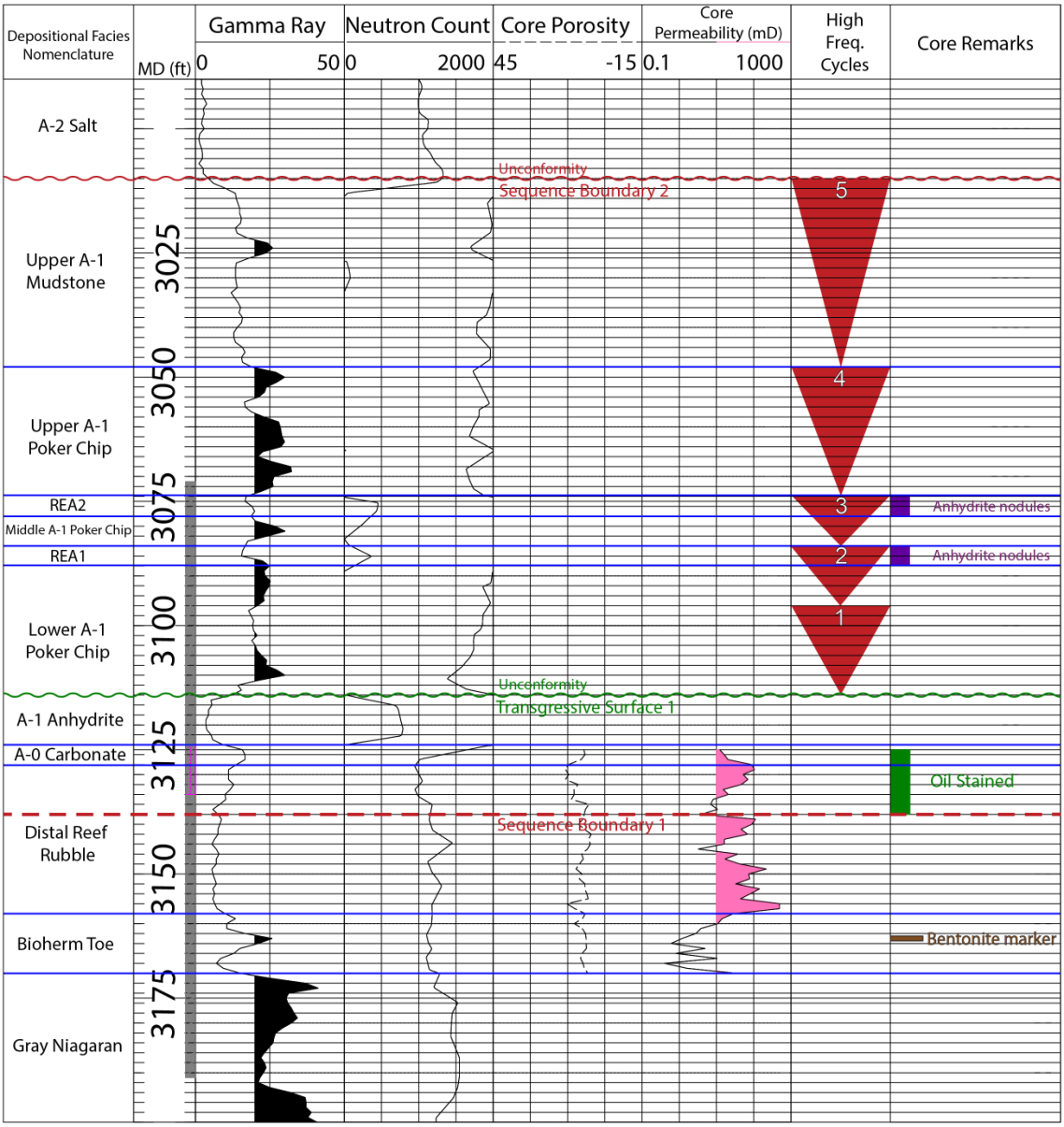

5: Leeward Distal Reef Apron PN 27606

*no core depth shift

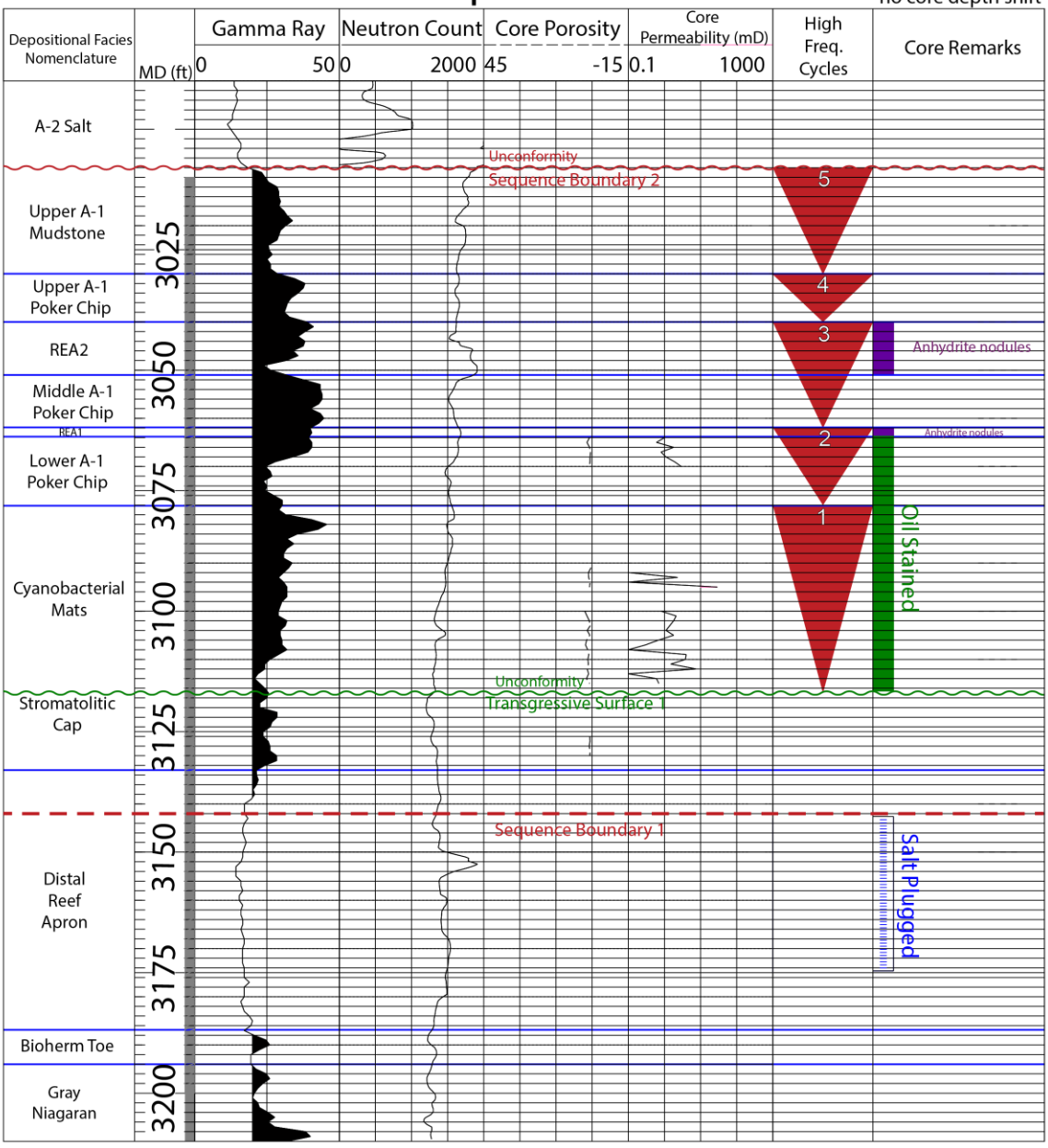

4: Leeward Proximal Reef Apron PN 27655

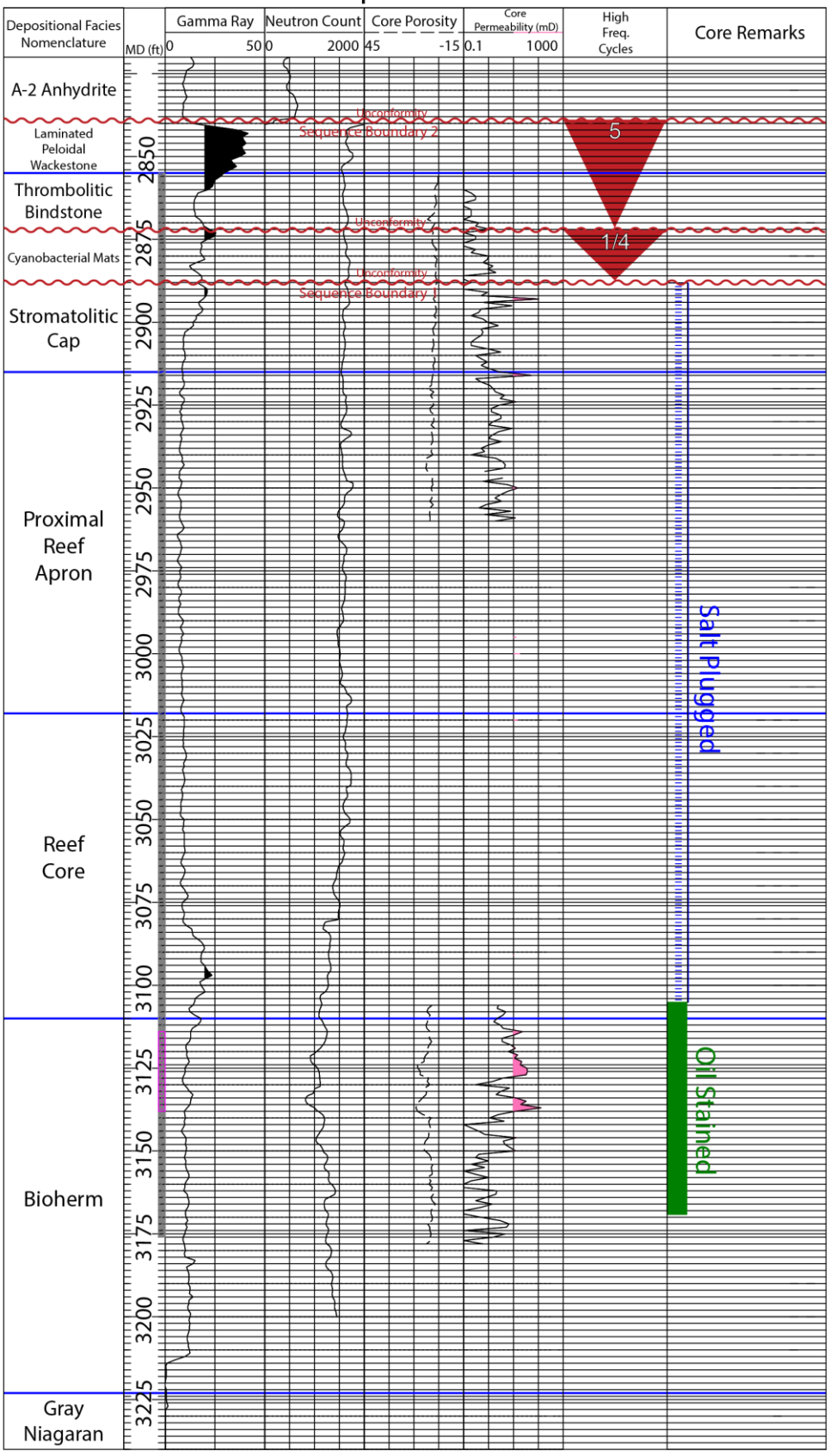

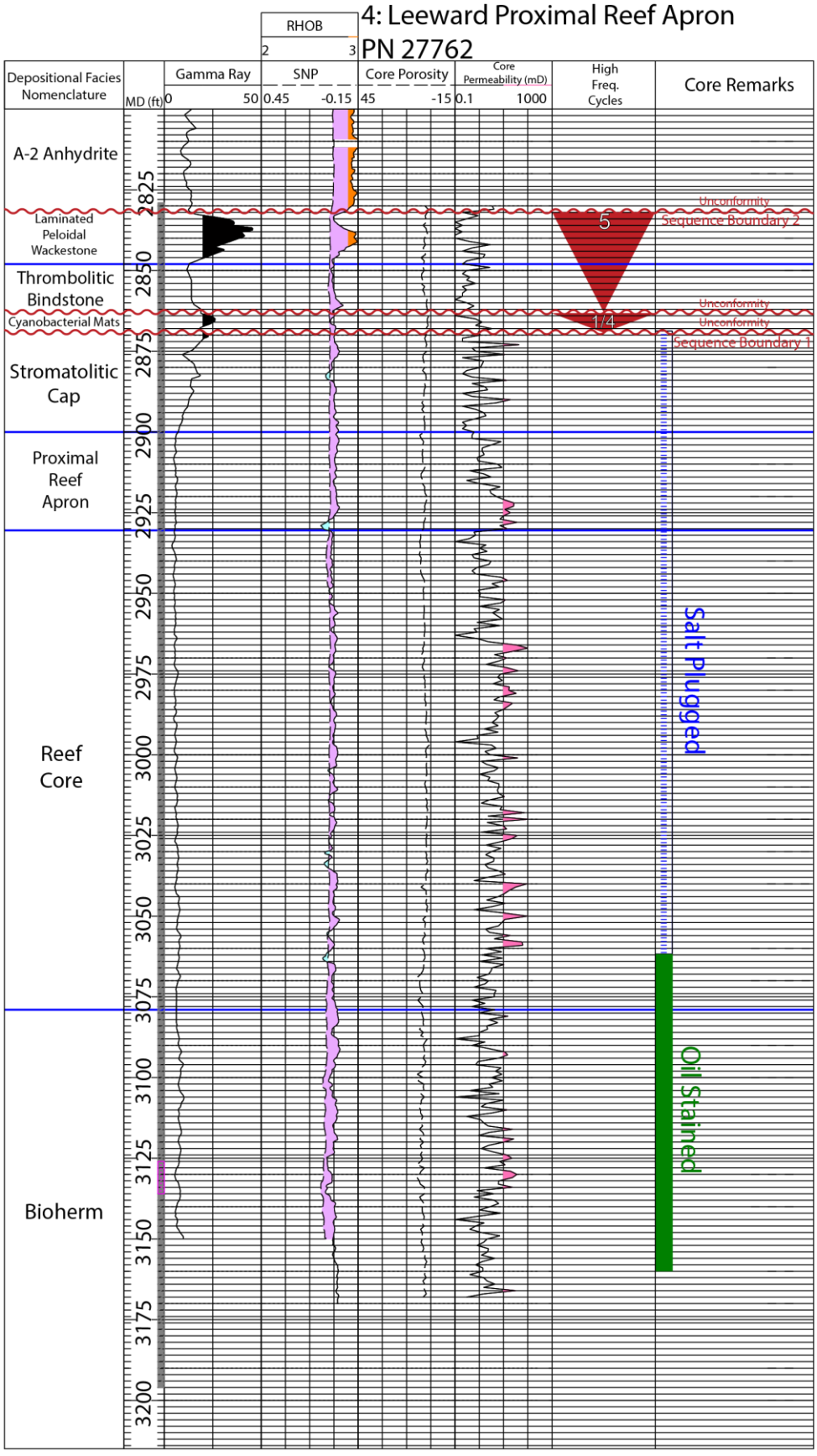
4: Leeward Proximal Reef Apron
PN 27762
RHOB
2
3
Depositional Facies Nomenclature
Gamma Ray
0
50
SNP
0.45
-0.15
Core Porosity
45
-15
Core Permeability (mD)
0.1
1000
High Freq. Cycles
Core Remarks
MD (ft)
A-2 Anhydrite
Laminated Peloidal Wackestone
Thrombolitic Bindstone
Cyanobacterial Mats
Stromatolitic Cap
Proximal Reef Apron
Reef Core
Bioherm
2825
2850
2875
2900
2925
2950
2975
3000
3025
3050
3075
3100
3125
3150
3175
3200
5
1/4
Unconformity
Sequence Boundary 2
Unconformity
Unconformity
Sequence Boundary 1
Salt Plugged
Oil Stained

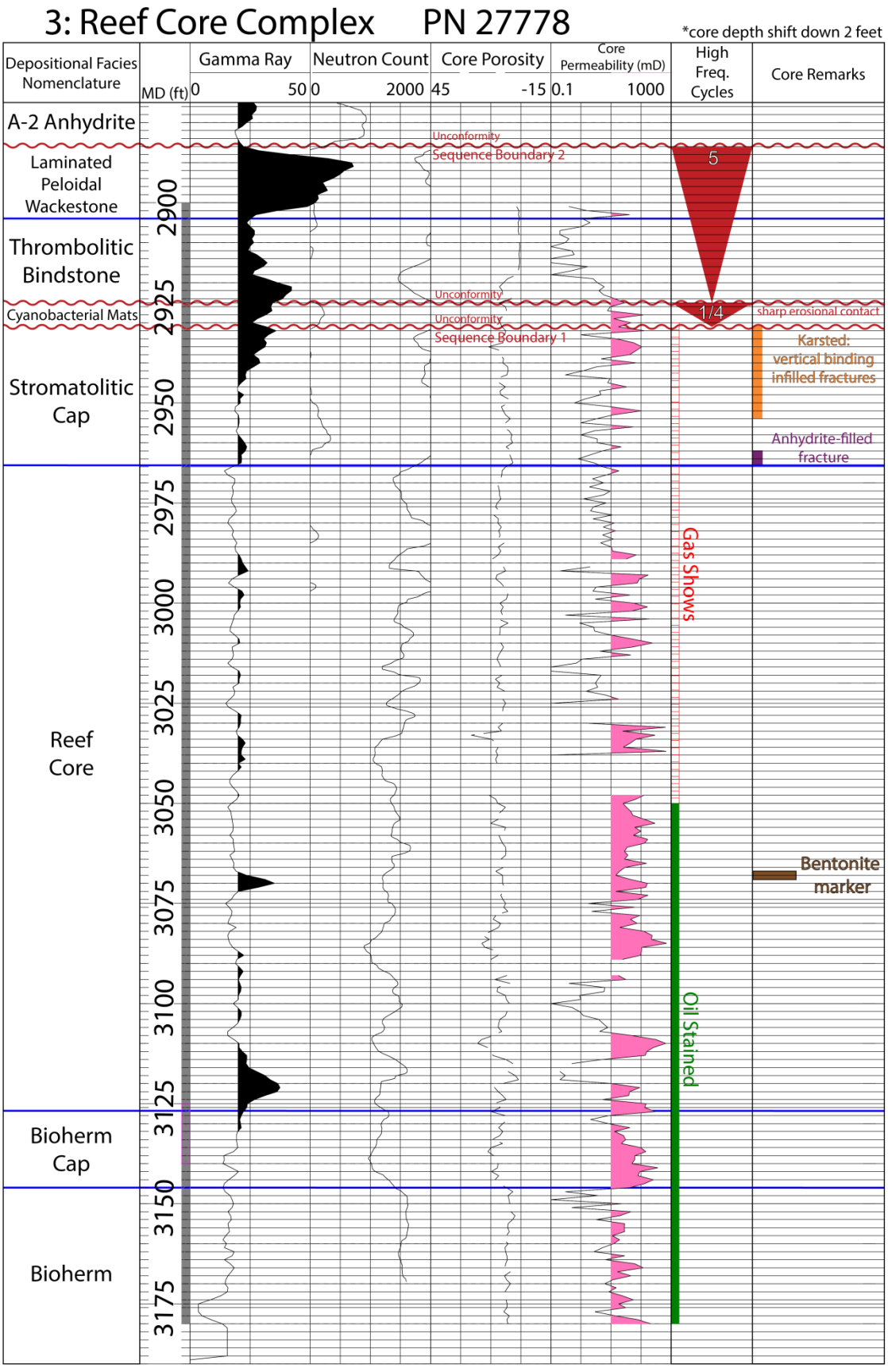
3: Reef Core Complex PN 27778
*core depth shift down 2 feet
Depositional Facies Nomenclature
MD (ft)
Gamma Ray
0
50
Neutron Count
0
2000
Core Porosity
45
-15
Core Permeability (mD)
0.1
1000
High Freq. Cycles
Core Remarks
A-2 Anhydrite
Laminated Peloidal Wackestone
Thrombolitic Bindstone
Cyanobacterial Mats
Stromatolitic Cap
Reef Core
Bioherm Cap
Bioherm
Unconformity
Sequence Boundary 2
Unconformity
Unconformity
Sequence Boundary 1
5
1/4
sharp erosional contact
Karsted: vertical binding infilled fractures
Anhydrite-filled fracture
Gas Shows
Oil Stained
Bentonite marker
2900
2925
2950
2975
3000
3025
3050
3075
3100
3125
3150
3175

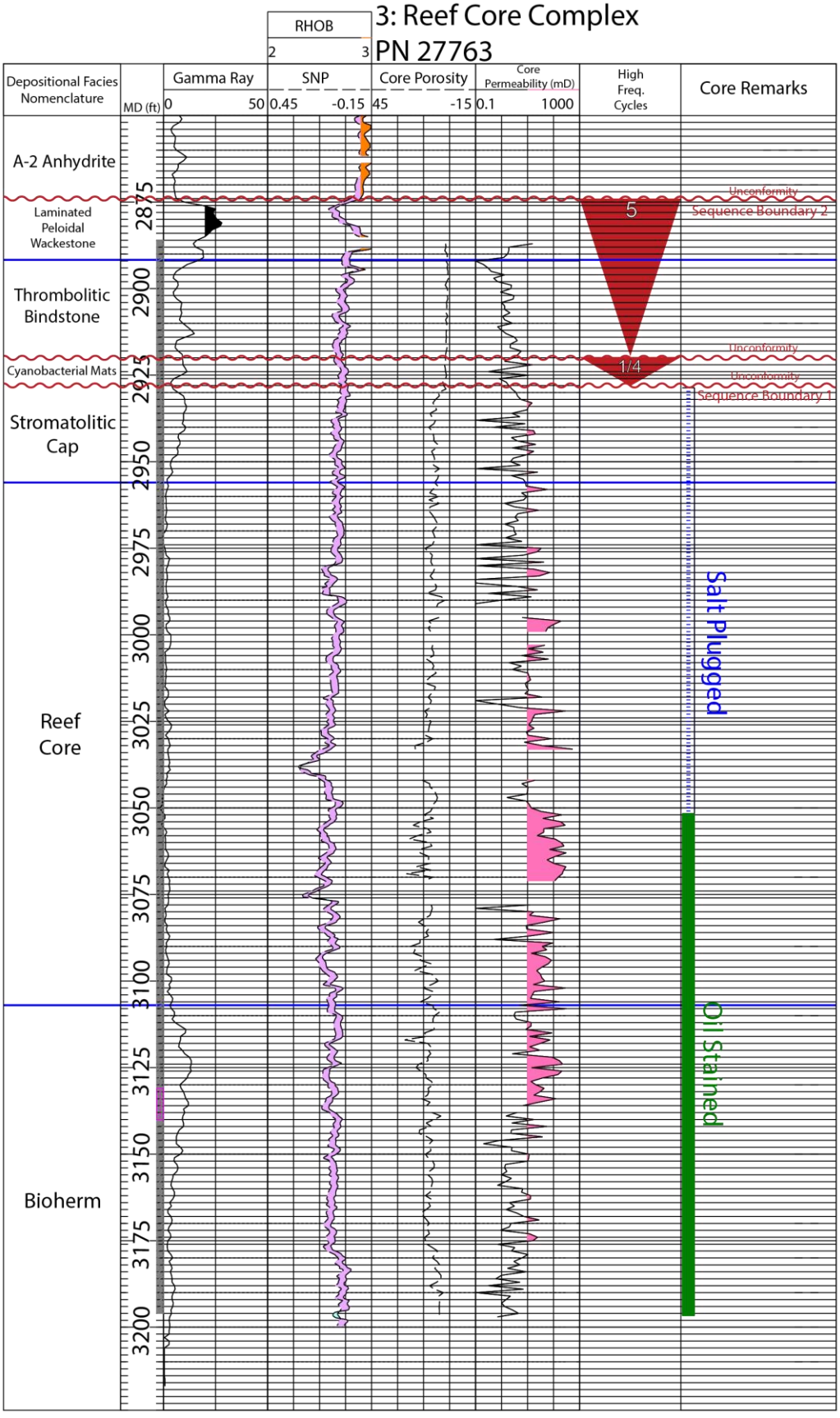
3: Reef Core Complex
PN 27763
RHOB
2
3
Depositional Facies Nomenclature
MD (ft)
Gamma Ray
0
50
SNP
0.45
-0.15
Core Porosity
45
-15
Core Permeability (mD)
0.1
1000
High Freq. Cycles
Core Remarks
A-2 Anhydrite
Laminated Peloidal Wackestone
Thrombolitic Bindstone
Cyanobacterial Mats
Stromatolitic Cap
Reef Core
Bioherm
2875
2900
2925
2950
2975
3000
3025
3050
3075
3100
3125
3150
3175
3200
Unconformity
Sequence Boundary 2
5
1/4
Unconformity
Unconformity
Sequence Boundary 1
Salt Plugged
Oil Stained

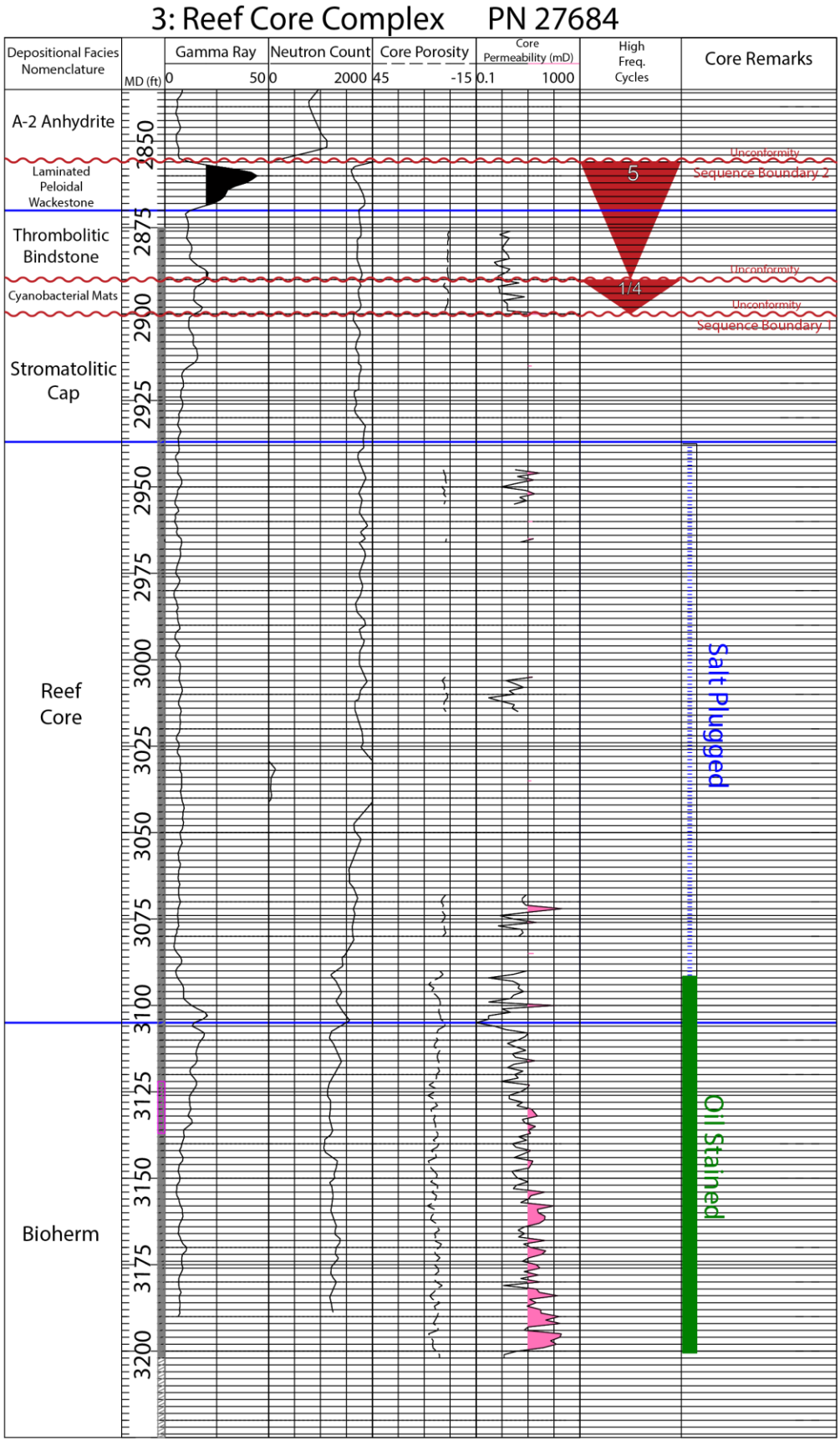
3: Reef Core Complex PN 27684
Depositional Facies Nomenclature
MD (ft)
Gamma Ray
0
50
Neutron Count
0
2000
Core Porosity
45
-15
Core Permeability (mD)
0.1
1000
High Freq. Cycles
Core Remarks
A-2 Anhydrite
Laminated Peloidal Wackestone
Thrombolitic Bindstone
Cyanobacterial Mats
Stromatolitic Cap
Reef Core
Bioherm
2850
2875
2900
2925
2950
2975
3000
3025
3050
3075
3100
3125
3150
3175
3200
5
1/4
Unconformity
Sequence Boundary 2
Unconformity
Unconformity
Sequence Boundary 1
Salt Plugged
Oil Stained

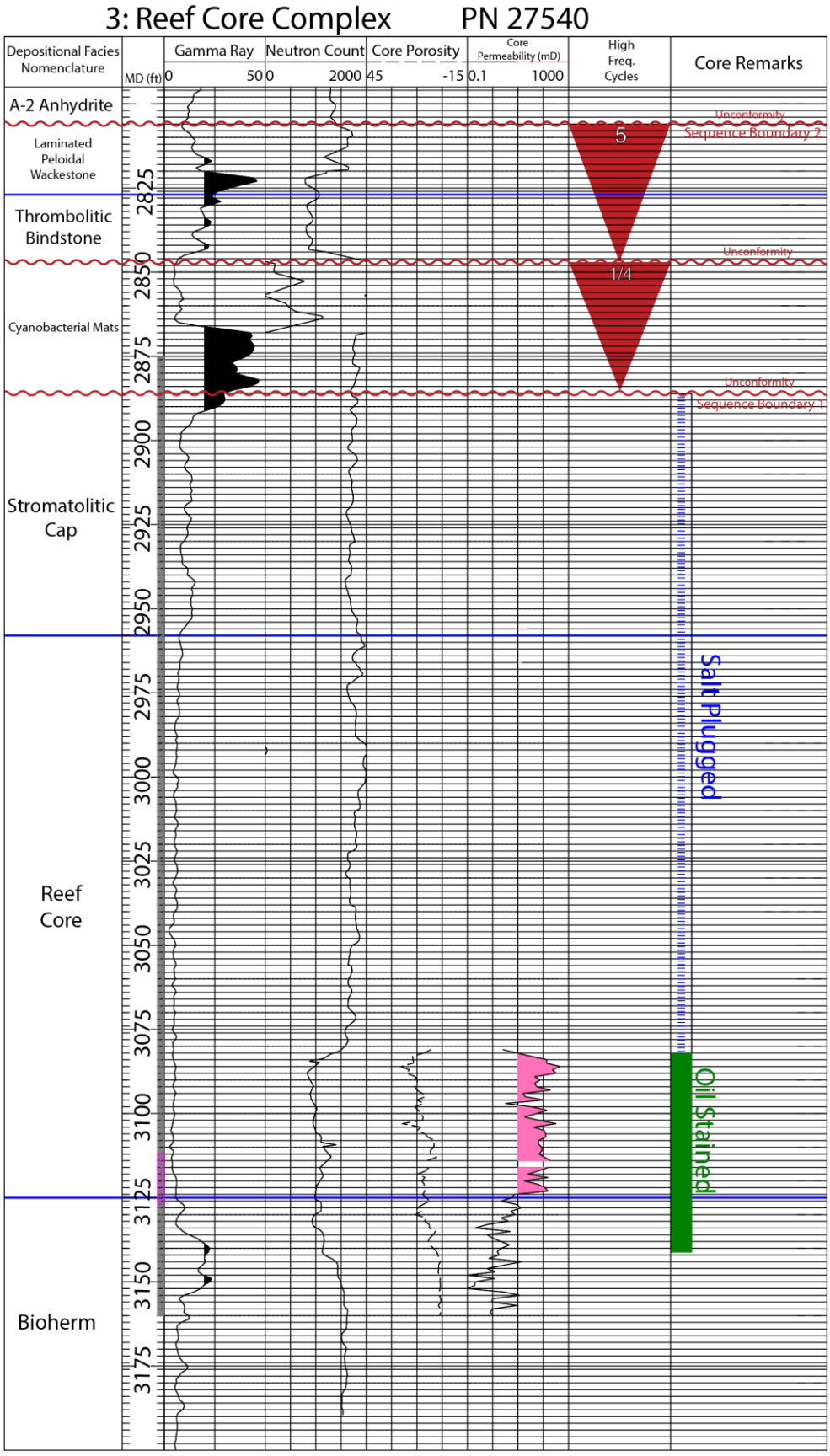
3: Reef Core Complex PN 27540
Depositional Facies Nomenclature
MD (ft)
Gamma Ray
0
50
Neutron Count
0
2000
Core Porosity
45
-15
Core Permeability (mD)
0.1
1000
High Freq. Cycles
Core Remarks
A-2 Anhydrite
Laminated Peloidal Wackestone
Thrombolitic Bindstone
Cyanobacterial Mats
Stromatolitic Cap
Reef Core
Bioherm
2825
2850
2875
2900
2925
2950
2975
3000
3025
3050
3075
3100
3125
3150
3175
Unconformity
Sequence Boundary 2
5
Unconformity
1/4
Unconformity
Sequence Boundary 1
Salt Plugged
Oil Stained

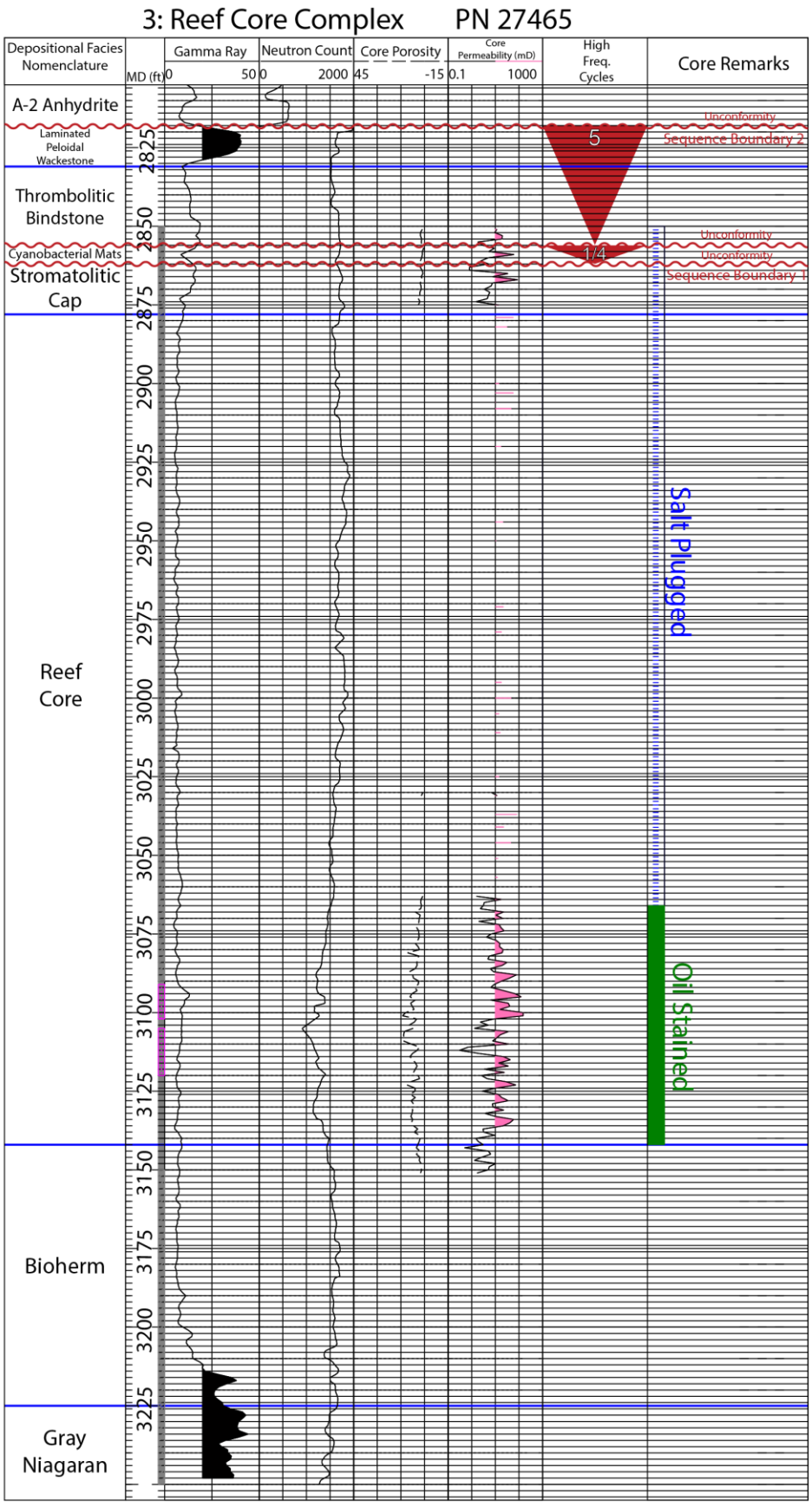
3: Reef Core Complex PN 27465
Depositional Facies Nomenclature
MD (ft)
Gamma Ray
0
50
Neutron Count
0
2000
Core Porosity
45
-15
Core Permeability (mD)
0.1
1000
High Freq. Cycles
Core Remarks
A-2 Anhydrite
Laminated Peloidal Wackestone
Thrombolitic Bindstone
Cyanobacterial Mats
Stromatolitic Cap
Reef Core
Bioherm
Gray Niagaran
2825
2850
2875
2900
2925
2950
2975
3000
3025
3050
3075
3100
3125
3150
3175
3200
3225
5
1/4
Unconformity
Sequence Boundary 2
Unconformity
Unconformity
Sequence Boundary 1
Salt Plugged
Oil Stained